A mineralogical approach to quantifying ore variability within a polymetallic Cu-Pb-Zn Broken Hill-type deposit and its implications for geometallurgy

Henry J.J. Gordon

A dissertation presented in partial fulfilment of the requirements for the degree of Master of Geology in the Faculty of Science at Stellenbosch University

Supervised by: Associate Professor Jodie Miller

Co-supervised by: Associate Professor Megan Becker

December 2019

DECLARATION

This dissertation is a presentation of my original research work. Wherever contributions of others are involved, every effort is made to indicate this clearly, with due reference to the literature, and acknowledgement of collaborative research and discussions. The work was done under the guidance of Associate Professor Jodie Miller, at the University of Stellenbosch, Stellenbosch, South Africa, and Associate Professor Megan Becker at the Centre for Minerals Research, Department of Chemical Engineering, University of Cape Town, South Africa.

Date: December 2019

ABSTRACT

A detailed two-part mineralogical study was undertaken on a polymetallic Cu-Pb-Zn ore from the Aggeneys-Gamsberg Ore District to quantify which mineral characteristics of the lithological ore types are problematic during flotation. The first part involved quantifying the bulk mineralogy, grain size distribution and textural characteristics from five primary lithological units (Quartz-Magnetite, Amphibole-Magnetite, Mineralised Schist, Sulphidic-Quartzite and Garnet-Quartzite) in order to propose early-stage geometallurgical domains prior to flotation testing. Strong bulk mineralogical and chalcopyrite grain size distribution patterns were selected as the partition between three early-stage geometallurgical domains. These domains were, the least variable Cu-rich quartz dominated Garnet-Quartzite domain, the Cu-Pb-rich quartz-dominated Lower Ore Body domain (consisting of the Mineralised Schist and Sulphidic Quartzite) and the most variable Cu-Pb-Zn rich magnetite dominated – Upper Ore Body domain (consisting of the Amphibole Magnetite and Quartzite-Magnetite).

Six bulk samples that represent the magnetite-dominated Upper Ore Body domain were selected to test the process mineralogical variability of the Quartz-Magnetite and Amphibole-Magnetite subordinate lithological units, and thereby prove or disprove the proposed early-stage Upper Ore Body geometallurgical domain. Distinct metal zonation (head grade), liberation and mineral association configurations within these ores proved to be the defining variables that influenced their respective flotation responses. From this approach, the Cu-Pb Quartz-Magnetite domain (medium grade, best liberated and most straightforward), the Zn-Cu-Pb Pyroxmangite-Quartz-Magnetite domain (highest grade, moderately liberated and most complex) and the Cu-Pb Amphibole-Magnetite domain (lowest grade, poorest liberated and poorest quality) were resultant.

However, provisions should be made to counteract the negative implications associated with the economic sulphide -, gangue sulphide - and non-sulphide gangue mineralogies of the three magnetite-dominated geometallurgical domains, if processed individually. Problematic process mineralogical features of the magnetite-dominated ores are: Slow floating sphalerite minerals (implications for Zn recovery); chalcopyrite disease (implications for selectivity between chalcopyrite and sphalerite); varying chalcopyrite and galena head grades (implications for Cu and Pb recovery); varying hardness and concentration ratios (implications for ore throughput); locked economic sulphide minerals (implications for recovery of gangue minerals) and fine-grained manganese minerals (implications for manganese entrainment). These problematic process mineralogical characteristics can potentially be neutralised through finer grinding (increased liberation and recovery of economic sulphide minerals), blending of Mn-rich and Mn-poor ores, and follow up quantitative mineralogical test work to ascertain the lower limit grain size at which manganese entrainment can be minimized.

Integration of the above-mentioned domain considerations back into the geological block model is challenging due to limited mineralogy data and the incompatibility of the mineralogy and chemical assay data that define geological block models. As a result, an elemental proxy, the Cu:S ratio was presented as a quantitative variable that could be used to illustrate the differences between these domains in a 2-D

and 3-D manner to inform the geologist and metallurgists about the expected variability. Secondly, a geometallurgical matrix was presented as a qualitative approach to ensure that the domains are accurately identified by the underground geologists and the variability of the mined feeds are efficiently communicated to the metallurgists.

The approach of this study can contribute to the way in which the geometallurgical domains within other deposits are formulated.

ACKNOWLEDGEMENTS

I would like to express my deepest gratitude and appreciation to Prof Jodie A. Miller, Earth Science Department, Stellenbosch University, and Prof. Megan Becker, Centre for Minerals Research, Department of Chemical Engineering, University of Cape Town. I have learnt a great deal from the two of you. Thank you for your time, patience, advice, criticism and correction of this thesis from the beginning up to the end of writing.

Thank you to everyone who has helped with the sample preparation and generation of flotation, optical microscopy, SEM-EDS, QEMSCAN, QXRD, XRF and ICP-AES data, in particular Kirsten Corin, Gaynor Yorath, Monde Bekaphi, Lorraine Nkemba, Kenneth Maseko, Keshree Pillay from the Centre for Minerals Research, Department of Chemical Engineering, University of Cape Town and Madelaine Frazenburg from the Central Analytical Facility, Department of Earth Science, Stellenbosch University.

A word of thanks goes to Black Mountain Mining (Pty). Ltd. for funding this project, in particular General Manager, Sean Jenniker; Metallurgical Manager, Adrian Landsberg and Geology Manager, Pieter Steinmann, who saw the value of this geometallurgical work.

Graeme Stroebel, thank you for making it possible for me to live and work in Aggeneys and still be able to obtain my MSc.

I would like to acknowledge that none of this would have been possible without God. Thank you for the patience, guidance, energy and perseverance throughout the investigation and preparation of this thesis.

To my wife, Jo-ann Gordon you have been as much a part of this project as I have. Thank you for being my anchor during this time. Without our talks and your encouragement, I would have given up long ago. Thank you for all the coffee and snacks you brought me at night when I was busy writing, but most of all, thank you for your love and patience during the last three years.

I would like to acknowledge and thank my parents, Henry and Bernadette Gordon, who always has all of the answers. Similarly, my in-laws, Alfred and Elizabeth for also supporting me.

To my friends who provided comfort in the least pleasant times, in particular, Sergio Jones, Duran Diergaardt, Griffen Makok, Isidor Malgas and Aydan Jansen. You are always there when I need you and you always find a way to make me laugh.

To my colleagues, Westley Price and Alan Johnson, my sincere apologies for talking your ears off about geometallurgy; nonetheless, thank you for listening and covering for me when I had to take off from work.

LIST OF PUBLICATIONS AND PRESENTATIONS

Gordon, H.J.J, Miller, J.A. and Becker, M. 2018. Using mineralogy for early-stage geometallurgical domain definition: A case study of the Swartberg polymetallic sulphide deposit. In Proceedings: The South African Institute for Mining and Metallurgy (SAIMM), Geometallurgy conference, pp. 121-131. 6-8 August 2018, Cape Town, South Africa.

Candidate contribution: *The candidate contributed 70 % to the conceptualisation of the early-stage geometallurgical domain approach presented in this work and 80 % to the data analysis and writing of this manuscript*

Gordon, H.J.J, Stroebel, G., Miller, J.A, Corin, K. and Becker, M. 2018. A process mineralogical study of the magnetite dominated ores of the polymetallic Swartberg deposit, Aggeneys. Presented at: MEI Process Mineralogy ’18, 19-21 November 2018, Cape Town

Candidate contribution: *The candidate contributed 70 % to the conceptualisation of the preliminary flotation trends presented in this work and 85 % to the data analysis and writing of this extended abstract*

Gordon, H.J.J., Stroebel, G., Miller, J.A., Corin, K. and Becker, M. 2019. Geometallurgical domain classification of magnetite dominated ores using ore mineral characteristics as geometallurgical proxies. Submitted to Minerals Engineering.

Candidate contribution: *The candidate contributed 70 % to the conceptualisation of the validation of early-stage geometallurgical domains presented in this work and 85 % to the data analysis and writing of this manuscript*

TABLE OF CONTENTS

LIST OF FIGURES

LIST OF TABLES

DEFINITIONS AND ABBREVIATIONS

A-GOD	Aggeneys-Gamsberg Ore District
AM	Amphibole Magnetite
Anh	Anhedral
BMC	Black Mountain Complex
BWI	Bond work index
ES	Economic sulphide minerals
euh	Euhedral
fol	Foliated
GQGD	Garnet quartzite geometallurgical domain
GQZ	Garnet Quartzite Zone
GS	Gangue sulphide minerals
ICP-AES	Inductively coupled plasma with atomic emission spectroscopy
LOB	Lower Orebody
LOM	Life of Mine
mass	Massive
MBZ	Magnetite Barite Zone
MC	Mineralised schist
MIBC	Methyl isobutyl carbinol
MLA	Mineral liberation analyzer
Non-fol	Non-foliated
NSG	Non-sulphide gangue minerals
PAX	Potassium amyl xanthate
PQM	Pyroxmangite Quartz Magnetite
QEMSCAN	Quantitative evaluation of minerals by scanning electron microscopy
QM	Magnetite Quartzite
QM Cu	Cu-rich Magnetite quartzite
QM Zn	Zn-rich Magnetite quartzite
QXRD	Quantitative x-ray diffraction
SAIMM	Southern African Institute for Mining and Metallurgy
SEX	Sodium ethyl xanthate
SQ	Sulphidic quartzite
S-QM	Sulphidic quartz magnetite

Sub	subhedral
UOB	Upper Orebody
UOBGD	Upper Orebody geometallurgical domain
Wt. percentage	Weight percentage
XRF	X-ray fluorescence spectroscopy

MINERAL NAMES, ABBREVIATIONS AND FORMULAS

Actinolite (act)	$Ca_2\ (Mg,\ Fe_2)_5\ Si_8O_{22}\ (OH)_2$
Albite (alb)	$NaAlSi_3O_8$
Almandine	$Fe_3Al_2\ (SiO_4)_3$
Amphibole (amph)	$Ca_2(Mg,Fe^{2+},Fe^{3+},Al)_5(Si,Al)_8O_{22}(OH)_2$
Andradite	$Ca_3Fe_2(SiO_4)_3$
Annite	$KFeAlSiO_{10}(OH,F)_2$
Anorthite	$CaAl_2Si_2O_8$
Apatite (ap)	$Ca_5(PO_4)_3(OH,F,Cl)$
Arsenopyrite	$FeAsS$
Augite	$(Ca,Na)(Mg,Fe,Al,Ti)(Si,Al)_2O_6$
Barite (ba)	$BaSO_4$
Biotite (bt)	$K(Mg,Fe)_3AlSi_3O_{10}(OH,F)_2$
Bismuthinite	Bi_2S_3
Bornite (bor)	Cu_5FeS_4
Chalcopyrite (cp)	$CuFeS_2$
Chlorite	$(Fe,Mg,Al)_6(Si,Al)_4O_{10}(OH)_8$
Chromite	$FeCr_2O_4$
Chromohercynite	$Fe(Al,Cr)_2O_4$
Covellite	CuS
Cordierite	$Mg_2Al_4Si_5O_{18}$
Cummingtonite	$Mg_7(Si_8O_{22})(OH)_2$
Diopside	$CaMgSi_2O_6$
Epidote (ep)	$Ca_2(Fe,Al)Al_2(SiO_4)(Si_2O_7)O(OH)$
Fayalite	Fe_2SiO_4
Feldspar (fsp)	$KAlSi_3O_8$
Fluorite (fl)	CaF_2
Ferrosilite	$(Fe,Mg)_2Si_2O_6$
Gahnite (gah)	$ZnAl_2O_4$

Galena (ga)	PbS
Grunerite (gru)	$Fe_7Si_8O_{22}(OH)_2$
Hedenbergite	$CaFe^{2+}Si_2O_6$
Hematite (hem)	Fe_2O_3
Hercynite	$FeAl_2O_4$
Hyalophane (hyal)	$(K,Ba)Al(Si,Al)_3O_8$
Ilmenite (ilm)	$FeTiO_3$
Jacobsite	$(Mn^{2+},Fe^{2+},Mg)(Fe^{3+},Mn^{3+})_2O_4$
Magnetite (mgt)	Fe_3O_4
Manganogrunerite	$Mn^{2+}Fe^{2+}{}_5(Si_8O_{22})(OH)_2$
Microcline	$KAlSi_3O_8$
Molybdenite	MoS_2
Monazite-Ce	$(Ce,La,Nd,Th)P_4$
Muscovite	$KAl_2(Si_3Al)O_{10}(OH,F)_2$
Pyrite (py)	FeS_2
Pyrolusite	MnO_2
Pyroxene	$(Na,Ca)(Mg,Fe,Al)(Al,Si)_2O_6$
Pyroxmangite (pxm)	$(Mn,Fe^{2+})SiO_3$
Pyrrhotite (po)	$Fe_{1-x}S$
Quartz (qtz)	SiO_2
Rhodonite	$(Mn,Fe,Mg,Ca)SiO_3$
Rutile	TiO_2
Sillimanite (sill)	$AlSiO_5$
Spessartine	$Mn_3Al_2Si_3O_{12}$
Sphalerite (sph)	$(Zn,Fe)S$
Spinel	$MgAlO_4$
Tremolite	$Ca_2Mg_5Si_8O_{22}(OH)_2$
Tennantite	$(Cu,Fe)_{12}As_4S_{13}$
Zircon	$ZrSiO_4$

GLOSSARY

Activator	Chemical compounds that facilitate the attachment of collectors onto mineral surfaces that they would not normally attach to.
Automated mineralogy	A term applied to the mineralogy products generated by automated SEM-based instrumentation such as SEM-EDS and QEMSCAN.
Base Metals	Common metals that are not considered precious, such as copper, lead, iron, tin, zinc.
Broken Hill-type	A metamorphosed sedimentary exhalative deposit characterised by copious amounts of Cu-Pb-Zn-Ag.
Collector	Chemical compounds that adsorb onto the surfaces of particles and induce hydrophobicity.
Depressant	Chemical compounds that prevent certain mineral surfaces from becoming hydrophobic.
Face	The surface where the mining work is advancing.
Frother	Compounds used to stabilise the bubbles induced by the airflow so that they remain well dispersed in the slurry for hydrophobic mineral attachment and removal before the bubble bursts.
Geometallurgy	A discipline that utilizes learnings from geology, mining, mine planning, metallurgy and mineral processing to exploit metals from an orebody with spatially orientated predictive models.
Geometallurgical domain	A single ore, ore a set of ores that can be treated as a single unit in a metallurgical environment because of similarities in its physicochemical makeup.
Grade control	A process that is concerned with the delineation of ore and waste within a mine, and the efficiency by which sufficient ore grade material is reaches the concentrator plant.
Hydrophobicity	A particle or a portion of a particle that is wettable/ wetted by water.
Hydrophilic	A particle or a portion of a particle that is water-repellent.
Physico-chemical	Relating to physics and chemistry or to physical chemistry.
Polymetallic	Containing or involving several metals or their ores.
Process Mineralogy	Focuses on the relationships between ore and gangue minerals. The data generated from such studies characterize the mineralogy and deportment (texture) of the various mineral phases in the ore to optimize recovery and selectivity and predict environmental sensitivities.
Stope	The process of extracting the desired ore or from an underground mine, leaving behind an open space known as a stope. As mining progresses the stope is often backfilled with tailings, or when needed for strength, a mixture of tailings and cement.

Stratabound	Confined to a single stratigraphic unit. The term can refer to a stratiform deposit, to variously oriented orebodies contained within the unit, or to a deposit containing veinlets and alteration zones that may or may not be strictly conformable with bedding.
Tailings	Materials left over after the process of separating the valuable fraction from the uneconomic fraction (gangue) of an ore.

CHAPTER 1: Introduction and background

1.1. Introduction

The global demand for base metals is ever increasing to match the growth rate of economies in developing countries (Base Metals Supply and Demand - CME Group, 2019). It is for this reason that the mining of base metals is highly profitable (Ndlovu et al., 2011; Cropp et al., 2013; Bradshaw, 2014). In the last five years (Fig. 1.1), the business cycle for base metals has forced a strong trend to emerge in the metals industry (Lotter et al., 2017). When metal prices are high, metal refiners are more inclined to accept the available metal in concentrate to meet the demand for processed metal products. However, metal refiners become fastidious regarding the quality of base metal concentrates when metal prices are low (Twidle and Engelbrecht, 1984; Lane et al., 2016). This proves difficult for the continuation of mining operations that rely on a lower grade, polymetallic mineral resource to sustain profit margins due to its physicochemically complex nature (Lotter et al., 2011, Williams, 2013; Bradshaw, 2014; Johnson, 2016). Ores are considered complex when there are problematic interrelationships of economic minerals to one another and gangue minerals. This mineral association in most cases is further complicated by grain size – and textural variability (Becker et al., 2016; Evans and Morrison, 2016). These factors prevent the successful separation of economic minerals from one another and their ore host. This translates to metal losses and contaminated concentrates. In an attempt to mitigate the financial risk associated with the mining of complex, polymetallic deposits in current metal markets, mining companies are reassessing their minerals processing strategies (Rule and Schouwstra, 2011; Lotter et al., 2017).

It has become the best practice to scrutinize the processability of the economic minerals to combat metal losses and the recovery of unfavourable minerals during the flotation of base metal ores (Lotter et al., 2017). This requires a specialist approach that is capable of addressing difficulties related to the flotation of ores by identifying problematic ore characteristics, the extent of their variability, and their distribution within deposits. Knowledge of these factors will allow informed, proactive decision making regarding the acceptable amount of ore variability that can be accommodated without compromising the quality of concentrate products. This approach is known as process mineralogy (Becker et al., 2016). Several studies have highlighted the value of a process mineralogical approach to complex, polymetallic deposits to an extent that it is now increasingly understood that mineral characteristics such as texture, mineral identity, grade, composition, grain size, shape, and association of valuable and gangue minerals underpin the flotation response (Howarth and Rowlands, 1987; Bojcevski et al., 1998; Strohmayr et al., 1998;

Petruk, 2000; Johnson and Munro, 2008; Baumgartner et al., 2011; Johnson, 2016; McKay et al., 2016 etc.).

Figure 1.1: *Rise and fall of copper prices over the past five years. Available. [Online]: Infomine 5 year Copper prices (2019, September 30). http://www.infomine.com/investment/metal-prices/copper/5-year/*

A common theme arising from each of these studies is mineralogical characterisation through quantitative image analysis, whether rudimentary (Petruk and Schnarr, 1983) or more specialised (McKay et al., 2016); quantitative mineralogical data by means of image analysis forms a key component of process mineralogical studies (Becker et al., 2016; Lotter et al., 2017). Technological advancements in automated mineralogy over the last decade have expanded the capability of imaging systems to an extent that the relationship between the abovementioned mineral characteristics and flotation response can be studied at greater depths to further understand their interdependence (Baum et al., 2004; Lotter and Fragomeni, 2010; Ayling et al., 2012; Becker et al., 2016; Bradshaw et al., 2016; Lotter et al., 2017). These types of datasets have implications for how process mineralogy and geometallurgy will be pursued in the future (Gottlieb, 2008; Ehrig et al., 2012).

One such implication is that it is becoming increasingly apparent that mineralogy and elemental data can be used independently of flotation testing to constrain ore variability and infer process mineralogical relationships. However, the acquisition of quantitative mineralogy data is costly and time extensive. Therefore strides have been made to go beyond the use of quantitative mineralogy and develop elemental proxies which would allow the integration of routine elemental data (Baumgartner et al., 2011; Ehrig et al., 2012; Lamberg et al., 2013; Butler et al., 2016; Schouwstra et al., 2017). When considering the logical hierarchy in which field observations of drill core informs image analysis and image analysis informs the elemental proxy, elemental proxies can be used to predict process mineralogical parameters. Even though these process mineralogical parameters are inferred, they provide an early indication of

geometallurgical domains. This approach will be applied to a complex, polymetallic Cu-Pb-Zn-Ag deposit in this study.

The Aggeneys-Gamsberg Ore District (A-GOD) is situated within the arid Namaqualand region of the Northern Cape Province, South Africa. Since the early 20th century, the rock outcrops and sub-outcrops surrounding four inselbergs in this area have been the subject of mineral prospecting -, exploration - and mining activities (Stedman, 1980). Through continued drilling and prospecting, four deposits have been found of which three are in production. The A-GOD Zn-Pb-Cu-Ag base metal deposits are the biggest source of lead and zinc metal in Southern Africa (Ryan et al., 1986). The main ore producing deposit is reaching its life of miner (LOM); therefore, the focus will be shifting to a different Black Mountain Complex (BMC) deposit to sustain production for the foreseeable future (Deposit names are omitted here for confidentiality purposes). This deposit is typified as lower-grade, and it is mineralogically and texturally complex. These characteristics present several limitations to the successful extraction of economic mineral potential (Twidle and Engelbrecht, 1984). Amongst the various limitations are inconsistent grade and recovery trends that arise from the sequential flotation of this ore. Previous metallurgical projects carried out on this orebody have been aimed at resolving short term operating issues and have been inconclusive with regards to the identification of key process affecting mineralogical characteristics.

Mineralogical and textural characterisation of the deposit will be carried out on the primary and secondary lithological units. This data will be used to infer similarities in flotation responses of the economic sulphide minerals towards establishing mineral-based geometallurgical domains, prior to flotation testing. Bulk mineralogy, grain size distribution and quantitative textural data will be acquired by means of QEMSCAN and QXRD analysis and will be supplemented by batch flotation testing to validate the accuracy of the mineral-based approach to geometallurgical domaining. Similarities in mineralogical - and flotation characteristics will be reviewed as process mineralogical relationships. Ores with similar process mineralogical relationships will be considered as geometallurgical domains. Upon the establishment of the geometallurgical domains, potential elemental proxies will be reviewed to ascertain if the domains and their respective process mineralogical parameters can be integrated back into the geological block model for subsequent use in mining and metallurgical processing.

1.1.1. *Research Hypothesis*

Mineralogical knowledge of the BMC ores is obtained through geological logging of drill core and the chemical assay data of the economic portions of drill holes. Metallurgical knowledge of the BMC ores is obtained via flotation and hardness testing, and the subsequent chemical assay data resulting from this test work. Geological and metallurgical data are largely collected independently of one another and the inefficiency of this is evident in the unpredictability of the mineralogical issues that arise during metallurgical processing of the ore. However, if the geological and metallurgical data are integrated, then an increase in the processing efficiency of the deposit will result. If the relationship between ore mineral characteristics and their respective metallurgical response is understood, then it will be possible to define

geometallurgical domains based on mineralogy data without flotation testing. If the approach of defining geometallurgical domains using mineralogy is validated by flotation results, then the approach can be applied to other deposits and mines.

1.1.2. *Aims and Objectives*

To validate the above research hypothesis, the following objectives and key questions have been articulated:

1. To integrate geological and mineral processing response knowledge to define mineral-based geometallurgical ore domains.
    - What are key mineralogical and textural characteristics of each of the lithological ore types associated with the BMC ore?
    - Is it possible to group lithological ore types that are mineralogical and texturally variable?
    - Can the predicted minerals processing response of the grouped lithological ore types be used to define geometallurgical domains?

2. To validate the mineral-based Upper Orebody geometallurgical domain proposed in Aim 1 with flotation testing.
    - What are the differences in the flotation performance of the six secondary Upper Orebody lithological domains for copper, lead and zinc?
    - Why are the geometallurgical domains that are based on the flotation performance of the six secondary lithological ore types different from the geometallurgical domains based on the mineralogical characteristics of the five primary lithological ore types?

3. To integrate the mineralogical characteristics with the flotation responses of the Upper Orebody secondary lithological domains to establish actual geometallurgical domains
    - How will these geometallurgical domains behave in a processing circuit?
    - What is the potential for mineralogical or elemental proxies?

1.2. Sulphide Mineral Flotation

Sulphide mineral flotation is a well-established, highly specialised process that involves the physical separation of economic sulphide minerals (ES; chalcopyrite, galena and sphalerite), sulphide gangue minerals (SG; pyrrhotite and pyrite) and non-sulphide gangue minerals (NSG) in a water slurry when air is bubbled through the slurry in a mechanical flotation cell (Fig. 1.2) (Kawatra and Eisele, 2002; Lotter and Fragomeni, 2010). This process is highly versatile and can be applied to a wide range of sulphide ore types and ore sizes that might be resistant to alternative processes such as gravity – and magnetic separation. The separation process is dependent upon the ability of the hydrophobic mineral surfaces of ES minerals to selectively adhere to air bubbles (Kawatra and Eisele, 2002). Particles attached to the air

bubbles are transported to the surface of the slurry because of the buoyancy of the air bubbles and removed as a low-bulk concentrate defined by a high amount of the ES mineral. SG - and hydrophilic NSG mineral particles remain behind suspended in solution. ES minerals that are not recovered by froth flotation go to the tailings. When there is selectivity between ES, SG and NSG minerals and these are efficiently separated as previously explained, the process is considered true flotation (Kawatra and Eisele, 2002). The opposite of true flotation is entrainment, a process whereby certain SG and NSG minerals are suspended in the water trapped between bubbles or attached to ES, carried into the froth and recovered to the concentrate. There is no selectivity in entrainment, and thus all minerals are recovered (Kawatra and Eisele, 2002; Lotter and Fragomeni, 2010).

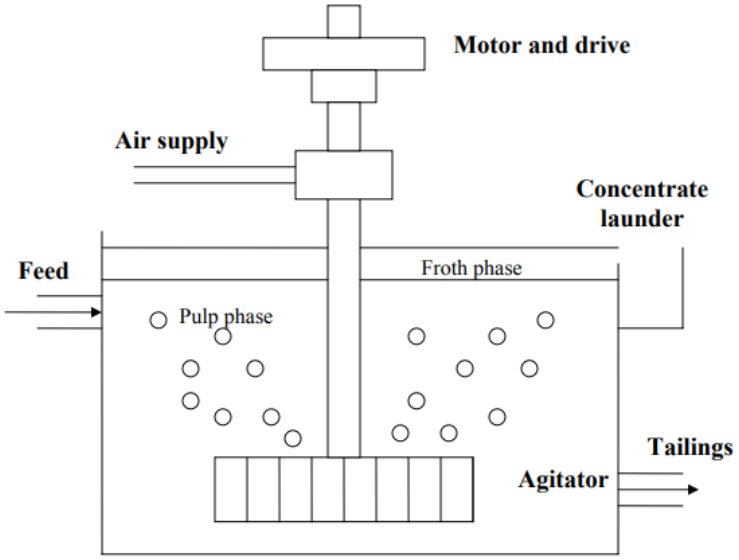

Figure 1.2: *Schematic illustration of a mechanical flotation cell. Taken from Kuan (2009).*

Depending on the nature of the mineralisation, the process is typically carried out either as sequential flotation wherein individual chalcopyrite, galena and sphalerite products are recovered in sequence, or as bulk flotation where chalcopyrite and galena are recovered as a product and sphalerite is recovered as a product (Petruk, 2000). Bulk flotation is generally less expensive than sequential flotation and thus more commonly used in base metal deposits devoid of silver. Because chalcopyrite, galena and sphalerite each behave distinctly during froth flotation, specialised reagents are often employed to temporarily or permanently modify the mineral surfaces to make them suitable for separation (Kormos et al., 2010; Lotter and Fragomeni, 2010; Bradshaw, 2014). This includes a combination of collectors, activators, depressants and frothers (See glossary). Common collectors for sulphide minerals are xanthates such as PAX (potassium amyl xanthate) or SEX (sodium ethyl xanthate). These compounds are highly selective between ES-SG minerals and NSG minerals, and facilitate the recovery of ES and SG minerals above the NSG minerals. Copper sulfate is typically used as an activator for sphalerite because it is a slow floating mineral. Cyanide is a common depressant for pyrite and sphalerite during

sequential flotation, whereas lime and sulphuric acid are very useful for stabilizing the pH during sulphide flotation (Twidle and Engelbrecht, 1984). A typical frother used in sulphide flotation are MIBC because it is more effective in fine-particle recovery than it is for coarse particle recovery (Kawatra and Eisele, 2002).

1.3. Geometallurgical Domains in Polymetallic Deposits

A geometallurgical domain is a single ore or a group of ores that are considered similar because of physicochemical characteristics that result in similar responses observed in metallurgical processing (flotation and milling) (Lotter et al., 2003; Fragomeni et al., 2005; Johnson and Munro, 2008). Geometallurgical domains facilitate the identification, quantification, characterisation and optimization of sulphide ore variability, and its respective minerals processing parameters (Gottlieb, 2008; Coward et al., 2009; Lund et al., 2013; Schouwstra et al., 2013; Lotter et al., 2017). This allows for targeted variability testing and the development of predictive models based on ore characteristics that can be integrated with geological block models (Fig. 1.3) to optimize the mining and processing of complex, polymetallic deposits. Such ore characteristics include alteration, grain size, texture, RQD, mineral grade, mineral type, metal ratios, hardnesses and grade-recovery curves etc. (Johnson and Munro, 2008; Lotter et al., 2017).

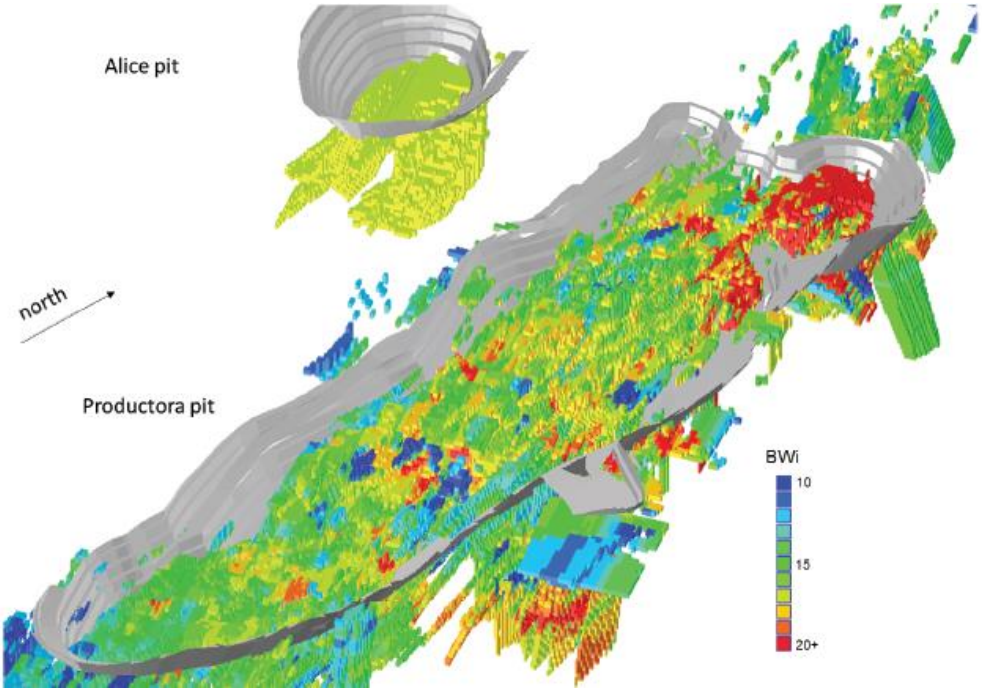

Figure 1.3: *A heat map of the Bond work index (BWI) values of the Productora Cu-Mo-Au deposit that have been integrated with the geological block model and pit design. Taken from King and McDonald (2016).*

Three key factors need to be considered prior to the establishment of geometallurgical domains. Firstly, to generate meaningful data that can be integrated back into the operation, representative samples need to be collected, either per lithology or geometallurgical domain. This will define a range of performance that can be expected from each of the geometallurgical domains. Secondly, care should be taken to

review the available geological data, in particular, ore characteristics that are known to affect metallurgical performance. Lastly, the number of domains should be practical to work with when validation testing is done (Johnson and Munro, 2008; Lotter et al., 2017).

1.4. Geological Setting

The Namaqua-Natal Metamorphic Province (NNMP) is a 1400 km long and 400 km wide mobile belt that wraps around the western and southern margins of the Archaean Kaapvaal Craton (Cornell et al., 2006). The NNMP stretches across from KwaZulu–Natal into the Northern Cape and across the border into Namibia (Fig. 1.4). Two sectors within the NNMP have been recognised: The Namaqua Sector and the Natal sector (Thomas et al., 1994). Mineral assemblages within granitic gneisses and sedimentary supracrustal rocks of the Namaqua Sector indicate Mesoproterozoic ages and low pressure – high-temperature amphibolite to granulite facies metamorphism associated with multiple phases of deformation (Thomas et al., 1994; Cornell et al., 2006; Macey et al., 2014). Key geographical differences in these metamorphic characteristics along with definitive structural and geochronological traits see the Namaqua Sector subdivided into the Richtersveld Subprovince (Vioolsdrift and Pella Terranes), the Bushmanland Subprovince, the Gordonia Subprovince (Kakamas/ Grünau Terrane), the Kheis Subprovince, Areachap and Kaaien Terranes (Hartnady et al., 1985; Thomas et al., 1993, Cornell et al., 2006; Macey et al., 2014) (Fig. 1.4).

The Bushmanland Subprovince is the largest of these subprovinces and its geographic extent is subdivided into several thrust-bound terranes differentiated based on stratigraphic and tectonic similarities (Cornell et al., 2006). These include the Okiep -, Aggeneys -, Grünau -, Pofadder -, Steinkopf - and Bladgrond Terranes (Colliston et al., 2012). Subsequently, the Wortel Formation, the Witputs Formation, the Skelmpoort Formation, the T'hammaberg Formation, the Hotson Formation and the Koeris Formation presented in Schoch et al. (1987); Colliston et al. (2012) and Cornell et al. (2006) define the Aggeneys Terrane, which is key to this study.

Distributed across and within the tectonostratigraphic formations mentioned above are generalized horizons that outcrop throughout the A-GOD. These are the Augen Gneiss formation followed upward by the Pink Gneiss formation, the Aluminous Schist formation, the White Quartzite formation, the Aggeneys Ore Formation/ Gams Member – and the Amphibolite and leucocratic Grey gneiss horizons (Rozendaal, 1975; Lipson, 1978, 1990; SACS, 1980; Ryan et al., 1986; Strydom, 1986; Schoch et al., 1987; Rudnick, 2016). The nomenclature of the stratigraphy relating to the A-GOD has been widely debated (Table 1.1). For the purpose of this study, the stratigraphy proposed by Rudnick (2016) is followed.

1.4.1. *Aggeneys-Gamsberg Ore Distinct (A-GOD)*

The Aggeneys Ore Formation hosts four economic Broken Hill-type base metal sulphide deposits arranged in a 10 x 30 km area (Rozendaal, 1975; Lipson, 1978, 1980; Ryan et al., 1986; Rudnick, 2016). The orebodies are arranged as a complex ridge system striking northeast to southwest (Fig. 1.5) (Neufeld,

2005). Economic metals intersected are Zn, Pb, Cu and Ag. Mineralization styles range from a Cu-Pb-Ag zonation in the west to a central Cu-Pb-Zn-Ag rich zonation and a Zn-Pb zonation in the east (Stedman, 1980; Rozendaal, 1975, 1982; Lipson, 1978, 1980; Ryan et al., 1986). The A-GOD base metal ore bodies are constrained within isoclinal fold closures that resulted from the main episode of deformation accompanied by upper amphibolite - lower granulite facies metamorphism (P-T conditions of 630 to 670 ºC and 2.8 – 4.5 Kbar respectively) (Rozendaal, 1975; Macey et al., 2014). Ore host rocks comprise a combination of heterogeneous chemically distinct metamorphosed chemical exhalites, including barite and manganese-rich iron formations and bedded major sulphide horizons that overlie mineralised metapelitic rocks (Lipson, 1978; Rozendaal, 1975; Ryan et al., 1986: Rudnick, 2016).

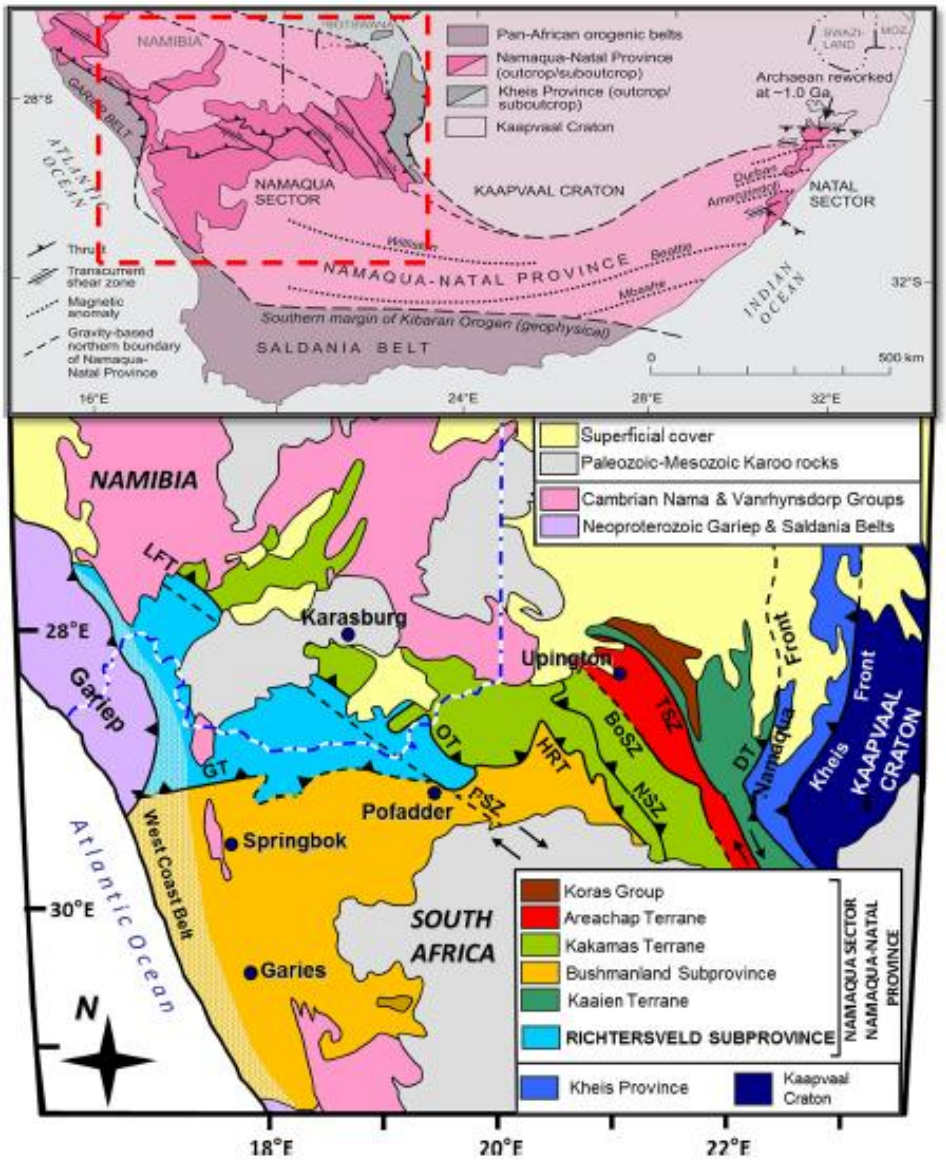

Figure 1.4: *Tectonostratigraphy of the Namaqua-Natal Metamorphic Province and subordinate subprovinces and terranes. Taken from Macey et al. (2017). GT: Groothoek Thrust; OT: Onseepkans Thrust; PSZ: Pofadder Shear Zone; VSZ: Vogelstruislaagte Shear Zone; HRT: Hartbeest River Thrust; BoSZ: Bovenrug Shear Zone; BBSZ: Brakbos Shear Zone; DT: Dabep Thrust; TSZ: Trioolapspan Shear Zone , NSZ: Neusberg Shear Zone.*

Table 1.1: *Tectonostratigraphic comparison of the hierarchy in the Aggeneys subgroup and the nomenclature proposed by previous works. Taken from Rudnick (2016)*

Rozendaal (1975)		Lipson (1978, 1990)		SACS (1980)	Ryan et al (1986)	Strydom (1986)		Schoch et al (1987)		McClung et al (2006)		Rudnick (2016)	
Formation	Member	Formation	Unit			Formation	Unit	Formation	Member	Subgroup	Formation	Subgroup	Formation/ Unit
Nousees Mafic Gneiss	Amphibolite Schist & Conglomerate	Grey Gneiss		Quartz-Muscovite Schist & Conglomerate	Amphibolite & Leucocratic Grey Gneiss			Koeris			Koeris		(Koeris Fm) *not present*
Gams Fm	C Member	Shaft Schist	Lower Footwall Schist	Gams Fm	Aggeneys Ore Fm	Soutkloof	Spring schist (not developed)	Hotson	Gams	Kouboom	Spring Schist	Kouboom	Gams Fm
			Upper Footwall Schist								Soutkloof		
	B Member	Ore Schist Ore Equivalent Schist	Lower Orebody				Sulphide-hosting rocks				Gams		
			Intermediate Schist										
			Upper Orebody										
	A Member		Hangingwall Schist										
Pella Quartzite	Dark Quartzite	Broken Hill Quartzite	Dark/Lower Quartzite	Metaquartzite Unit	White Quartzite Fm	Kouboom	Diamictcte Schist Grey & blue quartzite		Kouboom		Broken Hill Quartzite		Dark Quartzite
	Pelitic Schist		Median Schist				Schist		Schist	Wortel	Bloemhoek	Wortel	Aluminous Schist
	White Quartzite		White/Upper Quartzite			Zuurwater (removed)	White quartzite		Quartzite		Pella Quartzite		(White Quartzite) *removed*
Namies Schist		Namies Schist		Namies Schist	Aluminous Schist Fm		Qtz-bt-sill schist		Schist		Namies Schist		(Namies Schist) *removed*
Haramoep Gneiss		Basal Gneiss		Hoogoor Gneiss	Pink Gneiss Fm	Augen gneiss		Quartz-feldspar Gneiss		Hoogoor Gneiss		Pink Gneiss	
				Aroams Gneiss	Augen Gneiss Fm			Augen Gneiss		Achab Gneiss		Augen Gneiss	

unconformity

tectonic contact

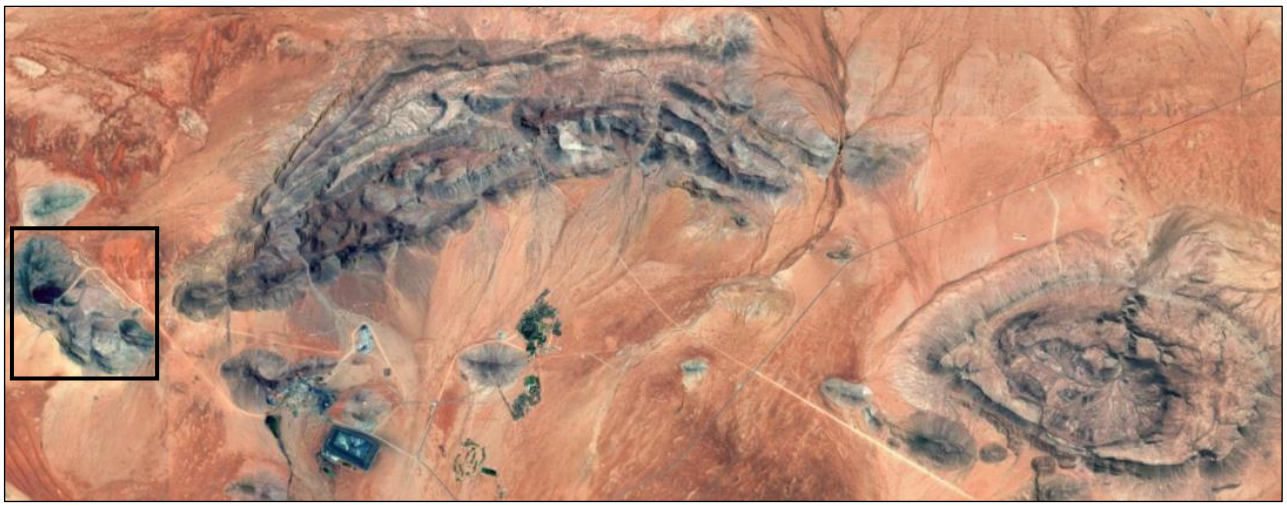

Figure 1.5: *The Aggeneys-Gamsberg Ore District illustrating the surface expressions of the four-polymetallic deposits. The study area is indicated by the black square.*

The study area comprises the westernmost part of the A-GOD base metal deposits (Fig. 1.5). On the surface, it is easily recognised because of its distinctive black colour (Stedman, 1980). The deposit is situated within a major recumbent isoclinal synformal fold in which the economic resource is structurally enclosed within the core of the fold. Four subdivisions are recognised: The Upper Orebody (UOB), the Lower Orebody (LOB), the Magnetite Barite zone (MBZ) and the Garnet Quartzite halo (GQZ) (Ryan et al., 1986).

Correlation between the lithostratigraphy proposed in previous works remains ambiguous, as is seen in the lithostratigraphic comparison (Stedman, 1980; Strydom, 1986; Ryan et al., 1986; Neufeld, 2005, Rudnick, 2016) (Table 1.2). For this study, the stratigraphic and mineralisation literature review is a summary of the works of Stedman (1980), Ryan et al. (1986) and Rudnick (2016) (Fig. 1.6)

As a result of polyphase deformation, the deposit is isoclinally folded and orientated in a recumbent position (Stedman, 1980; Fig. 1.7). Because of this, the succession contained within the upper limb of this fold is overturned and the stratigraphy reversed. Thus, the basal unit both overlies and underlies the sequence at the top, followed downward by the inverse of the stratigraphic profile (Stedman, 1980; Ryan et al., 1986; Rudnick, 2016) (Table 1.2). From top to bottom, the stratigraphic sequence of the deposit consists of Augen – and pink gneiss that are crosscut by metamorphic anatexites (leptite and amphibolite). Following downward, the start of the economic sequence is capped by the GQZ, which contains vitreous garnetiferous quartzites (GQ). Wherein contact with neighbouring schists due to top thrusting, the GQZ inherits a weakly developed foliation to form garnet schist. This unit forms an alteration halo around the lower-lying UOB. The protolith to the GQZ is considered the original sedimentary succession within the continental basin on top of which the metalliferous hydrothermal fluids of the UOB were deposited. The resulting GQZ is thus a testament to the hydrothermal alteration following the interaction between the country rocks and hydrothermal fluids that has subsequently been isoclinally folded around the overlying chemogenic following deformation (Stedman, 1980; Rudnick, 2016) (Fig. 1.7).

Table 1.2: *Lithostratigraphic comparison of the previous works done on the deposit focussed on during this study. Taken from Rudnick (2016)*

<table>
<tr><th>Stedman (1980)</th><th colspan="2">Strydom (1986)</th><th colspan="2">Ryan et al (1986)</th><th>Neufeld (2005)</th><th colspan="2">Rudnick (2016)</th></tr>
<tr><td rowspan="2">Magnetite barite rock
Magnetite amphibolite
Magnetite barite rock</td><td rowspan="2">Soutkloof Fm</td><td>Spring Schist</td><td colspan="2"></td><td rowspan="2">Iron formation and quartzite: amphibole- and quartz-magnetite; garnet- and/or magnetite-quartzite; ferrugenous schist; magnetite barite</td><td colspan="2">Gneiss (AG and PG), Leptite (L)</td></tr>
<tr><td>Sulphide-hosting rocks</td><td rowspan="5">Aggeneys Ore Fm</td><td>Lower ore body</td><td rowspan="2">GQZ and UOB</td><td>Quartzitic schist (QS) ±Mgt ±grt
Quartzitic schist (QS) + bar±mgt±grt
Magnetite rich rocks (QM and AM)</td></tr>
<tr><td rowspan="4">Mixed unit (schist, local garnet quartzite)</td><td rowspan="3">Kouboom Fm</td><td>Diamictite</td><td>Baritic quartz schist</td></tr>
<tr><td>Schist</td><td>Magnetite-barite rock</td></tr>
<tr><td rowspan="2">Grey to blue quartzite</td><td>Magnetite amphibolite</td></tr>
<tr><td rowspan="2">Quartzite</td><td>Magnetite quartzite</td><td>MBZ</td><td>Banded rock (BAND)
Baritic Quartzite (BQ)
Magnetite Barite (MB)</td></tr>
<tr><td rowspan="2">Aluminous schist</td><td>schist</td><td colspan="2" rowspan="3">Banded quartz schist</td><td>Upper schist conglomerate fm</td><td rowspan="4">LOB</td><td rowspan="4">Dark Quartzite (DQ)
Sulphidic pelitic schist (MixS)
Pelitic schist and quartzite (MixQ)</td></tr>
<tr><td rowspan="3"></td><td rowspan="3">Zuurwater Fm (absent from study area due to thrusting)</td><td rowspan="3">White quartzite, qtz-bt-sill schist</td><td>Upper dark quartzite fm</td></tr>
<tr><td>Lower schist conglomerate fm</td></tr>
<tr><td colspan="2">White quartzite</td><td>Lower white quartzite fm</td><td colspan="2">Median Schist (MS)</td></tr>
<tr><td>Pink gneiss</td><td colspan="3" rowspan="3">Augen gneiss</td><td colspan="2">Aluminous Schist</td><td>Aluminous schist fm</td><td colspan="2">White quartzite (WQ)
Aluminous schist (AS)</td></tr>
<tr><td>Calc-silicate rock</td><td colspan="2">Pink gneiss</td><td rowspan="2">Basement gneiss</td><td colspan="2">Pink gneiss (PG) and Leptite (L)</td></tr>
<tr><td>Grey augen gneiss</td><td colspan="2">Augen gneiss</td><td colspan="2">Augen gneiss (AG)</td></tr>
</table>

The UOB consists of magnetite quartzite (QM), amphibole magnetite quartzite (AM) and garnet magnetite quartzite (GM). The QM tectonically encloses the AM on both the hanging – and footwall side, whereas the GM has a gradational contact with the AM on the footwall of the core of the fold. The lower limb of the GQZ follows on after the footwall QM unit (Stedman, 1980; Rudnick, 2016) (Table 1.2).

The succeeding MBZ is a variable succession that consists of magnetite barite closest to the overlying UOB and grades into massive barite, baritic quartzite and banded quartz-iron oxide-barite-garnet-muscovite rock closest to the LOB. Strongly banded garnet magnetite also occurs along with the contact with the overlying UOB. The LOB defines the lower contact of the economic zone. The LOB is defined by a variable succession of dark quartzite, sulphidic pelitic schist (MC) and sulphidic pelitic quartzite (SQ). Below the LOB, the Median Schist, White Quartzite, Aluminous Schist, Pink Gneiss (with associated Leptite and Amphibolite) follows down to the basal augen gneiss. In conjunction with the stratigraphic profile being duplicated along strike by isoclinal folding, and top thrusting, the stratigraphic sequence is also duplicated down dip by thrusting in the following order: gneiss – schist – quartzite – schist and ore formation (Stedman, 1980; Rudnick, 2016) (Table 1.2; Fig. 1.6).

For this investigation, the following units containing economic sulphide mineralisation are reviewed in detail in the following section: the GQ (GQZ), the AM and QM (UOB), and SQ and MC (LOB).

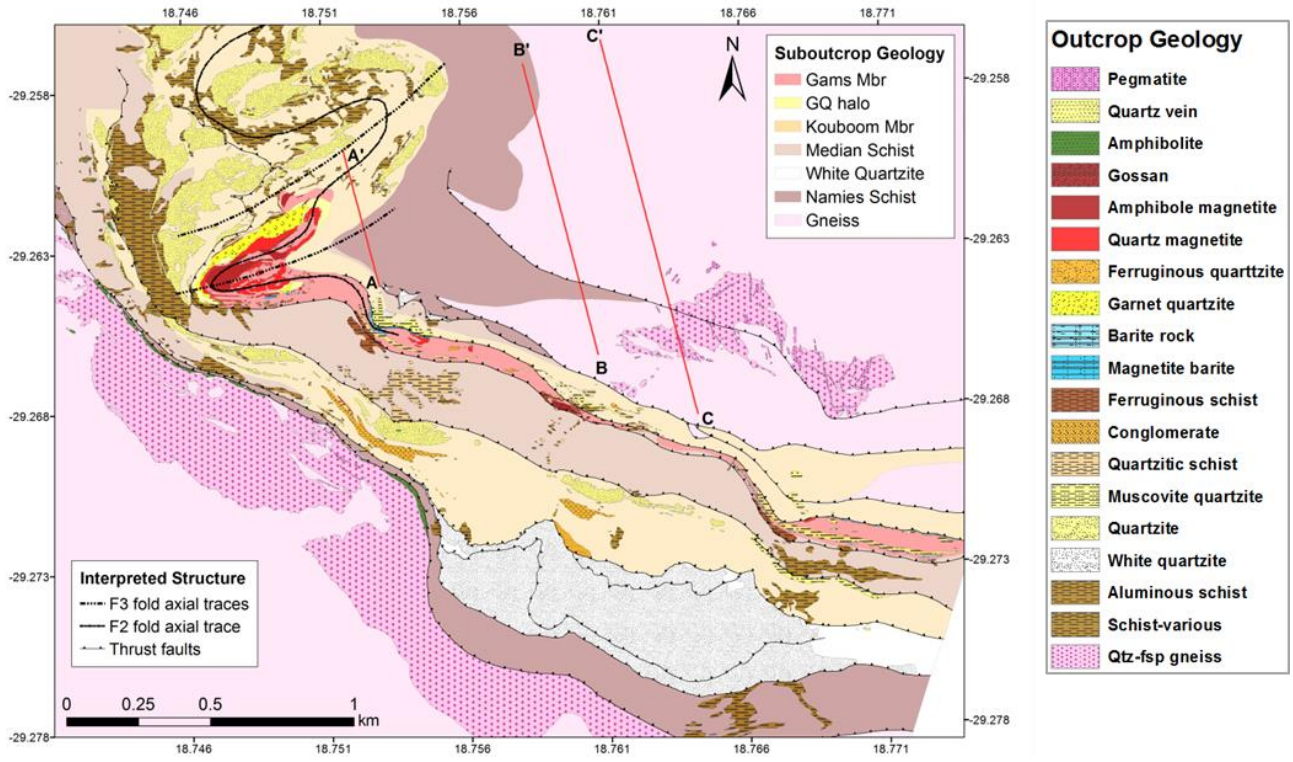

Figure 1.6: *Geological map of the deposit indicating the tectonostratigraphy. Taken from Rudnick (2016). The line A-A' illustrates a simplified cross-section of the deposit (Fig. 1.7).*

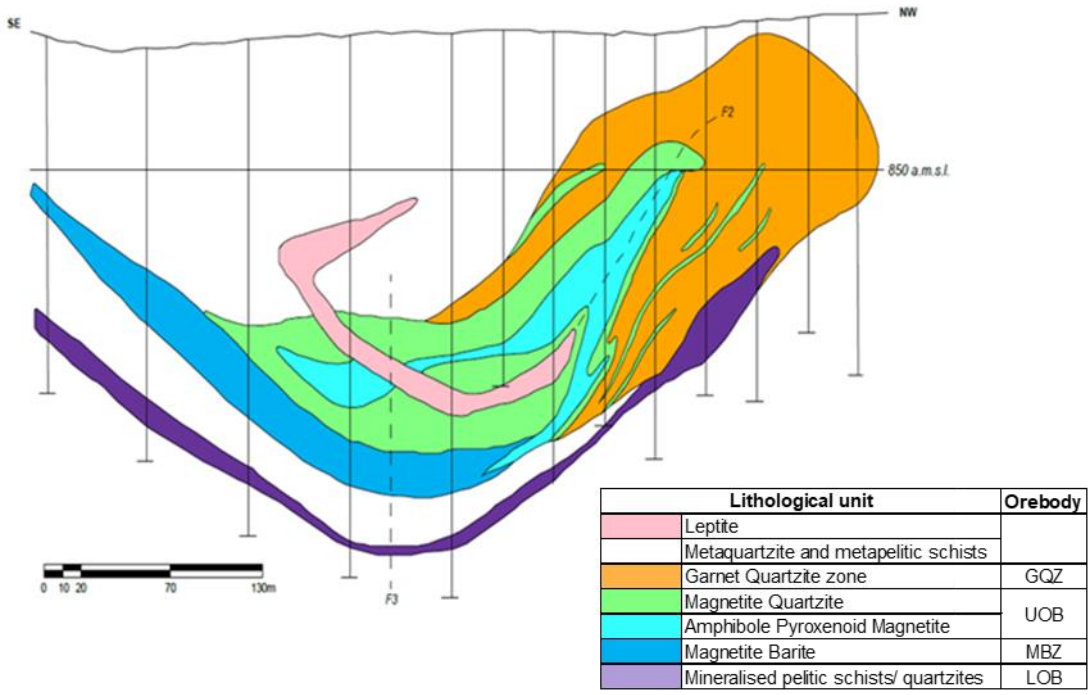

Figure 1.7: *A simplified cross-section of the deposit indicating the spatial relationship of the GQZ, UOB, MBZ and LOB orebodies to one another. Taken from a 2000 unpublished internal company report.*

1.4.2. ***Mineralisation***

1.4.2.1. *The Garnet Quartzite halo (GQZ)*

Coarse-grained quartz is highest in abundance (~80%), followed by almandine garnet and biotite in lesser amounts. Accessory minerals such as gahnite, cordierite or sillimanite have been encountered. Chlorite occurs as a retrograde product of biotite. Magnetite occurs sporadically dispersed in the GQ and decreases away from the UOB where it grades into vitreous garnet quartzite and garnet schist. Where in contact with the UOB, this unit is predominantly known for a metal zonation pattern of coarse-grained chalcopyrite-pyrite that progressively grades into the metal zonation pattern of chalcopyrite-galena-pyrrhotite of the UOB. Trace amounts of galena and sphalerite are noticed in the GQZ (Stedman, 1980; Ryan et al., 1986; Rudnick, 2016).

The protolith to the GQZ is believed to have undergone a strong hydrothermal overprint that subsequently formed a semi-concordant halo around the UOB following the precipitation of the UOB economic metals and their interaction with the country rocks and subsequent isoclinal folding (Stedman, 1980; Rudnick, 2016). Texturally the GQ is defined as massive or granoblastic with indistinct banding seen in the core (Fig. 1.8A). Closer to schistose contacts, the rock displays a gradational contact and inherits a distinct foliation defined by the neighbouring schist. The mineral assemblage here includes garnet, quartz, k-feldspar, sillimanite, muscovite, biotite and magnetite. Texturally, the garnet quartz schist is semi-massive due to the higher abundance of quartz; however, a schistosity within the rock is often defined by muscovite, biotite and sillimanite. The finer garnet minerals segregate into microbands whereas the

coarser garnets form poikiloblasts enclosed by biotite rims (Stedman, 1980, Ryan et al., 1986; Rudnick, 2016).

1.4.2.2. *The Upper Orebody (UOB)*

The UOB is a highly variable mixed clastic-chemogenic unit. This variability is expressed as distinct lithological -, textural -, mineralogical - and elemental zonation patterns that occur from the core of the isoclinal fold to the limbs. The UOB is defined by magnetite-rich iron formations that include a Magnetite Quartzite (QM) unit that encompasses a central Amphibole Magnetite Quartzite unit (AM). Sporadic Garnet Magnetite Quartzite (GM) is commonly also associated with the AM. Where present, these are defined by a gradational contact, whereas the QM-AM contact is characteristically sharp. Away from the core of the isoclinal fold, the iron formations grade into ferruginous quartzites and schists. The QM and AM are the only lithological units that have sufficient economic mineralisation, however, the extent and textural nature of the mineralization differs within each unit (Stedman, 1980; Ryan et al., 1986; Rudnick, 2016).

(a) Magnetite Quartzite (QM)

Quartz and Magnetite together account for approximately 70 – 100% of the mineralogy, however, magnetite often reaches massive proportions (>75 wt. %). Accessory minerals (barite, almandine – spessartine garnet, biotite, chlorite and apatite) make up the remaining portions. Trace amounts of ilmenite, hematite, amphibole, muscovite, sillimanite, gahnite and zircon have also been encountered. The QM accounts for the bulk of the Cu-Pb-Zn-Ag metal mined. Chalcopyrite is the dominant ES mineral; however, copious amounts of galena are also encountered. Pyrite is the dominant GS mineral. Texturally the QM displays a compositional banding (composed of layers of variable thicknesses) of medium to coarse-grained, equigranular magnetite (Fig. 1.8B). On the contact of the QM and AM, within the hinge, this compositional banding is almost completely overprinted by remobilized galena (Stedman, 1980; Ryan et al., 1986; Rudnick, 2016).

Four secondary end-member lithologies are recognised within the Magnetite Quartzite based on metal zonation: The normal QM end-member (QM; Fig. 1.9F), the High Cu end-member (QM high Cu, Fig. 1.9A) and the High Zn end-member (QM High Zn; Fig. 1.9B) and the Sulphidic Quartz Magnetite (S-QM; Fig. 1.9C). The S-QM end-member is characterised by a massive to banded stratiform lens of coarse-grained galena and sphalerite often reaching massive sulphide concentration. The S-QM unit is mostly present at the contact between the QM and AM. The high-Cu end-member is defined by variable grain sizes of chalcopyrite and accompanies the S-QM end-member on the hanging wall to the GQZ. Characteristically the QM Cu texture ranges from finely banded to disseminated sulphide minerals. The high-Zn end-member is predominantly lens-like and massive (Steinmann, pers. comm, 2016).

(b) Magnetite Amphibolite (AM)

Within the Magnetite Amphibolite unit, or the renamed Amphibole Pyroxenoid Magnetite unit (APM) (Rudnick, 2016), magnetite (in excess of 60 %) and cummingtonite-grunerite (in excess of 10 %) are the dominant phases with pyroxmangite, quartz, hedenbergite, spessartine garnet, fayalite and apatite present in lesser amounts. Trace amounts of chlorite, sillimanite and chlorite have also been encountered. AM varieties that commonly rich in pyroxmangite are typically poor in quartz. Dominant economic ore minerals are chalcopyrite and sphalerite (Stedman, 1980; Ryan et al., 1986; Rudnick, 2016).

Texturally, towards the QM contact, the AM displays both fine micro banding and coarse compositional banding defined by well-oriented grunerite, magnetite, quartz and pyroxmangite (Fig. 1.8C). This association often includes sulphide minerals. Within the core of the fold, the original fabric is destroyed resulting in a massive fabric defined by magnetite or pyroxenoid. Therefore, two subordinate AM end-member lithologies are recognised, the foliated AM end-member (Fig. 1.9D) and the non-foliated AM end-member (Fig.1.9E). Towards the MBZ, the modal mineralogy consists of dominant grunerite with subordinate spessartine and a decrease in magnetite and pyrrhotite. The dominant ore mineral here is galena (Stedman, 1980; Ryan et al., 1986; Rudnick, 2016).

1.4.2.3. *The Lower Orebody (LOB)*

Variability in the LOB is expressed in mineral assemblages and textures. The extension of the LOB around the UOB is seen as being obscured by the GQZ, however, it appears to follow the same trend of the UOB and GQZ, albeit in an altered form. The LOB is defined as well-bedded, narrow (22-50 m), and discontinuous in which the morphology of the mineralised portion is lens-like. The LOB consists predominantly of sulphide-rich metasedimentary units that include Mineralized aluminous quartzitic schists (MC) and Sulphidic Quartzites (SQ) that contain economic galena and chalcopyrite with sporadic sphalerite. Metal zonation patterns of the LOB indicate Pb>Ag>Cu>Zn. The mineralized aluminous quartzitic schists often reach massive sulphide concentration, whereas sulphidic quartzite is poorly mineralized in most cases. Down plunge, the Pb and Zn grades decrease, whereas Cu increases (Stedman, 1980; Ryan et al., 1986; Rudnick, 2016).

(a) Sulphidic Quartzite (SQ)

The SQ is a quartzitic to weakly schistose rock type that is considered a mixed quartzite (Rudnick, 2016). The SQ has highly variable mineralogy that includes quartz, barite, gahnite, garnet and biotite. Muscovite, chlorite, sillimanite, sericite and magnetite are subordinate minerals. Trace minerals include apatite, rutile, zircon, ilmenite, fluorite and monazite (Rudnick, 2016). This unit is often seen grading into gahnite quartzite and muscovite-magnetite where abundant amounts of gahnite and muscovite-magnetite are present (Rudnick, 2016). Texturally this unit is massive, however weakly developed compositional banding has been observed (Rudnick, 2016) (Fig. 1.8D).

(b) Mineralised schist (MC)

The MC is defined by a higher amount of muscovite and biotite that defines its strongly foliated texture (Rudnick, 2016) (Fig. 1.8E). Similar to the SQ, this unit is also significantly mineralogically variable. Muscovite, biotite, sillimanite and gahnite define the bulk mineralogy; however, the presence of economic mineralisation in pyrite-rich lenses is also a characteristic feature. Hyalophane is a common subordinate mineral (Rudnick, 2016). Pyrite is dominant with subordinate galena and sphalerite, and traces of chalcopyrite. This unit often reaches massive sulphide character (Ryan et al., 1986). Barite often occurs in concentrations reaching approximately 40%.

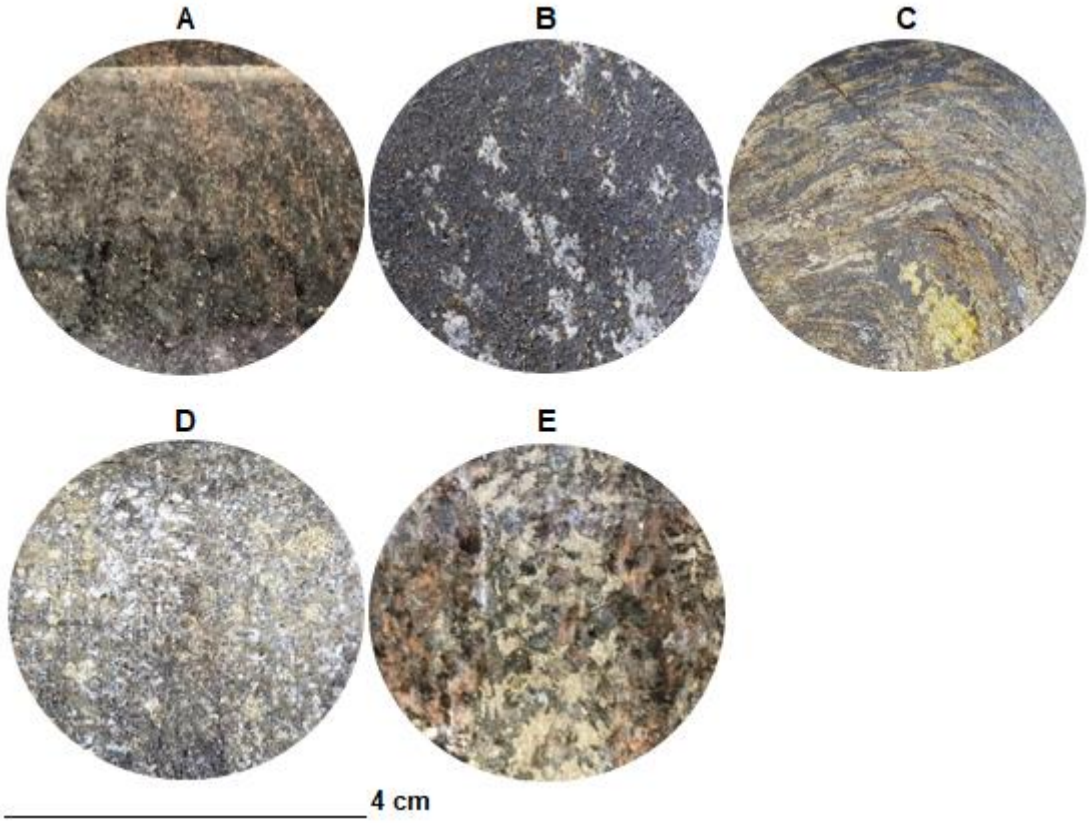

Figure 1.8: *Primary lithological ore types of the deposit (a). Garnet Quartzite, (b). Quartz Magnetite, (c). Amphibole Magnetite, (d). Sulphidic quartzite and (e). Mineralised schist*

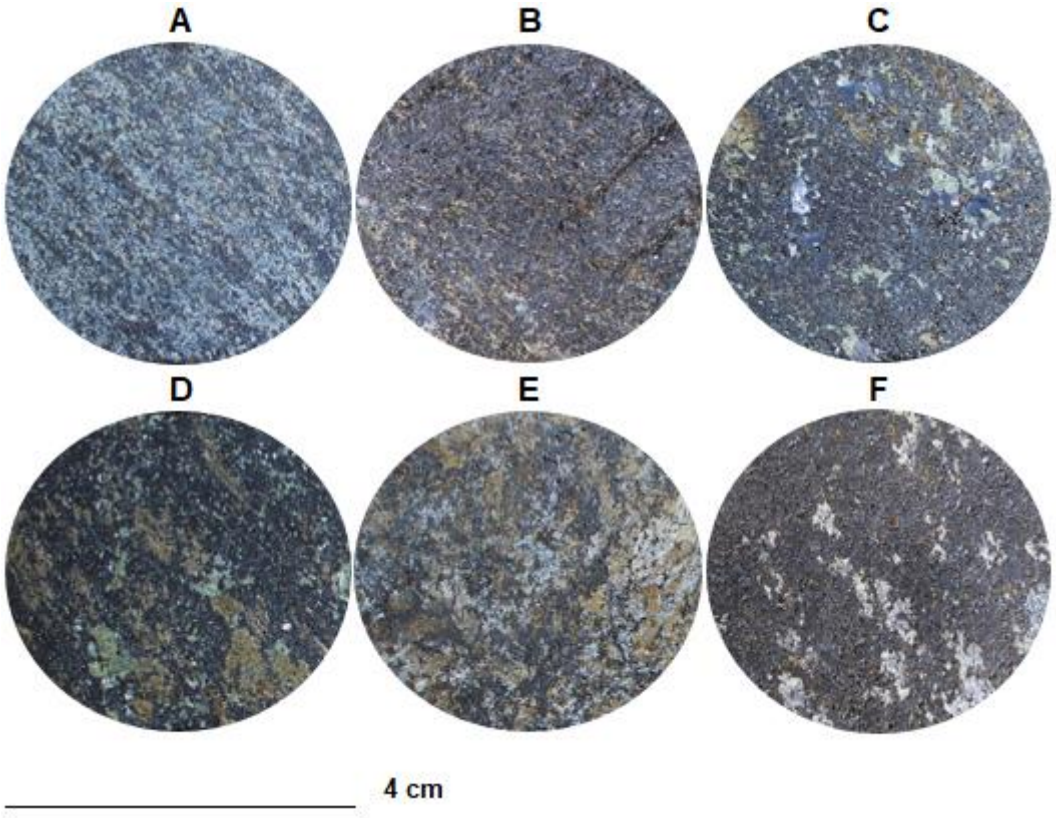

Figure 1.9: *Secondary lithological ore types of the Upper Orebody (a). QM Cu end-member, (b). QM Zn end-member, (c). S-QM end-member, (d). AM Foliated end-member, and (e). AM Non-foliated end-member and (f) conventional QM end member*

1.5. Thesis structure

This thesis consists of four chapters, of which Chapters Two and Chapter Three are written as manuscripts. Chapter Two is published as an extended conference proceeding for the SAIMM (South African Institute of Mining and Metallurgy) and Chapter Three is submitted to Minerals Engineering for review.

Chapter 1: This chapter provides background and geological context to the problem statement, aims and objectives of this study along with supporting literature on flotation and geometallurgical domains, the main topics that will be addressed in the ensuing chapters.

Chapter 2: This deals with the mineralogical and textural quantification of the primary lithological ore types of the deposit. Using the bulk mineralogy grain size distribution, textural characteristics and literature available in the public domain to propose mineral-based/ early-stage geometallurgical domains.

Chapter 3: This chapter deals with the validation of the magnetite-dominated mineral-based/ early-stage UOB domain proposed in Chapter 2. Six samples representing the mineralogical and textural variability of the magnetite-dominated domain were subjected to milling and flotation testing to confirm whether the mineralogical and textural variability identified in Chapter 2 can be constrained by a single geometallurgical domain. Based on size-by-size mineralogy-, milling and flotation data generated during

this work, an elemental proxy is suggested, through which the now established process mineralogical relationship can be integrated back into the geological block model.

Chapter 4: This chapter summarises the work conducted in this project by answering the aims and objectives through the now established process mineralogical relationships. This chapter also provides recommendations for dealing with problematic ores and proposes future topics that will contribute to the current geometallurgical understanding.

CHAPTER 2: Using mineralogy for early-stage geometallurgical domain definition: A case study of a polymetallic sulphide deposit

Publication Note - This chapter has been published as follows:

***Gordon, H.J.J**, Miller, J.A. and Becker, M. 2018. Using mineralogy for early-stage geometallurgical domain definition: A case study of the Swartberg polymetallic sulphide deposit. In Proceedings: The South African Institute for Mining and Metallurgy (SAIMM), Geometallurgy Conference, pp. 121-131. 6-8 August 2018, Cape Town, South Africa.*

***Candidate contribution:** The candidate contributed 70 % to the conceptualisation of the early-stage geometallurgical domain approach presented in this work and 80 % to the data analysis and writing of this manuscript.*

Stylistic changes have been made to ensure consistency of formatting throughout the thesis but the contents is unchanged. Refer to Appendix I for original publication.

Abstract

The deposit, Northern Cape Province, South Africa, is a low-grade, polymetallic base metal sulphide deposit. Reworking during the Namaquan Orogeny generated complex mineralogical and textural variability in the deposit. This variability is expressed through several different geological ore 'types' defined on texture and mineralogy. However, it is not clear how this petrographic definition of ore 'type' relates to the processing response of each ore type. In order to clarify the linkages between ore type defined geologically and ore type defined metallurgically, this study re-evaluates the geologically defined ore types by reviewing the silicate, oxide, and sulphide mineralogy, grain size, and mineral associations for each. Ore textures manifest as intricate intergrowths of sulphide, silicate, and oxide minerals, and are problematic for metallurgical processing, resulting in poor copper recovery. The geological ore types are then reclassified as distinct early-stage geometallurgical ore types on the basis of gangue mineralogy, copper mineral grain size distribution, and gangue mineral associations. The results have important implications for establishing controls on ore variability regarding mineral processing performance, and which mineralogical parameters ideally need to be incorporated when building a geometallurgical block model for the deposit.

Keywords: Polymetallic, block model, mineralogy

2.1 Introduction

The growth in demand for copper, lead, zinc, and silver, coupled with high base metal prices, is driving the need for more efficient extraction of larger metal tonnages (Bradshaw, 2014; Rosenkranz and Lamberg, 2014). At the same time, known high-grade, large-tonnage deposits are being depleted, causing mining companies to invest in the development of complex, lower-grade deposits. Ore variability in these types of deposits presents one of the most significant processing challenges (Lotter et al., 2017). Variability in mineralogy, mineralization style, grade, grain size, alteration, gangue mineral association, and the spatial arrangement of these characteristics within ores presents a limitation to metallurgical extraction, and hampers the development of these deposits (Lotter et al., 2011, 2017; Bradshaw, 2014; McKay et al., 2016a). The Pb-Zn ores of the Mount Isa deposit, Australia (Johnson, 2016) and the Zn-Pb-Ag-Ba ores of the Red Dog deposit, Alaska (McKay, Sztuke, and Lacouture, 2016b) are world-class examples illustrating the extent of such challenges. The block modelling of geometallurgical response variables, along with qualitative resource information, provides a new direction for proactive decision-making. This is especially so in an economic climate where financial sustainability of mining operations requires mitigation of mineralogical and metallurgical uncertainty (Coward et al., 2009; Lamberg, 2011, Sepulveda et al., 2015)

The Aggeneys-Gamsberg ore district (A-GOD) in South Africa's Northern Cape Province is a 10 × 30 km area known to host four polymetallic, sedimentary-exhalative and Broken Hill-type deposits in mid-Proterozoic metasediments (Bailie, Armstrong, and Reid, 2007; Rudnick, 2016). The westernmost portion of the A-GOD, forms the focus of this study. The metal distribution within the deposit follows the decreasing order of lead>zinc>copper>silver as disseminated, stratiform and recrystallized lead (galena), zinc (sphalerite), and copper sulphides (chalcopyrite and bornite) contained within an enclosing isoclinal fold nappe (Stedman, 1980). Two distinct stacked orebodies, the Upper (UOB) and Lower (LOB) orebody define the centre of the fold nappe, with an alteration halo, the garnet quartzite zone (GQ), defining a third orebody, encompassing the UOB and LOB (Ryan et al., 1986; Rudnick, 2016). Ore textures manifest as intricate intergrowths of sulphide, oxide, and silicate minerals, resulting in poor copper recovery during metallurgical processing. This has led to the recognition that established mineralogical end-member characteristics for the deposit as applied to processing have not yet been quantified on a geometallurgical end-member level.

This paper examines the current lithological domains as distinct early-stage geometallurgical ore types based on gangue mineralogy, copper mineral grain size distribution, and gangue mineral associations found within the main and down-plunge resource. A review of the mineralogical variability will have implications for constraining fixed boundaries between geological ore types, establish controls on ore variability regarding flotation performance, and identify which mineralogical parameters need to be incorporated when building a geometallurgical block model for the deposit. This paper focuses on attributes relevant to the copper flotation circuit. Characteristics relevant to the lead and zinc circuits will be addressed in a subsequent paper (Gordon et al. submitted).

2.2 Geometallugical Block Domaining

2.2.1 *Model Input*

A geometallurgical block model is a multivariate extension of a conventional 3D geological block model based on both geological and metallurgical data (Lotter et al., 2017). This model utilizes a combination of subordinate models, of which, focus is placed on developing mineralogical and metallurgical trends that are consolidated to display geometallurgical domains in a block-by-block, 3D spatial context (Coward et al., 2009; Lamberg, 2011; McKay et al., 2016a). Viewing orebodies by means of such domains defines the metallurgical variability and contributes toward the development of more robust mining and processing approaches (e.g., Butler et al., 2016; King and McDonald, 2016; Liebezeit et al., 2016). The geometallurgical programme as defined by Lamberg (2011) is based on joint input from three subordinate models that link geology and metallurgy through the consideration of minerals and particles: the geological model, particle breakage model, and the process model. The geological model provides quantitative mineralogical and textural information per ore block. The particle breakage model forecasts the resultant particle properties from the breakdown of different ore blocks, and the unit process model forecasts how particles will respond in a unit process. The combination of these three models feeds quantitative data into the geometallurgical model.

2.2.2 *Model Considerations*

This synergy between mineralogy and mineral processing starts with representative sample material regarding the type, size, and quantity of minerals (Lotter et al., 2017). A successful geometallurgical programme requires that the sampling strategy for the major domains within a deposit on which testing is conducted should be designed in accordance with the mineralization type (Coward et al., 2009). This ensures statistically sound chemical, mineralogical, and metallurgical data (Lotter et al., 2017). Representativity across samples requires that sample locations be spatially distributed throughout the deposit, or that the spatial location of drill-holes be optimized to allow for adequate coverage of the deposit as more drilling is done (McKay et al., 2016a, 2016b). The multivariate nature of geometallurgical domains can be missed when samples from different metallurgical units are blended and treated as one sample (Lotter et al., 2017). This is commonly considered the weak point of a geometallurgical programme as assumptions regarding the representativity of variability within the orebody are made at this stage (Lamberg, 2011).

Due care should be taken not to collect metallurgical samples based only on geological information, as the representativity and full variability within the deposit will be known only once metallurgical analysis has been completed (Lamberg, 2011). This makes for the case that using resource drill core in conjunction with bulk samples from underground workings and reject pulps from chemical assay analyses is beneficial towards establishing representativity and considering variability (McKay et al., 2016a, 2016b; Dominy, O'Connor, and Xie, 2016). From the work of Coward et al. (2009) there are three important

considerations associated with variability: (1) rock variables are classified as 'primary' in light of their characteristics, or 'response' in light of their response processes; (2) variables are often commodity, deposit-type, or mining/processing specific; and (3) the distinction between variables is not always apparent, but has important implications for their modelling capability, and defines the manner in which modelling is carried out. Directly measurable characteristics such as mineral grade, metal grade, mass, rock density, colour, grain size, and alteration are considered primary. Response variables describe the ore's reaction to processing and are often multivariate. Throughput, recovery, grindability, size distribution, particle density, and distribution are examples of response variables (Coward et al., 2009).

The revision of model inputs is beneficial towards the planning of a geometallurgical block model. As illustrated by Lotter et al. (2017), the foundation for a geometallurgical block model is existing data and prior knowledge. Within the scope of this paper, attention will be focused on the variability in bulk mineralogy, grain size distribution, and gangue mineral association, i.e. the primary variables, to gain an understanding of the variability within early-stage geometallurgical domains.

2.3 Materials and Methods

Thirty-five drill core samples were selected from the five main geological ore types of the deposit (See Appendix A), from which 30 mm samples were cut, impregnated in resin, polished, and carbon coated in a Quorum Q150T E coater for QEMSCAN analysis at the University of Cape Town. Polished blocks were run on a QEMSCAN 650F with two Bruker XFlash 6130 detectors operating at 25 kV, 10 nA using the field image analysis routine at a 1500 µm field size and a 15 µm pixel size. The Species Identification Protocol (SIP) was utilized to create a secondary mineral list from the primary list by using the iExplorer software offline. In the process of establishing and refining the mineral classifications, reference was made to previous works on the orebody (e.g. Rudnick, 2016).

2.4 Results

The main economic, geological end-members examined in this study are the magnetite quartzite (QM), amphibole magnetite quartzite (AM), garnet quartzite (GQ), mineralized quartz schist (MC), and sulphidic quartzite (SQ). The QM and AM, along with barite magnetite quartzite (MB) and garnet magnetite quartzite (GM), define the Upper Orebody, whereas the MC and SQ define the Lower Orebody. For the purpose of this paper, the MB and GM are disregarded due to their relatively low copper sulphide content in the down-plunge extent of the deposit. The following sections summarize the bulk mineralogy (Table 2.1), grain size distribution of copper minerals (Fig. 2.2), and main gangue mineral associations (table 2.3) of each of the copper minerals for the geological end-members listed above. Mineral percentages here are reported as mineral mass per cent, with 'trace' amounts indicating less than 1%.

2.4.1 ***Mineral and textural characterization of preliminary end-members***

2.4.1.1 *Garnet Quartzite (GQ)*

The GQ (Fig. 2.1a) end-member is composed of quartz (approx. 59%), magnetite (approx. 11 %), almandine garnet (approx. 6%), muscovite-chlorite mica (approx. 4%), as well as sillimanite (approx. 2.5%), with trace amounts of feldspars, apatite, and ilmenite, and contains around 17% sulphide minerals. The three dominant sulphides are chalcopyrite (approx. 13%), pyrrhotite (approx. 3%), and pyrite (approx. 1%), although minor amounts of bornite, galena, and sphalerite are present. The ratio of chalcopyrite to total sulphides is 2.5:1, and the ratio of chalcopyrite to other economic sulphides (galena and sphalerite) is 16:1. Chalcopyrite occurs as coarse and massive grains overprinting the fabric and is primarily associated with quartz, magnetite, sphalerite, sillimanite, and pyrrhotite. Bornite, galena, and sphalerite proportions are too low to establish statistical associations but these minerals appear to be associated with quartz and chalcopyrite. Of the main sulphide gangue minerals, pyrrhotite dominates pyrite in a 3:1 ratio. Pyrrhotite and pyrite, along with mica, occur as rims on chalcopyrite, or as pyrite-pyrrhotite-quartz inclusions within chalcopyrite.

2.4.1.2 *Magnetite Quartzite (QM)*

Magnetite (53%) and quartz (27%) together account for the bulk of the mineralogy in the QM unit. The remainder consists of chalcopyrite (7%), galena (4.5%), pyrite (approx. 2%), chlorite-muscovite mica (approx. 1.5%), barite (approx. 1%), amphiboles (approx. 1%), and trace amounts of garnet, sphalerite, apatite, pyrrhotite, and bornite. Chalcopyrite dominates galena in a 1.8:1 ratio, and the ratio of chalcopyrite to total sulphides is approximately 1:1. Chalcopyrite is commonly associated with magnetite, quartz, and pyrrhotite. Bornite is present in trace concentrations but may locally exceed 1.5%. Where present it is associated with chalcopyrite, quartz, garnet, and magnetite. Sphalerite does not exceed 2%. Pyrite is the dominant gangue sulphide mineral, with lesser sphalerite in an 8:1 ratio and pyrrhotite in a 6:1 ratio. A combination of coarse, euhedral and subhedral chalcopyrite and galena overprints an association of finely banded quartz, magnetite, pyrite, and pyrrhotite grains. The overall texture displays a combination of massive and well-defined compositional layering (Fig. 2.1b). Quartz-magnetite-chalcopyrite-galena interfaces are often arranged in triple junctions with distinct grain boundaries.

2.4.1.3 *Amphibole Magnetite Quartzite (AM)*

The AM unit is dominated by magnetite (approx. 56%), with lesser amounts of manganogrunerite-actinolite-amphibole (approx. 12%), quartz (approx. 10%), and manganese minerals (approx. 3%) with trace amounts of apatite. Galena (approx. 5%), sphalerite (approx. 4%), and chalcopyrite (approx. 3%) comprise the economic sulphides, whereas pyrrhotite (approx. 6%) and pyrite (approx. 1%) comprise the gangue sulphides. Chalcopyrite is primarily associated with manganogrunerite amphibole, magnetite, sphalerite, pyrrhotite, and pyroxmangite. The association of coarse-grained, massive galena-chalcopyrite-sphalerite-pyrrhotite-pyrite is common. Pyrite occurs as inclusions within pyrrhotite,

chalcopyrite, and sphalerite, and is rarely found outside this arrangement. The presence of pyroxmangite with rhodonite is widespread, and associated with manganogrunerite along the grain boundaries and as inclusions in quartz veins and magnetite grains. The AM texture is characterized by the presence of coarse-grained, centimetre-scale chalcopyrite, galena, and pyrrhotite overprinting a wavy compositional fabric defined by magnetite, elongated amphibole, and quartz with manganogrunerite and magnetite (Fig. 2.1c).

2.4.1.4 *Mineralized Quartzitic Schist (MC)*

The MC consists of quartz (approx. 45%), hyalophane (barium feldspar) (approx. 13%), biotite-muscovite (approx. 6%), gahnite (approx. 3.5 %), with lesser amounts of garnet (approx. 1%), sillimanite (approx. 1%), ilmenite (approx. 1%), magnetite (approx. 1.5%), and barite (approx. 1.5%). The sulphide population is dominated by galena (approx. 17%), with lesser amounts of pyrrhotite (approx. 4.5%), pyrite (approx. 2%), chalcopyrite (approx. 1%), and trace amounts of sphalerite and bornite. Chalcopyrite is randomly associated with the sulphide gangue minerals, most commonly as chalcopyrite-pyrrhotite-biotite and chalcopyrite-pyrrhotite-pyrite associations. Trace amounts of bornite are seen closely associated with chalcopyrite, Ba-feldspar, and quartz. Variability in the economic sulphides is common, where locally chalcopyrite dominates galena (62:1), and sphalerite concentrations exceed 5%. Pyrrhotite and pyrite are the main sulphide gangue minerals and although pyrrhotite is generally dominant, locally pyrite can dominate pyrrhotite in a ratio up to 5:1. Certain varieties of mineralized schist have hyalophane dominant over quartz in a 2:1 ratio. In the MC, compositional banding defined by gahnite-quartz-pyrrhotite with finer grained biotite-pyrrhotite-chalcopyrite-quartz alternates with the main fabric defined by muscovite-biotite-sillimanite and coarse-grained galena-gahnite-quartz (Fig. 2.1d).

2.4.1.5 *Sulphidic Quartzite (SQ)*

The SQ end-member is dominated by quartz (approx. 45%) and hyalophane (19%), with lesser amounts of magnetite (approx. 9%), biotite-muscovite mica (5%), garnet (2%), ilmenite (approx. 1.5%), sillimanite (approx. 1%), barite (approx. 1%) and alkali feldspar (1%). The sulphide population consists of galena (approx. 8%), chalcopyrite (approx. 4%), and pyrite (approx. 3%) with generally trace amounts of pyrrhotite, bornite, and sphalerite, although sphalerite can locally be up to approximately 5%. Chalcopyrite and galena are closely associated, with galena appearing on the rims of chalcopyrite grains. Chalcopyrite similarly displays occasional inclusions of pyrite and pyrrhotite. Bornite is associated with quartz and chalcopyrite. Quartz, Ba-feldspar, and mica comprise the matrix of the SQ unit, while quartz-galena-pyrite, mica-Ba-feldspar-magnetite, and quartz-chalcopyrite-galena-garnet associations define a compositional fabric (Fig. 2.1e). Disseminated chalcopyrite, pyrite, pyrrhotite, and galena also locally overprint the fabric.

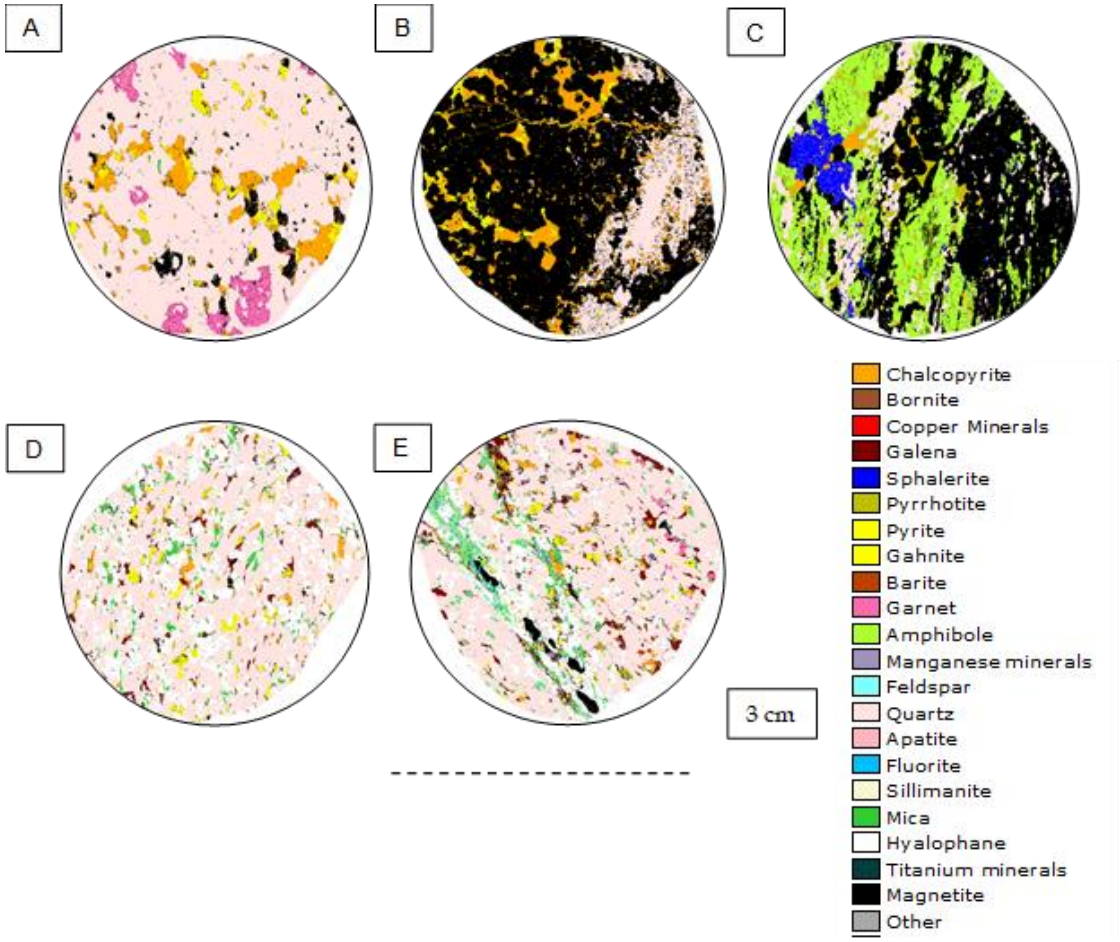

Figure 2.1: *QEMSCAN false-colour images generated for the five main geological end–members. (a) Garnet quartzite, (b) magnetite quartzite, (c) amphibole magnetite quartzite, (d) mineralized quartzitic schist, (e) sulphidic quartzite*

2.4.2 *Grain Size Distribution of Copper Minerals*

The grain size distribution of the copper minerals for the different rock types is illustrated in Figure 2.2. The grain size distributions show a clustering into two groups, a finer grained mineralization for the MC and SQ with a *d*50 (median grain size) of approximately 150 µm, and a coarser grained mineralization for the GQ, QM and AM with a *d*50 of approximately 250 µm. Given the dominance of chalcopyrite in the ore relative to bornite, the grain size distributions largely reflect those of chalcopyrite. In general, bornite is relatively fine-grained (< 50 µm) other than in the QM, where bornite grains can be as large as 150 µm.

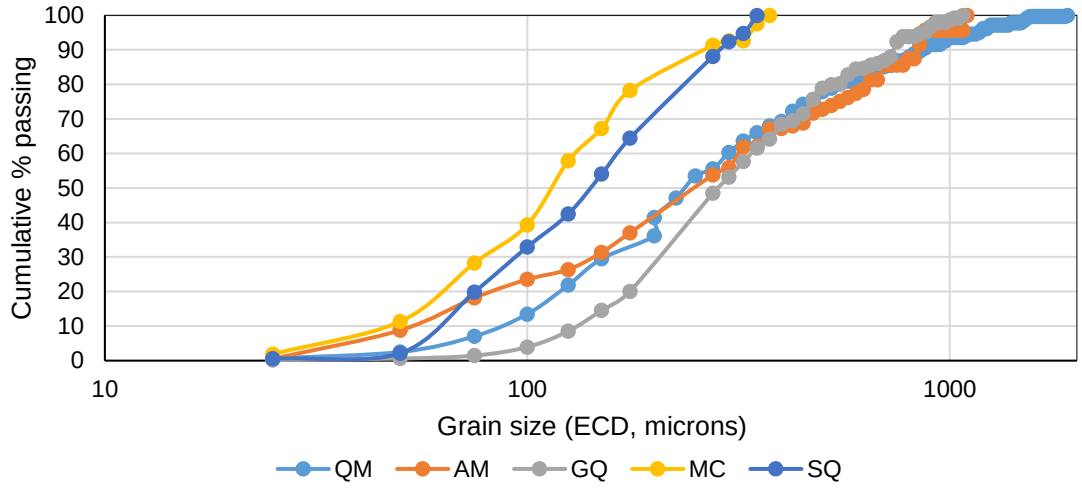

Figure 2.2: *Grain size distribution patterns of copper minerals within the GQ, QM, AM, MC, and SQ early-stage mineralogical ore types.*

2.5 Discussion

2.5.1 *Understanding the Mineralogical Characteristics for Geological Subdivisions of Ore Types*

Five potential ore types were investigated in an attempt to establish the foundation for early-stage geometallurgical domaining by verifying that these five geological end-members are distinct. Ore types were compared based on mineralogy (Tables 2.1 and 2.2) and textural characteristics (fabric and grain size) (Table 2.3). The UOB ore types (QM and AM) share similarities in their bulk mineralogy and are differentiated on the amounts of quartz and amphibole present. The QM displays the greatest textural variability. This is illustrated as a combination of fabrics and grain sizes ranging from micrometre-scale up to centimetre-scale. This characteristic feature of the QM ore, along with its mineralogical variability, has led to the establishment of subordinate ore types for improved underground grade control targeting. Three further variants of the QM ore type are identified: Sulphidic quartz magnetite (S-QM), the high-Cu end-member (QM Cu), and the high-Zn end-member (QM Zn) (Steinmann, 2016, personal communication). The main characteristic feature of the S-QM is the dominance of centimetre-scale euhedral-massive galena and chalcopyrite over all other sulphides. In comparison, the QM Cu ore is characterized by the absence of coarse galena and sphalerite, and the presence of coarse pyrrhotite and pyrite along with very coarse (centimetre-scale) chalcopyrite. The QM Zn is defined by centimetre-scale recrystallized, anomalous and lensoid massive sphalerite with subordinate galena and minor chalcopyrite.

The AM ore type displays both the greatest elemental and mineralogical variability, defined by a combination of amphibole, pyroxenoid, and manganese minerals. Mn-absent amphiboles such as

grunerite and actinolite, and similarly amphibole- and pyroxenoid-poor varieties are also considered characteristic of the AM ore. The mobility of manganese within the AM complicates the classification of amphiboles, pyroxenoids, and other manganese minerals. Manganese, iron, magnesium, and calcium can substitute for one another in these minerals, creating the possibility for a wide range of silicate and manganese minerals. Subordinate ore types might be required to constrain the variable nature of the abovementioned minerals into distinct classes, e.g. manganese-rich, manganese-poor, foliated, and non-foliated varieties, which might behave differently during metallurgical, processing based on the study by Schouwstra et al. (2010) on the neighbouring Gamsberg orebody. A close association of pyroxmangite and manganogrunerite is most prevalent in the AM ore. However, this association is also encountered in the QM ore where subordinate amounts of sphalerite are present. The manganese minerals might not necessarily be associated with only the AM ore type, but with sphalerite in general. The AM ore type is the only UOB ore type where sphalerite is widespread in high mineral grades, and this might explain why manganese minerals are concentrated here.

The variable amount of quartz in each of the UOB end-members is also problematic. Besides the QM and AM ore types described above, the GM and MB ores are also quartz-bearing. After discounting dominant magnetite, these ores are usually labelled according to the dominant silicate present. An important question is that where there is abundant quartz in these ore types, can the metallurgical responses of the QM, AM, MB, and GM ore types be distinguished from each other? The hardness of quartz overshadows that of the major silicate gangue minerals (amphibole and barite) with the exception of garnet. This raises a concern as to the metallurgical influence of garnet, amphibole, and barite relative to the amount of quartz, and how this can be better mitigated, i.e. forecasting the metallurgical performance (ore throughput) based on the ratio of quartz to the dominant silicate gangue mineral (garnet, amphibole, or barite).

The establishment of the LOB end-members, MC and SQ, is based on the presence of hyalophane, quartz, mica, sillimanite, and muscovite, generally without magnetite. The MC and SQ ore types also have distinctly finer-grained foliated and non-foliated economic chalcopyrite and galena (Table 2.3). The GQ is much closer in bulk mineralogy, grain size distribution, and mineral association to the LOB ore types.

The definitions of these early-stage ore types are still immature and will evolve depending on whether mineralogical or metallurgical variables have greater impacts on processing, e.g. the presence of pyrite and pyrrhotite vs. quartz, amphibole, and hyalophane (barium feldspar). Distinct mineral associations are present within each of the GQ, UOB, and LOB end–members. With the understanding of the elemental distribution within such geological ore types, the forecasting of mineral assemblages through element-to-mineral conversion (e.g. Nthlabane et al., 2018) as an alternative to QEMSCAN and XRD data allows for further refining of ‘early-stage mineralogical domains’.

2.5.2 *Development of Early Stage Metallurgical Domains*

The definition of geometallurgical domains is ultimately based on the response of the different ore types to mineral processing, as determined by experimental test work (Johnson and Munro, 2008). The effects of mineralogy on processing have been extensively described in the literature, specifically for polymetallic sulphide ores (e.g. Johnson, 2016; McKay et al. 2016a, 2016b; Bojcevski et al. 1998). This allows us to make some general inferences in terms of key characteristics affecting processing performance that can be used to explore possible early-stage metallurgical domains. The first of these is the relationship between grain size distribution and liberation – the coarser the grain size distribution of the valuable minerals, the better the liberation. The copper minerals in the GQ-QM-AM ores have a considerably coarser grain size distribution than in MC-SQ ores. This could present a natural subdivision into two different geometallurgical domains. Furthermore, valuable minerals cannot be recovered unless they are adequately liberated – the better the liberation, the better the flotation recovery. This presents a natural subdivision into the same two geometallurgical domains. It also highlights the potential need for finer grinding of the MC-SQ ores to liberate the copper minerals.

The second inference is the relationship between texture, rock strength, and mill throughput – the stronger the ore, the lower the throughput for a given set of milling conditions. Rock strength is a function of both the hardness of the individual minerals present and the texture, including both grain size distribution and grain orientation (Howarth and Rowlands, 1987). Considering the hardness of the major gangue minerals using Moh's scale, this suggests that quartz- (hardness 7) dominant rock types are likely to show a lower mill throughput than the amphibole- (hardness 5-6) and magnetite- (hardness 6) dominant rock types in the UOB. This is similar for the LOB ores, where there will be a difference in mill throughput for ores that are richer in quartz in comparison to hyalophane and micas. This presents a similar subdivision to that outlined above for liberation, except that the GQ ores are more similar to MC-SQ than to QM-AM. The third of these inferences is the effect of mineral association on the nature of composite particles and the possible effects on flotation concentrate grade. Because of the finer grain size distribution of the MC-SQ ores the mineral association becomes more relevant. Both these ore types show notable associations with economic (galena, sphalerite) and gangue sulphide minerals (pyrite, pyrrhotite). Both these ore types also have significant galena (> 10 wt.%) and as such are likely to exhibit similar problems relating to selectivity between the different sulphide concentrates (i.e. whether composite chalcopyrite-galena particles report to the Cu or the Pb concentrate). This affirms the logic in considering a single geometallurgical domain for the MC-SQ ores.

An additional factor to be considered is the role of the feed grade, which follows a general trend in that the higher the feed grade of the economic metals, the better the performance of the ore in processing (Bojcevski et al. 1998). In this case the GQ-QM ores would be expected to display the best copper grade and recovery during flotation (> 7% chalcopyrite in the feed), whereas the SQ-MC ores would be expected to display the best lead grade and recovery (> 8% galena in the feed). The reverse of this is, however, also possible, in that ores with the highest content of iron sulphide gangue minerals (pyrite, pyrrhotite)

are likely to be the most problematic in achieving selectivity during sequential flotation, i.e. the AM and MC ores. From the above discussion considering the five geological ore types, taking into account predicted response variables, three possible geometallurgical domains have been identified: (1) garnet quartzite, (2) magnetite quartzite and amphibole magnetite quartzite (both from the upper orebody), and (3) the mineralized quartz schist and sulphidic quartzite (both from the lower orebody). Further experimental work is needed to verify these divisions, and also to investigate whether the ore variability within each of these 'early-stage metallurgical domains' would warrant additional subdivisions (e.g. presence of S-QM and QM-Cu both within the QM ore type). Similarly, a more detailed investigation is needed to fully explore the variability within the Pb and Zn mineralization for this polymetallic sulphide orebody.

Table 2.1: *Average bulk mineralogical comparison of geological end-members (wt.%). Refer to Appendix B.*

Geological ore types					
Minerals	**GQ**	**QM**	**AM**	**SQ**	**MC**
Chalcopyrite (cp)	12.6	7.2	2.9	3.7	1.1
Bornite (bor)	<0.1	0.2	<0.1	<0.1	<0.1
Galena (ga)	0.6	4.6	4.8	8.1	17.3
Sphalerite (sph)	0.3	0.6	4.0	0.1	0.2
Pyrrhotite (po)	2.9	0.3	5.9	0.7	4.4
Pyrite (py)	0.8	1.9	0.9	2.9	2.0
Gahnite (gah)	0.1	<0.1	<0.1	<0.1	3.5
Barite (ba)	<0.1	1.0	<0.1	0.8	1.4
Garnet (gt)	5.5	0.6	<0.1	2.0	1.2
Amphibole (amph)	<0.1	0.7	12.1	0.1	0.1
Manganese minerals (mn)	<0.1	0.4	2.7	<0.1	<0.1
Feldspar (fsp)	0.2	0.1	<0.1	1.0	0.6
Quartz (qtz)	59.1	27.0	9.7	44.9	44.6
Apatite (ap)	0.3	0.3	0.5	0.1	0.1
Fluorite (fl)	<0.1	<0.1	<0.1	0.1	<0.1
Sillimanite (sill)	2.3	0.2	<0.1	1.0	1.2
Mica	4.5	1.5	<0.1	5.0	6.3
Hyalophane (hyal)	<0.1	<0.1	<0.1	19.0	13.4
Ti-minerals (ilm)	0.2	0.1	<0.1	1.4	1.0
Magnetite (mgt)	10.6	53.3	56.3	9.2	1.5
Other (oth)	0.1	0.1	<0.1	0.1	0.2

Table 2.2: *A summary of sulphide, oxide, silicate, and trace minerals present within the geological end-members. Refer to Table 2.1 for mineral abbreviations.*

Ore type	Sulphides		Oxides	Silicates	Trace
	Economic	Gangue			
GQ	cp	po, py	mgt	qtz, gt, mic, sill	
QM	cp, ga, sph, bor	py , po	mgt	qtz, ba, mica, amph, mn	amph, pyrox, ap
AM	ga, sph, cp	po, py	mgt	amph, qtz, pyrox, ap	ap, bor, py, gt, gah, fsp, fl, ilm
MC	ga, cp, sph	po, py	mgt, ilm	qtz, hyal, mica, gah	gt, fsp, sill, ap
SQ	ga, cp	Py	mgt, ilm	qtz, hyal, mica, gt	bor, sph, po, ba, ep, amph, ap, fl, sill

Table 2.3: *Grain size, mineral association, and textural arrangements as summarized from the geological end-members. Refer to Table 2.1 for mineral abbreviations.*

Ore body	Ore type	Grain size (µm)			Mineral association (%) **	Textural arrangement of chalcopyrite***	
		Copper minerals			Copper minerals	Grain shape	Fabric
		Min.	Max.	Med.		Euh/sub/anh	Fol/band/brec
GQ	GQ	<25	<1075	225-275	qtz, mgt, sph, sill, po	anh (massive)	mass/ non-fol
UOB	QM	<25	<2000	100-150	mgt, qtz, po	euh/ anh	mass/ fol/ non-fol
	AM	<25	<1100	50-100	amph, mgt, sph, po, pyrox	anh (stretched)	fol
LOB	MC	<25	<375	100-150	po, py, mica	sub	fol
	SQ	<25	<350	50-100	ga, py, po	anh (massive)	mass/ fol

** See Table 1 for mineral abbreviations

*** Grain shapes as euhedral (euh), subhedral (sub), anhedral (anh), and fabric as massive (mass), foliated (fol), and non-foliated (non-fol)

2.6 Conclusions

The deposit is a complex polymetallic sulphide orebody, for which there is motivation to initiate the development of a geometallurgical block model. Mineralogical variability within the ore manifests as an intricate association of sulphide, oxide, and silicate minerals across different lithological domains. A quantitative mineralogical study of the five geological ore types was essential to understand the disposition of these ores, specifically with a focus on copper mineralization. The resultant early-stage mineralogical domains, as based on the association of copper mineralization with silicate gangue minerals, is immature, and will evolve.

Mineralogical attributes such as chalcopyrite head grade, grain size distribution, mineral grades of economic sulphide, gangue sulphide, and other major gangue minerals, were most critical during the review of mineral processing responses. Characteristics of this nature should henceforth be primary variable inputs into the geometallurgical block model, and will prove useful towards the rationalization

and interpretation of mineral relationships. Consideration of the potential mineral processing response of the five mineralogical ore types on the basis of liberation, mill throughput, and flotation grade, recovery, and selectivity revealed three 'early-stage geometallurgical domains'. Defining subordinate geometallurgical domains within these early-stage geometallurgical domains might have further implications for mitigating elemental variability during mineral processing, and developing element-to-mineral conversion parameters for the generation of quantitative mineralogy from chemical assays. It is recommended that subordinate ore types be pursued by expanding the focus of the geometallurgical block model to incorporate lead-zinc-dominated ores.

2.7 Acknowledgements

The authors would like to acknowledge the efforts of employees at Black Mountain Mining (Pty) Ltd. in providing logistical support during sampling, travelling, site visits, and block analysis, and the executive management team for financial support. This work is based on research supported in part by the National Research Foundation of South Africa (grant numbers 86054, 99005). The authors would also like to acknowledge Gaynor Yorath and the QEMSCAN team for assistance with the QEMSCAN analysis.

2.8 References

Bailie, R., Armstrong, R., and Reid. D. (2007). Composition and single zircon U-Pb emplacement and metamorphic ages of the Aggeneys Granite Suite, Bushmanland, South Africa. *South African Journal of Geology*, 110: 87-110.

Bojcevski, D., Vink, L., Johnson, N.W., Landmark, V., Mackenzie, J., and Young, M.F. (1998). Metallurgical characterization of George Fisher ore textures and implications for ore processing. *Proceedings of the AusIMM Mine to Mill Conference*, Brisbane, Australia, 11-14 October. Australasian Institute of Mining and Metallurgy, Melbourne. pp. 29-41.

Bradshaw, D.J. (2014). The role of 'process mineralogy' in improving the process performance of complex sulphide ores. *Proceedings of IMPC 2014*, Santiago, Chile. Gecamin, Santiago. pp. 1-23.

Butler, C., Dale, R., Robinson, S., and Turner, A. (2016). Geometallurgy – Bridging the gap between mine and mill: A case study of the DeGrussa geometallurgy program. *Proceedings of the Third AUSIMM International Geometallurgy Conference,* Perth, WA, 15-16 June 2016. Australasian Institute of Mining and Metallurgy, Melbourne. pp. 77-88.

Coward, S., Vann, J., Dunham, S., and Stewart, M. (2009). The primary-response framework for geometallurgical variables. *Proceedings of the Seventh International Mining Geology Conference.* Australasian Institute of Mining and Metallurgy, Melbourne. pp. 109-113.

Dominy, S.C., O'Connor, L.O., and Xie, Y. (2016). Sampling and test work protocol development for geometallurgical characterisation of a sheeted vein gold deposit. *Proceedings of the Third AUSIMM*

International Geometallurgy Conference, Perth, WA, 15-16 June 2016. Australasian Institute of Mining and Metallurgy, Melbourne. pp. 97-112.

Howarth, D.F. and Rowlands, J.C. (1987). Quantitative assessment of rock texture and correlation with drillability and strength properties. *Rock Mechanics and Rock Engineering*, 20, 57-85.

Johnson, N.W. (2016). Sphalerite and galena liberation levels for the Mount Isa concentrator. *Process Mineralogy*. Becker, M, Wightman, E.M., and Evans, C.L. (Eds). Julius Kruttschnitt Mineral Research Centre, University of Queensland, Australia. pp. 234-249.

Johnson, N.W. and Munro, P.D. (2008). Methods for assigning domains in the primary sulfide zone of a sulfide orebody. *Proceedings of the Ninth International Congress for Applied Mineralogy*, Brisbane, Queensland, 8-10 September. Australasian Institute of Mining and Metallurgy, Melbourne. pp. 597-603.

King, G.S. and MacDonald, J.L. (2016). The business case for early-stage implementation of geometallurgy – an example from the Productora Cu-Mo-Au deposit, Chile. *Proceedings of the Third AUSIMM International Geometallurgy Conference*, Perth, WA, 15-16 June 2016. Australasian Institute of Mining and Metallurgy, Melbourne. pp. 125-133.

Lamberg, P. (2011). Particles – the bridge between geology and metallurgy. https://www.researchgate.net/publication/267386265

Liebezeit, V., Ehrig, K., Robertson, A., Grant, D., Smith, M., and Bruyn, H. (2016). Embedding geometallurgy into mine planning practices – Practical examples at Olympic Dam. *Proceedings of the Third AUSIMM International Geometallurgy Conference*, Perth, WA, 15-16 June 2016. Australasian Institute of Mining and Metallurgy, Melbourne. pp. 135-143.

Lotter, N.O., Baum, W., Reeves, S., Arrué, C., and Bradshaw, D.J. (2017). The business value of best practice process mineralogy. *Minerals Engineering*, http://dx.doi.org/10.1016/j.mineng.2017.05.008

Lotter, N.O., Kormos, L.J., Oliveira, J., Fragomeni, D., and Whiteman, E. (2011). Modern process mineralogy: Two case studies. *Minerals Engineering*, 24, 638–650.

McKay, N.A., Vann, J., Ware, W., Morley, C., and Hodkiewicz, P. (2016a). Strategic and tactical geometallurgy – a systematic process to add and sustain resource value. *Proceedings of the Third AUSIMM International Geometallurgy Conference*, Perth, WA, 15-16 June 2016. Australasian Institute of Mining and Metallurgy, Melbourne. pp. 29-36.

McKay, N. A., Sztuke, J.C. and Lacouture, B. (2016b). Red Dog Zinc concentrator optimization study 2009. *Process Mineralogy.* Becker, M., Wightman, E.M., and Evans, C.L. (Eds). Julius Kruttschnitt Mineral Research Centre, University of Queensland, Australia. pp. 250-260.

Nthlabane, S., Becker, M., Charikinya, E., Voight, M., Schouwstra, R., and Bradshaw, D. (2018). Towards the development of an integrated modelling framework underpinned by mineralogy. *Minerals Engineering*, 116, 123-131.

Rosenkranz, J. and Lamberg, P. (2014). Sustainable processing of mineral resources. *International Journal of the Society of Materials Engineering for Resources*, 20 (1), 17-22.

Rudnick, T.K. (2016). The genesis of the Swartberg base-metal sulphide deposit, South Africa. Master's dissertation, University of Stellenbosch.

Ryan, P.J., Lawrence, A.L., Lipson, R.D., Moore, J.M., Paterson, A., Stedman, D.P., and van Zyl, D. (1986). The Aggeneys base metal sulphide deposits, Namaqualand district. *Mineral Deposits of South Africa.* Anhaeusser, C.R. and Maske, S. (Eds). Geological Society of South Africa, Johannesburg. pp. 1447-1473.

Schouwstra, R., de Vaux, D., Hey, P., Malysiak, V., Shackleton, N., and Bramdeo, S. (2010). Understanding Gamsberg – A geometallurgical study of a large stratiform zinc deposit. *Minerals Engineering,* 23 (11-13), 960-967.

Sepulveda, E., Dowd, P., and Xu, C. (2015). Modelling geometallurgical response variables using Projection Pursuit regression. Proceedings of the 11th International Mineral Processing Conference. Gecamin, Santiago.

Stedman, D.P. (1980). The structural geology and metamorphic petrology of Black Mountain, Namaqualand. Master's dissertation. University of the Witwatersrand, Johannesburg.

Steinmann, P.G. (2016). Grade Control Geologist, Black Mountain Mining, Aggeneys. Personal communication

CHAPTER 3: Geometallurgical domain classification of magnetite-dominated polymetallic ores using ore mineral characteristics as proxies

Publication Note: This chapter has been submitted for review to Minerals Engineering.

***Gordon, H.J.J**., Stroebel, G, Miller, J.A., Corin, K.C. and Becker. M. Submitted. Geometallurgical domain classification of magnetite-dominated polymetallic ores using ore mineral characteristics as proxies*. *Minerals Engineering*

***Candidate contribution:** The candidate contributed 70 % to the conceptualisation of the validation of early-stage geometallurgical domains presented in this work and 85 % to the data analysis and writing of this manuscript*

This chapter validates the early-stage mineral-based Upper Orebody geometallurgical domain (UOBGD) that was proposed in Chapter 2. Flotation testing is used to test whether the UOBG does in fact behave as a single coherent domain.

Abstract

Geometallurgical domains provide a way to constrain metallurgical variability within complex sulphide deposits by isolating key physiochemical similarities within ores. In this study, six secondary lithological units that define the magnetite-dominated ores of a Cu-Pb-Zn-Ag Broken Hill-type deposit were investigated. Key mineralogical characteristics in conjunction with metallurgical indicators were used to define three geometallurgical domains. The quartz-, pyroxmangite- and grunerite-dominant nature are characteristic features of the Quartz Magnetite (QM), Pyroxmangite Quartz Magnetite (PQM) and Amphibole Quartz Magnetite (AM) domains respectively - each of which also has distinct metal zonation patterns as well as distinct economic sulfide liberation and association. The QM ore is the best performing ore. Its excellent mass pull, grade and recovery are underpinned by coarse-grained, well-distributed chalcopyrite and galena. Some key findings on the processing responses of these ores was the need to account for selectivity (especially when dealing with exsolution textures between chalcopyrite and galena), as well as the need to address the undesirable recovery of the penalty element Mn to the concentrate. The Cu:S ratio was identified as a potential elemental proxy that can readily be used for upfront classification of ore types into their respective geometallurgical domains. The value of the mineralogical approach used here is attributed to the efficient use of a representative quantitative mineralogical dataset.

Keywords: Polymetallic Cu-Pb-Zn, flotation, mineralogy, geometallurgical domains, elemental proxies

3.1. Introduction

For many years, 3-D geological block models have provided the core information that enabled mining companies to predict the minerals processing response of polymetallic deposits. Such models have underpinned financial decisions and hence have directly affected mining profitability (Coward et al., 2009; Lund et al., 2013; Dominy et al., 2016). In recent years though, as ore deposit grades have declined and the mineralogical complexity of deposits has increased, the limitations with considering only the geological block model and by extension chemical assay data have become increasingly apparent (Williams, 2013; Bradshaw, 2014; Lotter et al., 2017). In such cases, geological block models typically over-estimate the feed grade, resulting in inefficiencies in downstream metallurgical processing circuits, leading to metal loss due to lower than forecasted metal recoveries and concentrate grades (Kormos et al., 2010; Lamberg et al., 2013). Such inefficiencies result because the block model cannot accurately quantify the complexity of the mineralogical and textural characteristics of the ore, and thus its accuracy on the minerals processing responses of complex ores is limited (McKay et al., 2016).

Quantification of mineralogical and textural ore variability aids in understanding the complexity of a deposit and hence is necessary to differentiate between ores that are easy to process and those that are more challenging (Williams, 2013; Lotter et al., 2017). This is because the physical and chemical characteristics of minerals (grade, grain size and shape, and mineral association) underpin the processing response (Johnson and Munro, 2008; Kormos et al., 2010). However, the abovementioned process-mineralogical relationship often remains ambiguous in mines due to limited availability of fit for purpose process mineralogical data (Johnson and Munro, 2008). The interdependence of geology and metallurgy (ore characteristics vs. ore processability), is not yet fully appreciated, which is evident in the way geological data is collected (limited metallurgical data consideration), and downstream minerals processing issues are addressed (limited geological data integration) (Kormos et al., 2010; Williams, 2013). Geometallurgy, which aims to combine geological and minerals processing data as it pertains to the extraction of metals from an orebody, provides a platform for geologists and metallurgists to understand the significance of process-mineralogical relationships in ores, and their variability within deposits as geometallurgical domains (Kormos et al., 2010; Lamberg et al., 2013).

By definition, geometallurgical domains are one or more groups of ore types that, because of the similarities in their physicochemical makeups, are expected to behave similarly in a processing circuit (Lotter et al. 2003; Fragomeni et al., 2005). Geometallurgical domains aim to characterise the variability of the relationship of ore characteristics in deposits (mineralogy, mineral association and liberation) and their respective flotation responses (grade, recovery, entrainment and deportment) (Kormos et al., 2010; Williams, 2013). Upon establishing this link between the mineralogical characteristics and their flotation responses, geometallurgical domains can be assigned a certain set of process mineralogical parameters that will indicate how it, as an individual domain or as part of a group of domains, should be metallurgically

treated (Johnson and Munro, 2008). These process mineralogical parameters allow predictions to be made regarding the flotation response of ores from such domains and support proactive decision making to selectively target or blend ores to meet the strategic or tactical needs of the mining operation (Strohmayr et al., 1998; Lotter et al., 2003; McKay et al., 2016). This ensures reduced business risk and allows for optimization of the operational model in the event of process mineralogical inefficiencies due to ore variability (Lotter et al., 2003; Williams, 2013; Gu et al., 2014; Becker et al., 2016).

In this study, a complex, low-grade deposit from the Aggeneys – Gamsberg Ore District (A-GOD) of the Northern Cape Province, South Africa was used to test a mineralogy-based approach to geometallurgical domaining. The Black Mountain Complex (BMC) ore deposits have unique and complex mineralogies across multiple ore bodies resulting from multiple, prolonged geological deformation and metamorphic events (Rozendaal, 1975; Ryan et al., 1986; Cawood and Rozendaal, 2019). The Black Mountain concentrator produces three concentrates from a blend of Cu-Pb-Zn-Ag ores derived from two mines through sequential Cu, Pb, and Zn flotation. Historical recovery data from this circuit indicates that recoveries are variable, particularly the recovery of copper minerals (Fig. 3.1; units omitted for confidentiality purposes). Twidle and Engelbrecht (1984) were the first to notice the problematic copper recoveries of this BMC ore. This variability is largely interpreted to be due to grain size variability and mineralogical and textural complexity associated with the BMC ores. This variation in ore characteristics – mineral grade, elemental grade, grain size and association - poses a challenge towards forecasting the ore's physiochemical response to mineral processing derived from the geological block model alone.

The abovementioned factors have motivated a comprehensive mineralogical investigation of the ore to ascertain the key factors contributing to ore variability, and to establish how these relate to processing domains. Based on their bulk mineralogy, grain size distribution, head grade and texture, three geometallurgical domains have been proposed in a paper by Gordon et al. (2018) who investigated a set of drill cores from the deposit. Two of the proposed geometallurgical domains consist of multiple different lithological ore types, whereas the third represented one homogeneous ore type (Table 3.1). The Upper Orebody geometallurgical domain (UOBGD) consists of the QM and AM lithological units whereas the Lower Ore body geometallurgical domain (LOBGD) consists of the mineralised schist (MC) and sulphidic quartzite (SQ) lithological units. The Garnet Quartzite geometallurgical domain (GQGD) is a standalone unit.

The overarching objective of this paper is to test whether the magnetite-bearing lithological ore types that make up the UOB geometallurgical domain proposed by Gordon et al. (2018) do behave as a single coherent geometallurgical ore domain. An additional aim is to establish which mineral characteristics can act as suitable proxies for delineating geometallurgical domains in these ore types generally. For this, six separate secondary lithological ores that define the magnetite dominated geometallurgical domain were collected and subjected to quantitative mineralogical measurements (bulk mineralogy, mineral association and liberation), coupled with laboratory-scale bulk sulphide flotation tests (grade, recovery and selectivity). The results and interpretations from this study have application in the development of

early-stage geometallurgical domains in Cu-Pb-Zn-Ag magnetite-dominated broken-hill type ores in the absence of, or prior to the acquisition of, comprehensive geometallurgical data.

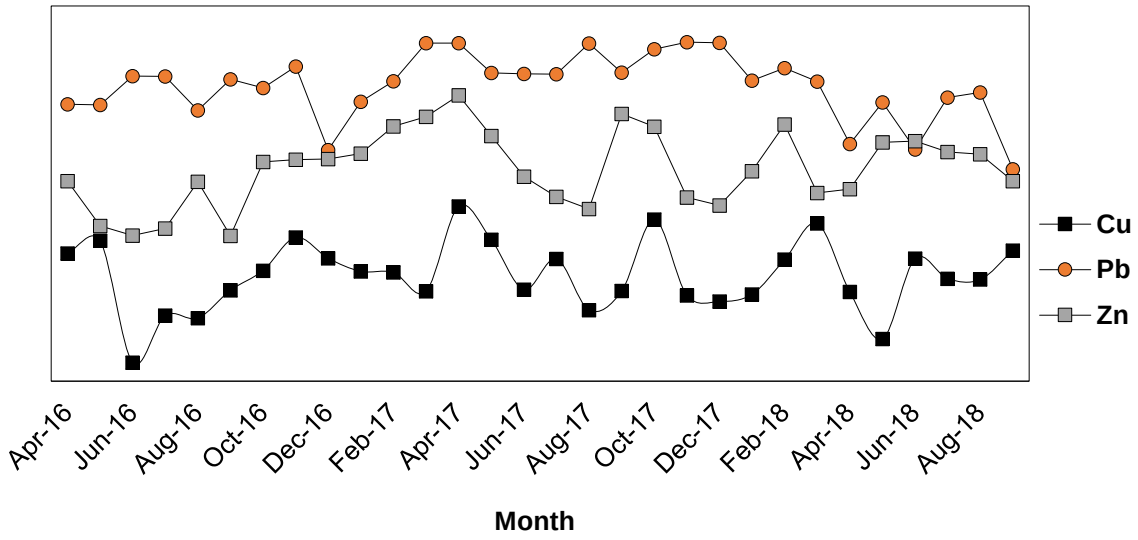

Figure 3.1: *Average monthly copper, lead and zinc recovery data from the BMM concentrator ranging over time.*

Table 3.1: *The subdivisions of lithostratigraphic orebodies and ore types of the deposit and its proposed geometallurgical domains (Gordon et al. 2018).*

Geomet Domain	**Lithostratigraphic**	**Primary**	**Secondary**
	Orebody	**Ore type**	**Ore type**
GQGD	Garnet Quartzite (GQZ) comprising 'quartz dominant' ores	Garnet Quartzite (GQ)	
UOBGD	Upper Orebody (UOB) comprising 'magnetite dominant' ores	Quartz Magnetite (QM)	Ores A-F
		Amphibole Magnetite (AM)	
LOBGD	Lower Orebody (LOB) comprising 'quartz dominant' ores.	Sulphidic Quartzite (SQ) Mineralised Schist (MC)	

3.2. Geological setting

The A-GOD deposits are polymetallic Zn-Cu-Pb-Ag Broken Hill-type sulphide ore deposits that occur in the Aggeneys Subgroup of the Bushmanland Subprovince, in the Namaqua-Natal Metamorphic Province (Cornell et al., 2006; McClung et al., 2007). The stratigraphic succession of the A-GOD is defined as repetitive thrust bounded sequences of quartzo-feldspathic gneisses, aluminous metapelitic schist, metaquartzite, and the Aggeneys/ Gams Ore Formation (AOF/ Gams Member). Ore bearing lithologies

of the AOF range from iron formation, metapelitic, ferruginous, garnetiferous and sulphidic quartzites and schists (Rozendaal, 1975; Ryan et al., 1986; Cawood and Rozendaal, 2019). Reworking of the original mineralogy during the poly-deformational history undergone by the deposit generated an intricate arrangement of primary and secondary silicate, sulphide and oxide minerals aligned in an array of micro – and mesoscopic textures (Neufeld, 2005; Cawood and Rozendaal, 2019).

Following deformation and surface erosion, the AOF was preserved within the core of a major recumbent isoclinal fold structure that defines the deposit reviewed in this study (Fig. 3.2). Within the core of the fold, three separate economic orebodies are differentiated, based on bulk mineralogy, ore mineral textures and metal zonation patterns (Stedman, 1980; Ryan et al., 1986; Cawood and Rozendaal, 2019). These are the Garnet Quartzite alteration halo (GQZ), the Upper Orebody (UOB) and the Lower Orebody (LOB) (Fig. 3.2). The UOB, LOB and GQZ orebodies collectively contain five primary (GQ, QM, AM, MC and SQ) and six secondary ore-bearing lithostratigraphic units (Ore A: QM Cu, Ore B: QM Zn, Ore C: S-QM, Ore D: AM Foliated, Ore E: AM Non-foliated and Ore F: QM). Primary ore-bearing units are differentiated according to strong mineralogical and textural differences whereas secondary ore-bearing units are subordinate units within primary ores that are differentiated based on differences in economic sulphide (ES) mineral grade zonation. The primary and secondary lithostratigraphic ore units are simultaneously extracted and blended to produce the run of mine material feeding the concentrator (Table 3.1).

The Cu-rich GQZ horizon wraps around the UOB thus forming both the stratigraphic hanging wall and footwall to the UOB in the fold hinge. The GQZ is between 10 and 70 m thick and contains varying amounts of coarse-grained chalcopyrite, quartz and garnet. The Pb-Zn-Ag-rich LOB is a well-bedded, 5 to 50 m succession of micaceous and siliceous mineralized schists (MC) and sulphidic quartzites (SQ) containing lensoidal and stratiform galena, sphalerite and chalcopyrite. This unit occurs stratigraphically below the UOB and GQZ in the lower limb of the isoclinal fold (Stedman, 1980; Ryan et al., 1986; Cawood and Rozendaal, 2019).

The Cu-Pb-Zn-Ag-rich UOB forms the core of the deposit and is a 25 – 30 m thick magnetite-quartz-amphibole-pyroxenoid bearing unit. Two dominant end member lithological ore types, the quartz magnetite (QM) and the amphibole magnetite (AM)/ amphibole pyroxenoid magnetite (APM), define the UOB. Stratigraphically, the amphibole pyroxenoid magnetite is tectonically enclosed by the quartz magnetite on both the hanging – and footwall sides of the core (Stedman, 1980; Ryan et al., 1986; Neufeld, 2005; Cawood and Rozendaal, 2019). Key mineralogical differences between the three lithologies are based on the relative dominance of magnetite vs quartz (QM vs AM), and the ratio of pyroxenoid to amphibole (AM vs APM). Variable amounts of chalcopyrite, galena and sphalerite are hosted within each. The mineralogical and textural complexity of the AM/ APM and QM ore-bearing lithostratigraphic ore units are the focus of this study.

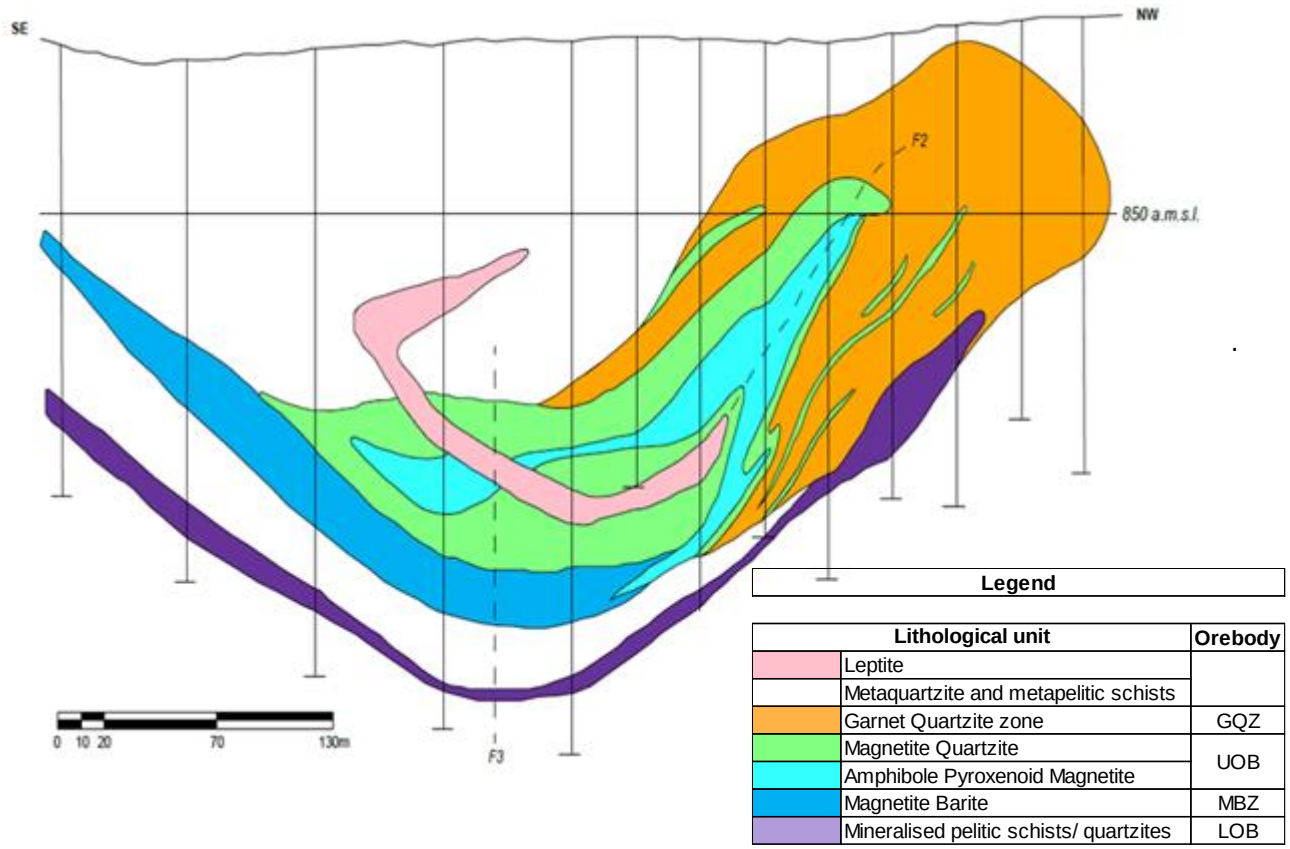

Figure 3.2: *Geological model of the Broken Hill-type polymetallic Cu-Pb-Zn-Ag deposit reviewed in this study. Reworked from an internal company report from 2000.*

3.3. Materials and methods

Six bulk samples (labelled A to F, approximately 75-100 kg of each sample) (Table 3.1), representing the heterogeneity of the magnetite dominant UOB ores, viz quartz magnetite (QM) and amphibole magnetite (AM/ APM) were collected in-situ from underground workings (See Appendix A). A sixth ore sample (Ore F) was collected from six resource drill holes drilled during the 2016 financial year due to limited stope availability underground to sample this ore. All analytical work was carried out in the Department of Chemical Engineering at the University of Cape Town unless otherwise specified.

3.3.1. Crushing, milling and flotation procedure

The ore samples were manually reduced in size with a sledgehammer (where required) and thereafter fed through a TERMINATOR jaw crusher, with jaw width set to 3 mm. All crushed ores were thereafter split using a ten-way rotary riffle splitter to produce 1.3 kg aliquots for batch flotation. Ores A to C however, were used for Julius Kruttschnitt Rotary Breakage Tester (JKRBT) ore characterisation entailing the extraction of drill cores prior to flotation (Hill Unpubl. data), and the progeny from this experimental work was thereafter milled and prepared for flotation tests. Milling curves were established for each of the ore types to produce a flotation feed size distribution of 65% passing 75 µm using a 10 L rod mill fitted with

twenty rods of varying sizes (six - 258mm x 25 mm, eight - 285 mm x 20 mm and six - 285 mm x 15 mm). Special care was taken throughout to avoid any cross-contamination between samples during milling. Ore E required the least amount of time to reach 65 % passing 75 µm (11 minutes). When the milling times of all the other ores were normalised to the milling time of Ore E, Ore D required 1.33x, Ore C required 1.39x, Ore F required x1.49 and Ores A and B required 1.5x as long to reach 65 % passing 75 µm.

All flotation tests were conducted in triplicates using a 3 L Barker bench flotation cell at the University of Cape Town, run at 1250 rpm using an airflow rate of 7.5 L/m. To simplify the laboratory flotation procedure, batch floats were set up as bulk sulphide floats rather than sequential floats (as used on-site at Black Mountain using a reagent suite similar to that used on-site at BMM). To allow comparisons between ore types, the reagent suites were kept as constant as possible and not optimized for the individual ore characteristics. Two collectors were added, 80 g/t of 1 % (w/v) Sodium Ethyl Xanthate (SEX) along with 6 g/t Senkol 700, and allowed to condition for two minutes. After two minutes, 25 g/t Methyl Isobutyl Carbinol (MIBC) frother was added followed by a further conditioning time of one minute. The froth height was kept at a constant 15-20 mm using in-house synthetic plant water. The Eh and pH of the floats were not measured. Flotation experiments were conducted in the absence of copper sulphate as an activator to allow for more selectivity between the economic (chalcopyrite, galena and sphalerite) and gangue sulphides (pyrite and pyrrhotite). After three minutes, the airflow was switched on. Concentrates were collected at four, six, nine and eighteen minutes, with scraping done every fifteen seconds. The water recovery was monitored. All flotation products, including those of the feed and tails, were filtered and dried overnight before weighing.

3.3.2. Elemental analyses

Duplicate feed, concentrate and tailings samples best representing each of the triplicate floats were thereafter assayed for Cu, Pb, Zn, Fe and Mn using a three acid digestion (HCl, HNO_3 and $HClO_4$) and ICP-OES. In conjunction with the 5-element ICP-OES assays, 33-element ICP-OES analysis was also conducted on each of the flotation feeds. A Spectro Acros ICP-OES operating at 1400W plasma power, 30 rpm pump speed, 14 L/min coolant flow, 2.1 L/min auxiliary flow and 0.8 L/min nebuliser flow (crossflow) was used to analyse the samples at Scientific Services in Cape Town. Silica blanks and certified reference material samples were also included for control.

3.3.3. Mineralogical analyses

One milled feed sample (from a representative aliquot of each ore) was physically wet screened into four size fractions: < 10 µm, +10/-38 µm, +38/-75 µm and +75 µm and prepared as a transverse/vertical section mounted in polished epoxy blocks for QEMSCAN (Quantitative Evaluation of Minerals by Scanning Electron Microscopy) analysis. Samples were run at 25 kV, 10 nA using the field scan analysis routine at a 1465.2 µm field size and a 14.65 µm pixel size. Both the bulk mineralogical analyses and specific mineral search were run at 1372.5 µm field size and 3.66 µm particle size for -300/+75, whereas

the -75/+38, -38/+10 and -10 µm were run at a field size of 686.25 µm and a particle size of 1.83 µm. Regrinds of the -300/+75 and +75/-38 µm size fractions of some of the ores were run at a field size of 975.69 µm and a particle size of 2.93 µm.

A combination of the bulk mineralogical analysis, field image analysis and specific mineral search routines were used to characterise the mineralogy of the samples. A unique QEMSCAN species identification protocol was created for the Black Mountain ore, which made use of the mineralogy reported in Stedman (1980), and Ryan et al. (1986), and quantitative mineral chemistry data reported in Rudnick (2016). ICP-OES data from the feed products were also used to validate QEMSCAN assay data.

QXRD (Quantitative x-ray diffraction) was used as a validation measure for QEMSCAN on bulk unsized samples only. The QXRD measurements were done using a Bruker D8 Advance with Lynx-eye detector and CoKα radiation over a range of 5 to 90° 2θ. The step size was kept consistent at 0.02 degrees, whereas the counting time was one second per step. Bruker EVA and Topas version 5 Rietveld refinement software were used to refine the spectra.

3.4. Results

Based on milling, flotation and quantitative elemental - and mineralogical data, the following observations can be made for the magnetite-dominated ores (Tables 3.2-3.5; Figs. 3.3-3.10).

3.4.1. Ore feed metal grade

There are distinct metal zonation patterns across the magnetite-dominated ores (Table 3.2). Ores A and B display a metal zonation trend of Zn>Cu>Pb, Ore C displays a metal zonation trend of Pb> Zn>Cu. Ores D, E and F display metal zonation trends of Cu>Pb>Zn. Ores A and B are the only ores in which there are significant amounts of Zn. When comparing total elemental grade, within each of these ores, Ore C has the highest combined elemental grade (6.2 wt. % Cu+Pb+Zn) followed in decreasing amounts by ores F (2.9 wt. % Cu+Pb+Zn), and A and B (2.8 wt. % Cu+Pb+Zn). Ores D and E have the lowest combined elemental grade (1.1 and 2.9 wt. % Cu+Pb+Zn respectively). High Mn elemental grades are noticed in ores A, B, C and D (4.58 - 9.37 wt. %), whereas Ore E and F have lower Mn values (0.89 and 0.26 wt. % respectively). The Fe content within the ores ranges from (46.99 – 54.25 wt. %).

Table 3.2: Bulk elemental breakdown of magnetite dominated ores.

Bulk elemental composition of magnetite dominated ores							
Element	Unit	Ore A	Ore B	Ore C	Ore D	Ore E	Ore F
Cu	wt. %	0.56	0.71	0.24	0.51	0.36	1.33
Pb	wt. %	0.48	0.56	5.53	0.21	0.66	1.30
Zn	wt. %	1.74	1.48	0.45	0.09	0.05	0.24
Fe	wt. %	47.43	46.99	48.47	51.14	47.78	54.25
S	wt. %	2.42	2.34	1.59	1.03	0.46	1.65
Mn	wt. %	4.58	4.60	5.81	9.37	0.89	0.26
Al	wt. %	0.06	0.09	0.08	0.17	0.21	0.18
Ca	wt. %	0.39	0.30	0.28	0.32	0.43	0.24
K	wt. %	<0.01	<0.01	<0.01	<0.01	<0.01	0.01
Mg	wt. %	0.73	0.61	0.41	1.85	1.75	0.05
Na	wt. %	<0.01	<0.01	<0.01	0.01	0.01	<0.01
P	wt. %	0.18	0.13	0.11	0.15	0.20	0.11
Ti	wt. %	<0.02	0.01	<0.01	0.01	0.02	0.01
Sr	ppm	16.71	17.01	15.82	18.05	32.38	29.81
Th	ppm	<5	<5	<5	<5	<5	<5
Tl	ppm	<5	<5	<5	<5	<5	<5
U	ppm	5.10	<5	5.13	<5	<5	<5
V	ppm	<1	<1	0.88	<1	<1	<1
W	ppm	26.30	20.70	6.31	<5	<5	9.74
Cu+Pb+Zn	wt. %	2.8	2.8	6.2	0.8	1.1	2.9
Cu:S		0.2	0.3	0.2	0.5	0.8	0.8

3.4.2. Ore feed bulk mineralogy

Associated with the head elemental grades are distinct bulk mineralogies (Table 3.3). Due to the similarity of ores D and E in hand specimen, QXRD mineralogy and flotation response, the mineralogy of ore E was not quantified using QEMSCAN. For simplification during the data presentation, three groupings of mineral types are used. Chalcopyrite, galena and sphalerite define the economic sulphide minerals (ES), pyrite and pyrrhotite define the sulphide gangue minerals (SG), whereas all other minerals are grouped as non-sulphide gangue minerals (NSG).

Mineral phases whose presence within the bulk mineralogical breakdown does not exceed one wt. % has been grouped as “other” minerals. These include arsenopyrite, sillimanite, feldspar (albite and microcline), mica (muscovite and biotite (annite and phlogopite)), chlorite, fluorite, barite, rhodonite, pyrolusite, garnet (spessartine, almandine and andradite), pyroxene (augite and diopside), monazite, bismuthinite, molybdenite and spinel (gahnite, hercynite and chromohercynite). Secondary sulphide and

oxide minerals (< 0.1 wt. %) found during the mineralogical analysis include bornite, covellite and tennantite (grouped with chalcopyrite) and chromite, ilmenite and jacobsite are grouped with magnetite. The various end-member varieties of the feldspar-, mica-, garnet- and pyroxene minerals are found as distinct mineral species within the magnetite-dominated ores (Rudnick, 2016).

3.4.2.1. Ores A, B and C

Magnetite is the dominant mineral throughout Ores A, B and C (53.8 – 58.8 wt. %) with the remainder of the NSG minerals making up (31.9 – 34.6 wt. %). NSG minerals include pyroxmangite (21.0 – 27.7 wt. %), grunerite (amphibole) (0.6 – 5.5 wt. % split into grunerite with 0 – 0.2 wt. % and manganogrunerite with 0.5 - 5.4 wt. %), and quartz (2.5 - 6.8 wt. %). Sphalerite (0.6 - 3.1 wt. %), galena (0.5 – 6.4 wt. %) and chalcopyrite (0.6 – 2 wt. %) define the ES, whereas pyrrhotite (0.8 - 2 wt. %) and pyrite (0.9 - 1.1 wt. %) are the SG minerals. Notable minerals within the “other” category for QEMSCAN include annite (0.14 wt. %), spessartine (0.55 wt. %) and pyrolusite (0.2 wt. %). Sphalerite is the dominant ES mineral in Ores A and B, whereas galena is dominant in Ore C. Pyrrhotite dominates pyrite in Ores A and B; however, the opposite is true for Ore C. The greatest concentration of magnetite and pyroxmangite is present within Ore C, which subsequently also has the least amount of quartz and grunerite-manganogrunerite. Quartz and grunerite concentrations are more or less equal for Ores A and B, whereas Ore B has a greater concentration of pyroxmangite in comparison to Ore A.

Examination of the particle characteristics illustrated in the false colour QEMSCAN images in Fig. 3.3A, B and C, indicates the following textural features are prevalent throughout ores A, B and C. A pervasive association of chalcopyrite and sphalerite dominates the ES mineral textures. Sphalerite grains are well distributed displaying pronounced chalcopyrite disease (chalcopyrite grains as an exsolution feature within sphalerite grains; Fig. 3.3G). Chalcopyrite is rarely observed not associated with sphalerite. Similarly, chalcopyrite and sphalerite also display a strong association with pyrrhotite and pyrite as alteration rims and sulphide mineral intergrowths. These intergrowths are texturally variable as can be seen from their overgrowths onto magnetite and pyroxmangite and their filling of interstitial spaces between and within magnetite and pyroxmangite grains as veins (Fig. 3.3A). Where galena is present, it is associated with sphalerite and chalcopyrite. NSG mineral textures include a clear association of magnetite and pyroxmangite, with or without an association of grunerite-manganogrunerite, quartz and apatite (Fig. 3.3A and B). This association is commonly displayed as a compositional fabric or as a foliation in grains dominated by manganogrunerite and quartz separately. However, within Ore C, no discernible fabrics were observed (Fig. 3.3C).

Table 3.3: Bulk mineralogy[1] of the magnetite-dominated ores along with applicable sulphide mineral ratios

Bulk mineralogy (wt. %)						
Minerals	**Chemical formula**	**A**	**B**	**C**	**D**	**F**
Sphalerite	$(Zn_{0.9}Fe_{0.1})S$	3.1	2.6	0.6	0.1	0.4
Chalcopyrite	$CuFeS_2$	1.6	2.0	0.6	1.4	3.7
Galena	$Pb_{1.3}S$	0.5	0.5	6.4	0.2	1.7
Economic sulphides (ES)		5.3	5.2	7.6	1.7	5.8
Pyrrhotite	FeS	2.0	2.0	0.8	0.2	0.2
Pyrite	FeS_2	1.1	0.9	1.0	1.2	0.5
Fe-sulphide gangue (SG)		3.1	2.9	1.8	1.4	0.7
Total sulphide		8.4	8.1	9.4	3.0	6.5
Magnetite	$Fe^{2+}Fe^{3+}{}_2O_4$	57.1	53.8	58.8	65.6	74.1
Quartz	SiO_2	6.8	6.8	2.5	9.2	16.8
Grunerite	$(Mg_{2.5}Fe_{2.8}Mn_{1.6})[Si_8O_{22}](OH)_2$	5.5	3.5	0.6	20.4	0.1
Pyroxmangite	$(Mn_{0.6}Fe_{0.3})[SiO_3]$	21.0	26.2	27.7	0.4	0.1
Apatite	$Ca_{4.8}(PO_4)_{2.9}(OHF_{1.4})$	0.9	0.7	0.5	0.8	0.5
Other		0.4	1.0	0.6	0.7	2.0
Non-sulphide gangue (NSG)		91.6	91.9	90.6	97.0	93.5
Mineral ratios						
ES/SG		1.7	1.8	4.3	1.2	8.6
ES/NSG		0.1	0.1	0.1	0.0	0.1
NSG/(ES+SG)		10.9	11.3	9.7	32.0	14.5

[1]Notes:

1. Average chemical formulas from Rudnick (2016).

2. Bornite and covellite are grouped with chalcopyrite

3. Chromite, ilmenite and jacobsite are grouped with magnetite

4. Other minerals include arsenopyrite, sillimanite, feldspar (albite, microcline and anorthite), mica (muscovite, biotite and annite), chlorite, fluorite, barite, rhodonite, pyrolusite, garnet (spessartine, almandine and andradite), pyroxene (augite and diopside), monazite, bismuthinite, molybdenite and spinel (gahnite, hercynite, chromohercynite).

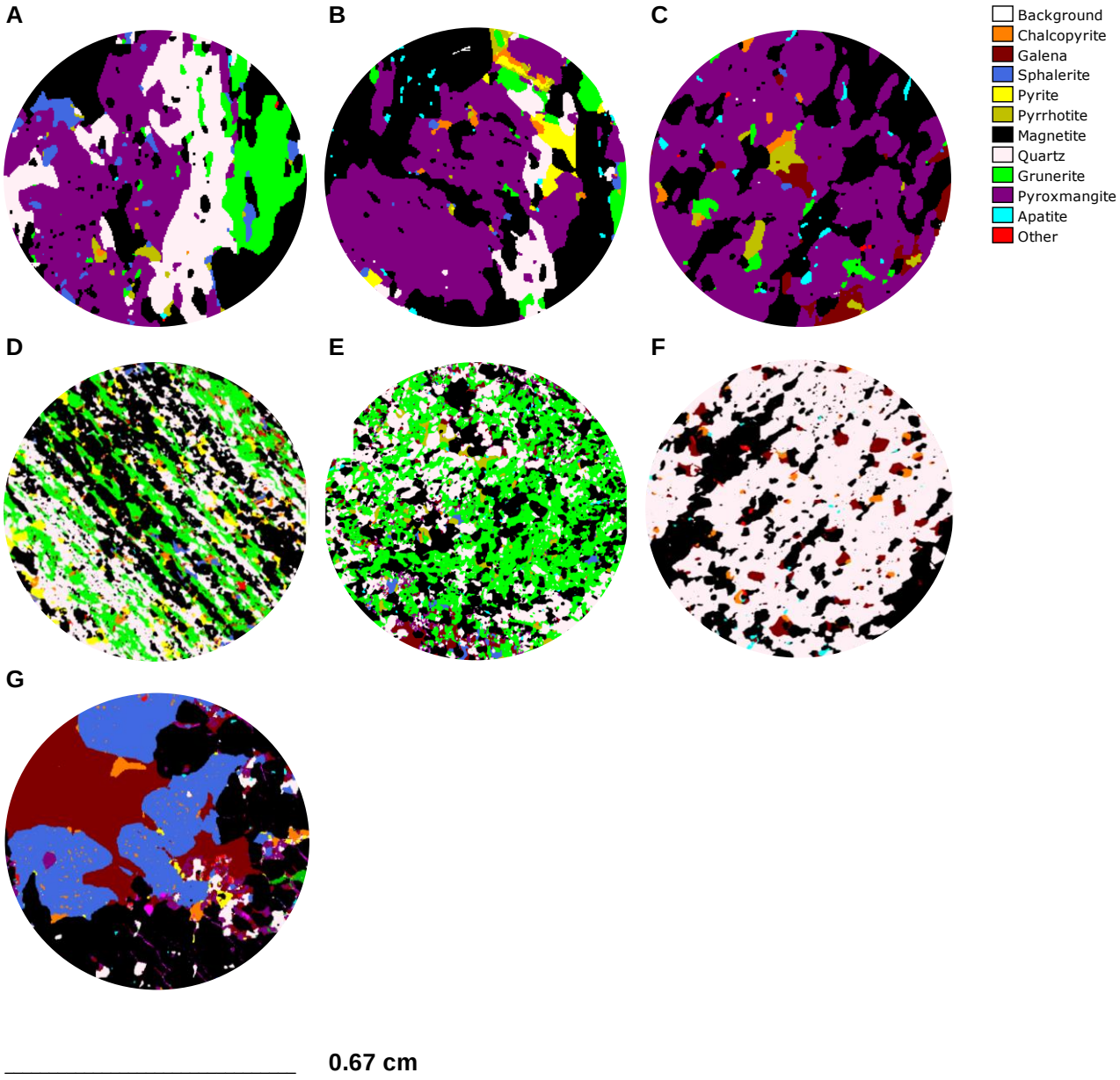

Figure 3.3: *QEMSCAN false colour field images of the magnetite dominated ores. Labels A through F represent the six secondary lithological ore types focussed on during this study. Note. The image for Ore E was generated from drill core during the primary ore characterisation (Gordon et al., 2018). Image G represents the observed chalcopyrite disease in Ores A, B and C*

3.4.2.2. Ore D (and by inference E)

ES minerals are present in quantities equalling 1.7 wt. %, whereas SG minerals define 1.4 wt. % of the bulk mineralogy. NSG minerals occupy the remaining 97 wt. % of Ore D. Ores D and E are dominated by magnetite (65.5 wt. %), grunerite (15 wt. % grunerite and 5.3 wt. % manganogrunerite) and quartz (9.2 wt. %). Chalcopyrite (1.4 wt. %) dominates sphalerite (0.1 wt. %) and galena (0.2 wt. %) as the main ES mineral, with pyrite (1.2 wt. %) dominating pyrrhotite (0.2 wt. %) as the main SG mineral. Notable minerals within the 'other' category include annite (0.2 wt. %), apatite (0.8 wt. %) and almandine (0.1 wt. %). Where

noticeable amounts of economic sulphides are present, there is a strong association of galena and sphalerite (with chalcopyrite disease). The association of pyrrhotite with galena is also prevalent. The main textural feature of Ore D is the strong foliation defined by elongated grunerite-manganogrunerite, quartz and magnetite (Fig. 3.3D), although massive varieties also occur. The bulk mineralogical data presented here is in agreement with QXRD data of Ore E.

3.4.2.3. Ore F

The ES mineral content within Ore F is 5.8 wt. %, the SG mineral content is 0.7 wt. %, while NSG minerals define the remaining 93.5 wt. % of the bulk mineralogy. Ore F is dominated by magnetite (74.1 wt. %) and quartz (16.8 wt. %). Chalcopyrite is the dominant ES mineral (3.7 wt. %) and galena, the subordinate ES mineral (1.7 wt. %). Sphalerite is present in lesser amounts (0.4 wt. %). Pyrite (0.5 wt. %) is the dominant SG mineral followed by pyrrhotite (0.2 wt. %). Notable minerals within the 'other' category include sillimanite (0.6 wt. %), annite (0.3 wt. %), barite (0.2 wt. %), spessartine (0.2 wt. %) and almandine (0.3 wt. %). Gangue mineral textures indicate a foliation defined by magnetite and quartz. A strong association of chalcopyrite and galena often overprints this fabric (Fig. 3.3F).

3.4.3. Flotation experiments

Solids-water recovery curves of the ES minerals show high solids recovery at the start of the float that thereafter levels off (Fig. 3.4). Ores C, B and A achieved the highest overall solids-water recovery (137.9, 135.9 and 130.3 g respectively), Ore F achieved an intermediate solids-water recovery (89.12 g) while Ores D and E achieved the lowest overall solids-water recovery (49.8 and 46.7 g respectively) (Fig. 3.4a). Ore F achieved the highest Cu-water recovery (15.9 g) (Fig. 3.4b), Ore C achieved the highest Pb-water recovery (54.7 g) (Fig. 3.4c), while ore A achieved the highest Zn-water recovery (23.8 g) (Fig. 3.4d). The recovery vs water of Fe and Mn shows a continued increase of Fe and Mn throughout the float in Ores A, B and C with linear solids-water recovery curves of Mn and Fe. Ore B recovered the highest Fe (50 g), whereas Ore C recovered the highest Mn (6.5 g) (Figs. 3.4e and f).

All ores achieved over 90% Cu recovery (lowest recovery is at 92.6 and highest at 98.1 %), whereas both Pb and Zn recoveries were more variable (Table 3.4B). Pb recoveries varied between 79.6 and 96.0 %, while Zn recoveries were even more variable between 40. 9 % and 92.0 %. Ore F achieved the highest Cu concentrate grade (17.9 %), Ore C the highest Pb concentrate grade (39.9 wt. %), and Ore A the highest Zn concentrate grade (18.4 wt. %). Ore B has the highest Fe grade (34.9 wt. %) and Ore C has the highest Mn grade (4.71 wt. %). When comparing recovery trends across the ores, Ore F achieved the highest Cu and Pb recoveries (98.1 and 96 wt. % respectively) (Figs. 3.5a and b), whereas Ore A achieved the highest Zn recovery (92 wt. %) (Fig. 3.5c). Similar to the concentrate grade patterns, Ore B achieved the highest Fe recovery (6.4 wt. %), whereas Ore C achieved the highest Mn recovery (7.8 wt. %) (Figs. 3.5d and e).

Table 3.4: ***Average metal recovery and concentrate grade of the magnetite-dominated ores following bulk sulphide flotation. Error, indicated in brackets, from chemical assay data of duplicate floats.***

Concentrate grade (wt. %)					
Ores	**Cu**	**Pb**	**Zn**	**Fe**	**Mn**
Ore A	5.8 (0.0)	4.3 (0.0)	18.4 (0.0)	34.9 (0.0)	3.5 (0.2)
Ore B	6.4 (0.0)	4.7 (0.0)	14.5 (0.0)	36.4 (0.3)	3.6 (0.1)
Ore C	1.9 (0.0)	39.9 (0.4)	3.1 (0.0)	21.5 (0.0)	4.7 (0.0)
Ore D	10.3 (1.3)	4.1 (0.4)	1.2 (0.1)	33.4 (0.7)	0.9 (0.1)
Ore E	9.1 (0.8)	20.5 (1.6)	0.5 (0.0)	22.9 (1.5)	0.9 (0.1)
Ore F	17.9 (0.3)	18.6 (0.0)	3.2 (0.0)	25.2 (0.4)	0.2 (0.0)
Concentrate recovery (wt. %)					
Ores	**Cu**	**Pb**	**Zn**	**Fe**	**Mn**
Ore A	95.2 (0.1)	79.7 (0.6)	92 (0.0)	5.6 (0.1)	5.8 (0.3)
Ore B	94.3 (0.3)	81.1 (0.9)	90.1 (0.3)	6.4 (0.1)	6.4 (0.2)
Ore C	93.5 (0.8)	91.6 (0.9)	71.5 (0.2)	4.2 (0.1)	7.8 (0.1)
Ore D	92.6 (0.4)	79.6 (1.8)	52.7 (3.9)	2.4 (0.1)	3.6 (0.1)
Ore E	94.1 (0.3)	90.8 (0.5)	40.9 (2.1)	1.7 (0.0)	3.7 (0.3)
Ore F	98.1 (0.9)	96 (1.3)	89.9 (0.7)	3.3 (0.0)	5.4 (0.0)

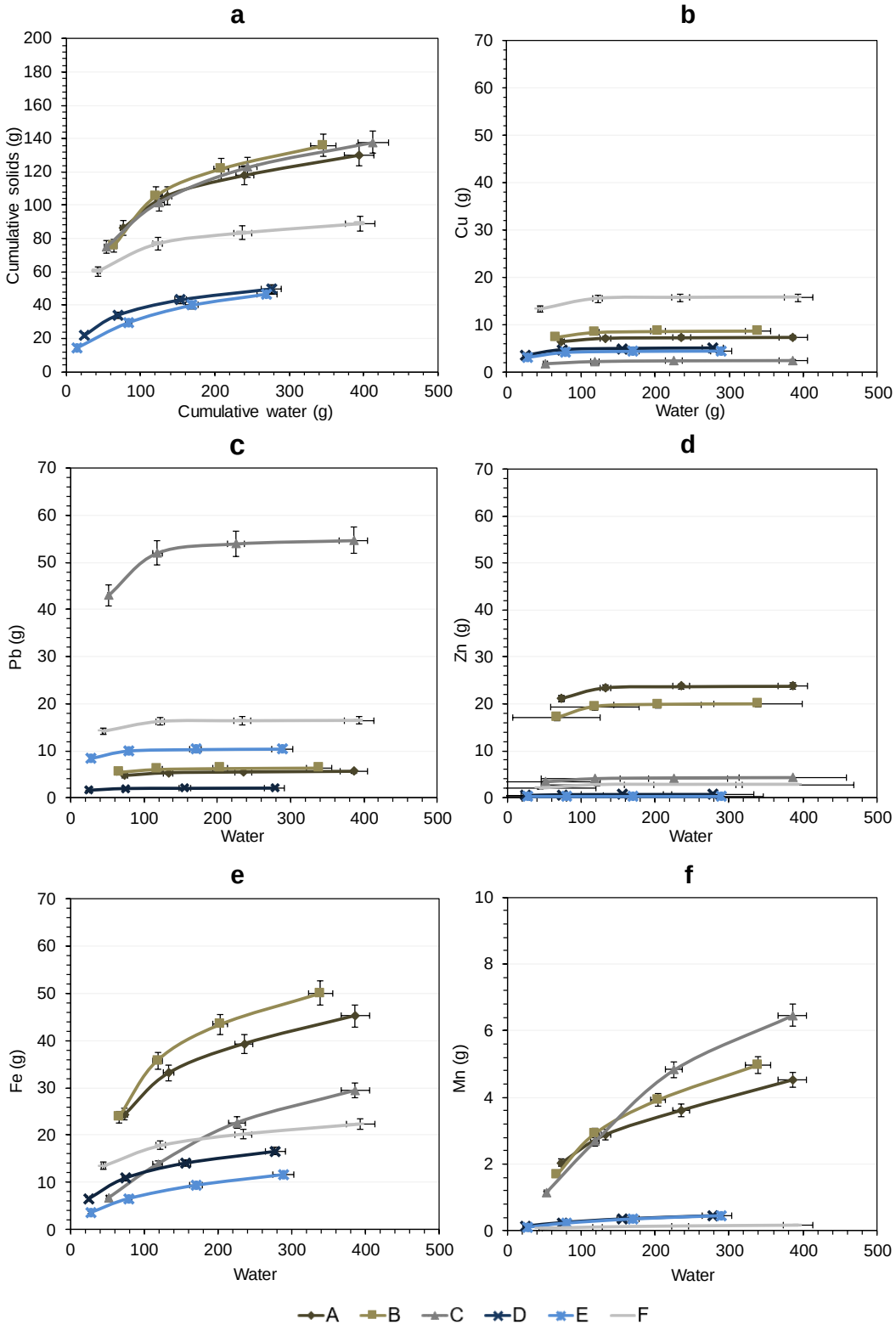

Figure 3.4: *(a) Total solids vs water recovery; (b) Cu element mass vs water recovery; (c) Pb element mass vs water recovery; (d) Zn element mass vs water recovery; (e) Fe element mass vs water recovery; and (f) Mn element mass vs water recovery. Error bars represent standard deviation between the chemical assay data of duplicate floats. Note the difference in scales of Fe and Mn.*

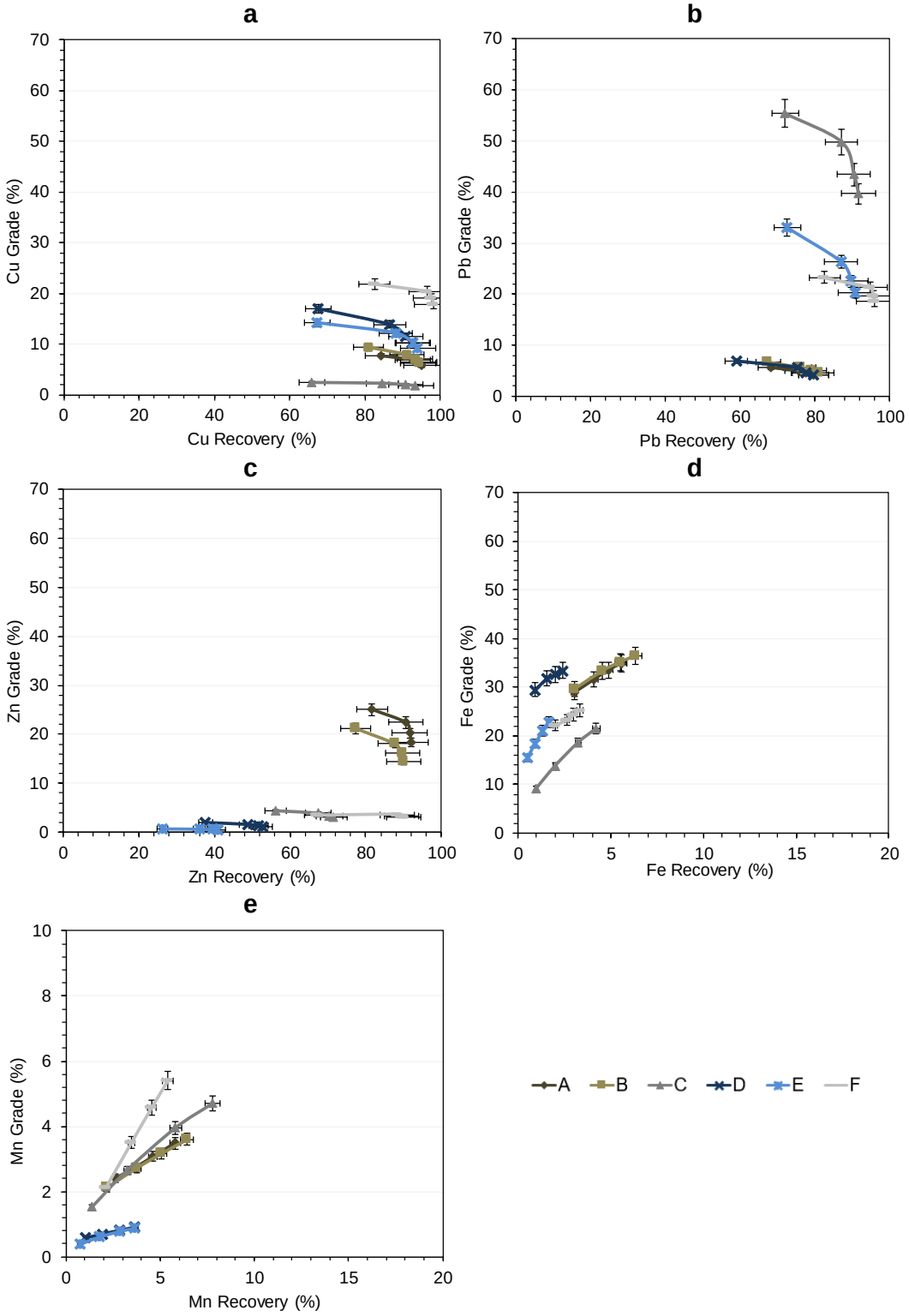

Figure 3.5: *(a) Elemental grade recovery curves of Cu; (b) Elemental grade and recovery of Pb; (c) Elemental grade and recovery of Zn; (d) Elemental grade and recovery of Fe; and (e) Elemental grade and recovery of Mn. Error bars represent the standard deviation between the chemical assay data of duplicate floats. Note the difference in scales of Fe and Mn.*

3.4.4. Mineral liberation and association characteristics

Table 3.5 summarises the liberation states for chalcopyrite, galena and sphalerite within the different magnetite dominated ores Liberation here is defined as the percentage of the mineral (by weight) greater than 90 % within the particle of interest. Ore F is most liberated for chalcopyrite (88 % liberated), followed by Ores C, A and B (64, 63 and 61 % respectively). The lowest chalcopyrite liberation occurs for ore D (50 % liberated). Ores B, A and D have the lowest amount of liberated galena (42 – 47 %), whereas Ores C and F are the best-liberated (64 % and 78 % respectively). Sphalerite is well liberated in Ores A and B (73–78 %), whereas Ores C, D and F are poorly liberated (33-45 %). Overall, Ores A and B are similarly liberated for chalcopyrite, galena and sphalerite. Ore D illustrates a similar liberation state as Ores A and B for galena and sphalerite. Ore F is most liberated for chalcopyrite and galena, and least liberated for sphalerite. Ore C closely follows this pattern.

Table 3.5: *Mineral liberation across the different magnetite dominated ore types. A liberated particle here is defined as the mineral of interest (by area) making up greater than 90 % of the particle of interest. ES particle count in brackets.*

Mineral liberation of ES minerals					
	Ore A	**Ore B**	**Ore C**	**Ore D**	**Ore F**
Economic sulphides	(74,516)	(81,644)	(127,286)	(22,706)	(52,292)
Chalcopyrite	63 (25,866)	61 (35,436)	64 (15,636)	50 (19,158)	88 (35,227)
Galena	47 (6,831)	42 (6,146)	64 (99,441)	43 (1,971)	80 (13,798)
Sphalerite	77 (41,819)	73 (40,062)	45 (12,209)	33 (1,577)	78 (3,267)

Figure 3.6 illustrates the association of unliberated chalcopyrite, galena and sphalerite within the magnetite ores. The association percentage quantifies the relationship between unliberated ES mineral grains to one another and gangue minerals. Unliberated chalcopyrite in ores A-B-C shows a strong association with pyroxmangite (16 – 22 %) and sphalerite (6 – 12 %). In contrast, unliberated chalcopyrite in ore D shows a strong association with iron sulphides (16 %), pyroxmangite (11 %) and grunerite (7 %) (Fig. 3.6a). Particles with low galena liberation are associated with pyroxmangite (8 – 41 %), Fe sulphides (5 -11 %), grunerite (0 – 12 %) and magnetite (3 – 10 %) (Fig. 3.6b). Unliberated sphalerite within this ore is associated with chalcopyrite (12 – 14 %), magnetite (16 – 18 %) and pyroxmangite (4 – 16 %) (Fig. 3.6c).

Theoretical grade-recovery curves for each ore (Fig. 3.7) take into account the liberation states of chalcopyrite, galena and sphalerite as well as their associations to other SG and NSG minerals. Hence, the relationship between the ores in terms of their theoretical grade-recovery curves (Fig. 3.7) can be considered an early indication of the potential grade-recovery similarities expected from the magnetite-dominated ores. Ore F is most liberated for both chalcopyrite and galena, and hence the greatest recovery potential. Ores A and B cluster very tightly for chalcopyrite, galena and sphalerite, whereas Ore D

infrequently follows the same trend as Ores A and B. Ore C is closer to Ore F for both galena and sphalerite, but closer to Ores A and B for chalcopyrite.

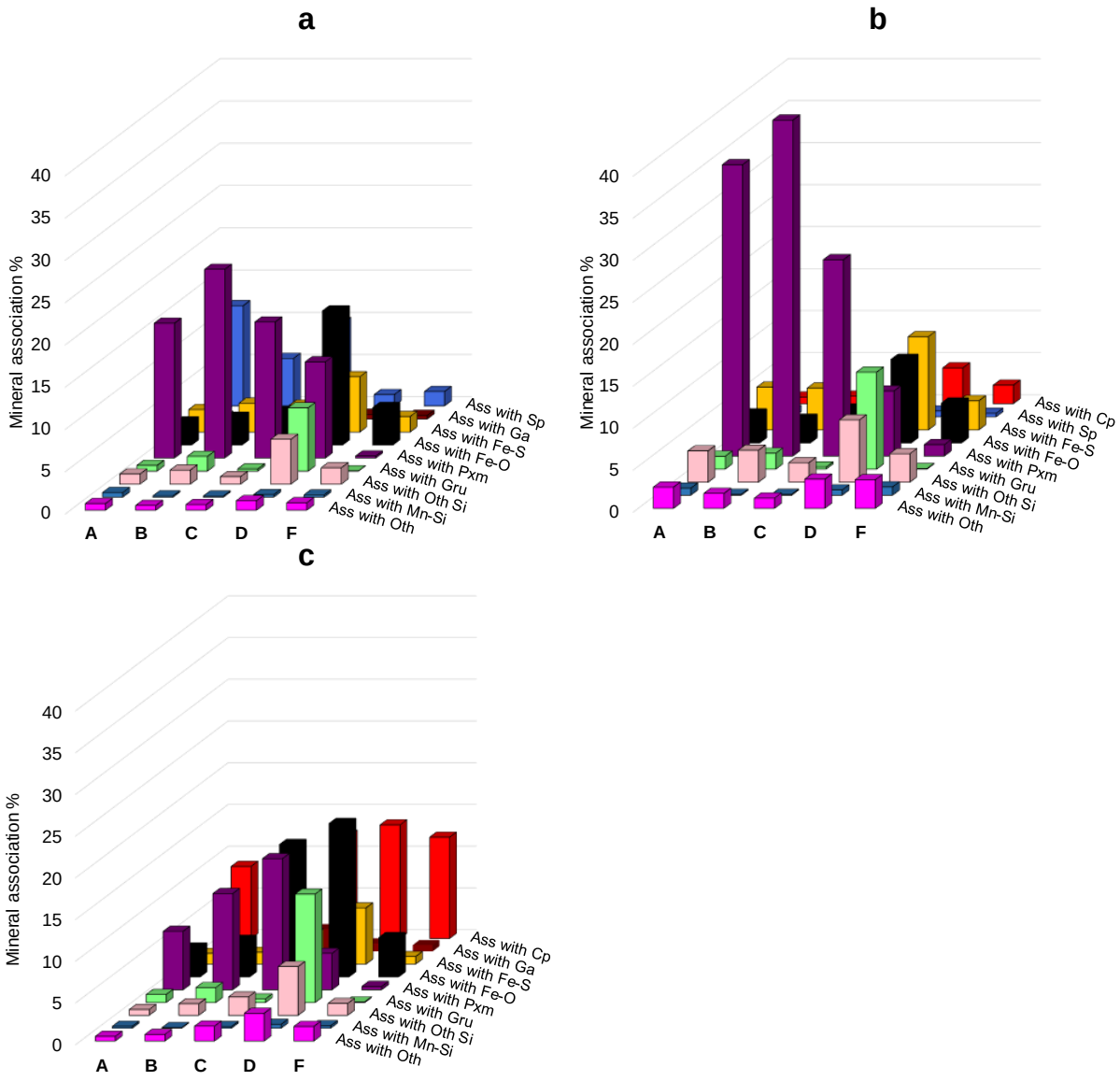

Notes: *Cp: Chalcopyrite, covellite and bornite,*
Sp: Sphalerite, Ga: Galena,
Fe-S: Pyrite, pyrrhotite and arsenopyrite,
Fe-O: Magnetite, jacobsite, chromite and ilmenite,
Pxm: Pyroxmangite, Gru: Grunerite,
Oth Si: Quartz, sillimanite, feldspar, mica, chlorite, garnet (almandine and andradite) and pyroxene,
Mn-Si: Rhodonite, pyrolusite and spessartine,
Oth: Fluorite, apatite, barite, gahnite, bismuthinite, molybdenite, monazite and spinel.

Figure 3.6: *Mineral association data for (a) unliberated chalcopyrite grains; (b) unliberated galena grains; and (c) unliberated sphalerite grains across the different magnetite dominated ore types.*

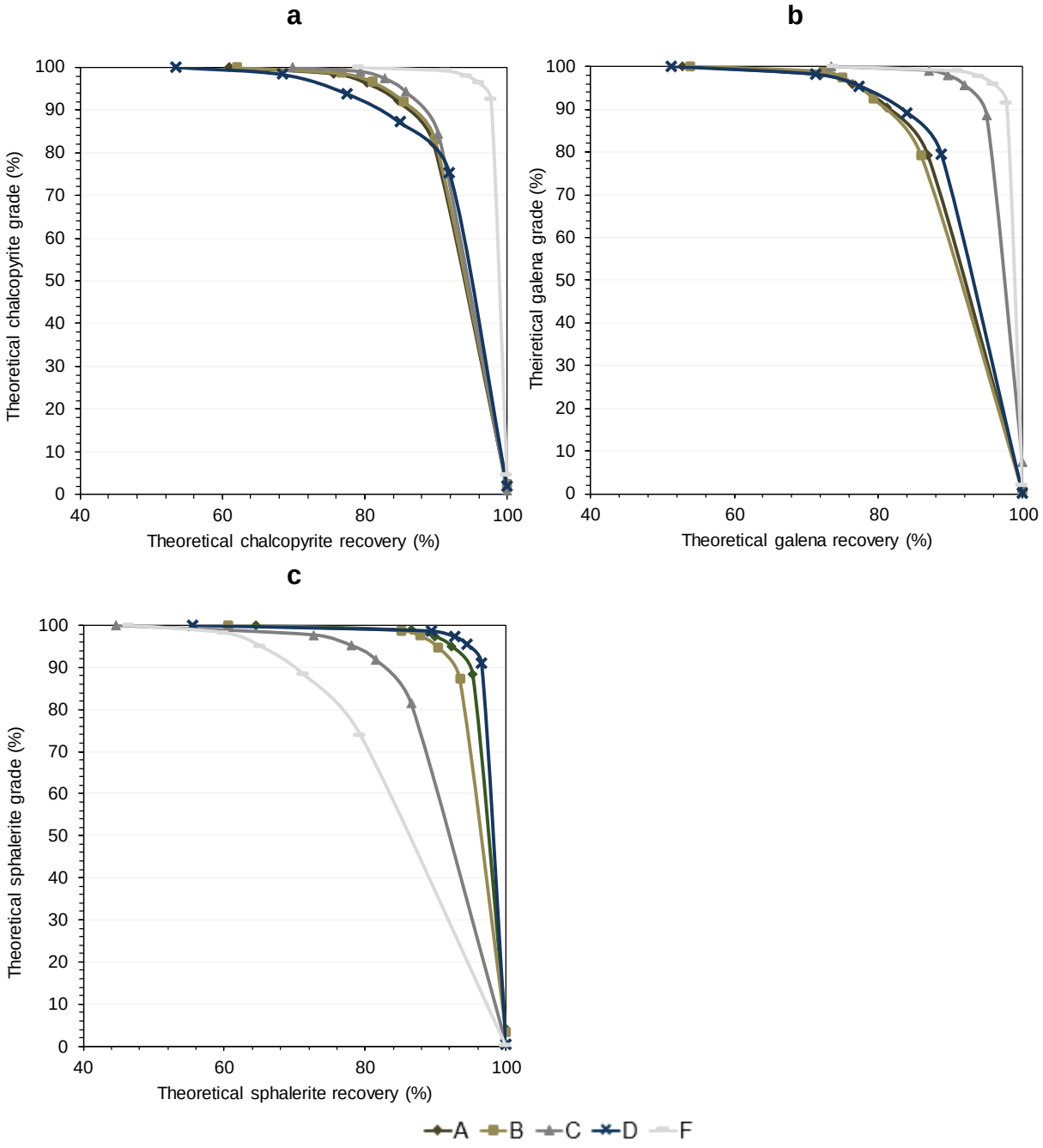

Figure 3.7: *Theoretical grade-recovery curves for magnetite-dominated ores: (a) chalcopyrite; (b) galena; and (c) sphalerite*

3.5. Discussion

Through assessment of the information presented in section 4, groupings of ore types based on mineralogical characteristics and flotation responses are discussed in the following section. This discussion is aimed at understanding why these domains are behaving differently than the minerals-based domains that were proposed in Gordon et al. (2018); what are the process mineralogical considerations attached to these domains and what are the capabilities of the current dataset to support predictive elemental proxies.

3.5.1. Validating the magnetite-dominated geometallurgical domains

The magnetite-dominated geometallurgical domain proposed by Gordon et al. (2018) was based on differences in the bulk mineralogy, chalcopyrite grain size distribution and textural characteristics of the AM and QM lithological units. The mineralogical and textural variability between the QM and AM units was considered to be less significant than the difference between these units and the LOB and GQZ domains. Since textural and mineralogical variability are indicators of processing response (throughput, liberation, grade and recovery), the grouping of the AM and QM into one geometallurgical domain was justified. This was even though there were differences in the NSG population and chalcopyrite grain size distribution. However, the mineralogical and textural variability documented in this study for both the AM and QM units has now shown that the AM and QM units define three distinct geometallurgical domains. These domains are differentiated based on the processing responses of quartz -, grunerite - and pyroxmangite-dominated ores. This has resulted in the AM being divided into two geometallurgical domains (previously considered as one lithological unit; Stedman (1980) and Rudnick (2016)), and the QM defined as a domain in its own right. These domains are defined as (Table 3.3): (1) a PQM domain where ores are dominated by magnetite and pyroxmangite with subordinate amounts of manganogrunerite (Ores A, B and C); (2) an AM domain where ores are dominated by magnetite and grunerite with subordinate amounts of quartz with little pyroxmangite (Ores D and E); (3) a QM domain where ores are dominated by magnetite and quartz with no pyroxmangite or grunerite (Ore F).

The PQM domain has a definitive chalcopyrite-galena-sphalerite zonation that is associated with several other NSG minerals. In spite of this, excellent mass pull and ES concentrate grades and recoveries were attained. This is supported by the high solids recovery during flotation of Ores A, B and C (Figs. 3.4 and 3.5). However, associated with this domain is the potential for problematic ES-pyroxmangite middlings () and pyroxmangite entrainment that could result in elevated Mn values in the concentrate (Figs. 3.4f, 3.5e and 3.6; Table 3.4). Lower-grade, finer-grained and locked ES particles (in middlings with a wide variety of SG and NSG) are prevalent within the AM domain. This translates to its poor liberation and flotation performance (Figs. 3.4 and 3.5; Table 3.5). The QM domain has the most straightforward mineralogical breakdown with associated coarser-grained and well-distributed chalcopyrite-galena zonation (Table 3.3, Fig. 3.3F). This translates to excellent liberation and best overall flotation performance, supported by elemental recovery-water curves (Fig. 3.4), grade-recovery curves (Fig. 3.5) and the liberation state of chalcopyrite and galena (Table 3.5).

3.5.2. Considerations associated with the processing of polymetallic sulphide ores

The interdependence of the mineralogical - and elemental characteristics and their respective minerals processing behaviour has been used to define distinct domains. These domains are further explored to propose how their respective feeds would behave in a processing circuit without blending (since the ores were processed distinctly within this study to obtain the process mineralogical differences). Considering the nature of the mineralogical characteristics within the domains, some potential issues are discussed

in the section below. Some of these issues will be site-specific based on the characteristics of the BMC ore, whereas others may be common issues within polymetallic Cu-Pb-Zn ores.

Chalcopyrite and galena are commonly fast-floating minerals; however, sphalerite is known to vary in this regard (Johnson, 2016). Low recoveries of sphalerite can be attributed to a slower flotation rate. Taking into consideration that sphalerite is normally activated using copper sulphate, which was not done during this study, where problems arise with sphalerite recovery; care should be given to ascertain the specific flotation rate of sphalerite within such ores and modify the flotation parameters accordingly (Lotter and Fragomeni, 2010; Johnson, 2016).

There is a well-established link between feed grade, grain size, liberation and recovery (Evans and Morrison, 2016). Variability in the grain size, ES mineral grade and sulphide mineral texture will induce variability in the throughput of ores, concentrate grades and recoveries of ES (Bradshaw et al., 2016; Johnson, 2016). To achieve consistent recoveries, concentrator plants need to process a blend of ores that have consistent feed grades, grain sizes, and liberation states.

Exsolution textures of chalcopyrite and galena can be advantageous in bulk sulphide flotation where chalcopyrite and galena are recovered together, and sphalerite recovered as a separate product; however, the opposite is true for associations of chalcopyrite and sphalerite, or galena and sphalerite in bulk sulphide flotation (Bojcevski et al., 1998). These associations are also problematic in sequential flotation and will induce chalcopyrite-galena-sphalerite selectivity issues whereby sphalerite and galena are recovered in the copper concentrate and lost to the Pb and Zn concentrates resulting in low Pb and Zn recoveries.

Where Mn is recovered to the concentrate, it is problematic and could lead to smelting penalties if not carefully monitored (Lane et al., 2016). The recovery of Mn to the Zn concentrate from the ores of the neighbouring Gamsberg deposit has been attributed to the presence of Mn as a solid solution element within sphalerite, or the mineral alabandite (MnS). Silicate minerals such as spessartine and a variety of pyroxenes and pyroxenoids also host Mn at Gamsberg. (McClung and Viljoen, 2010; Schouwstra et al., 2010). Mineral chemistry data from Rudnick (2016) confirms that Mn is not present as a solid solution element within sphalerite minerals for this deposit and none of the mineralogical examinations has revealed the presence of alabandite. Examination of the Mn distribution highlights that the major host of Mn in these ores is pyroxmangite and grunerite (Fig. 3.8). Therefore, potential mechanisms responsible for elevated Mn in the concentrate in this study are the recovery of locked ES-pyroxmangite composite particles or entrainment given the high grade of Mn minerals for some of the ores in this study (Table 3.3). More detailed size-by-size concentrate mineralogical analyses would inform whether the treatment strategy to minimise this requires additional liberation of ES-Mn mineral composites, or simply blending of ores to manage Mn feed grades.

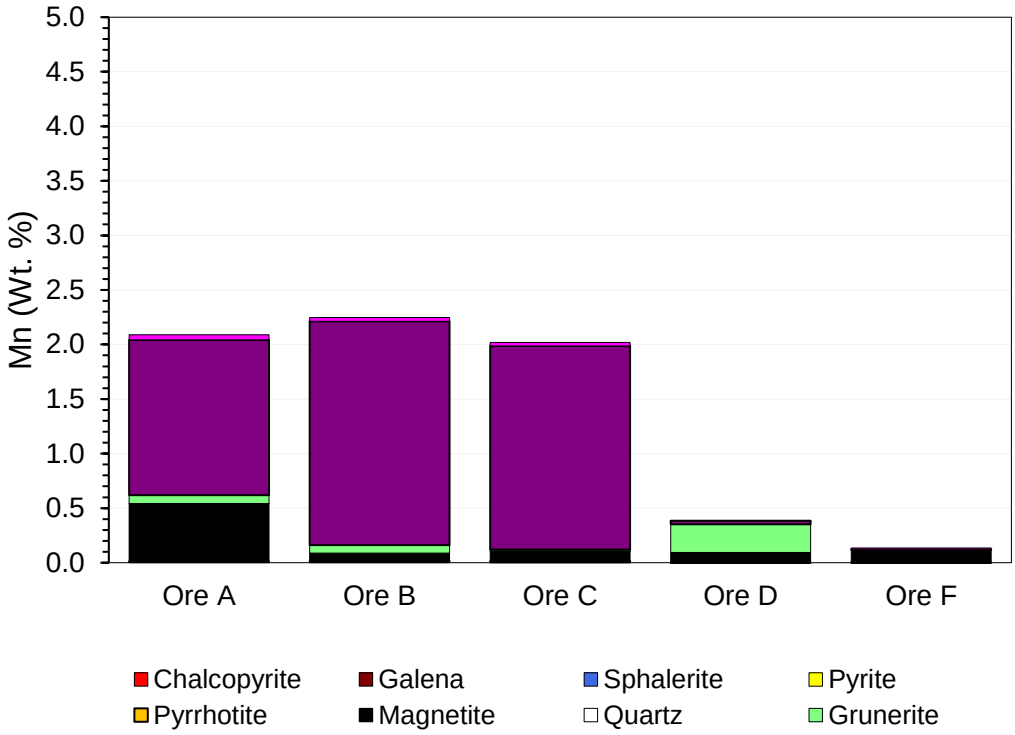

Figure 3.8: *Combined manganese deportment in all magnetite-dominated ores.*

When considering the comminution of ores, it is also important to consider the concentration ratios for the same set of ores. The concentration ratio is defined as the weight of the metal in the feed relative to the weight of the metal in the concentrate (Kawatra and Eisele, 2002). The calculated value indicates how many ROM tonnes is required to produce one tonne of Cu, Pb and Zn concentrate respectively. Note however that these numbers should not be considered absolute, given the calculations are based solely on batch flotation behaviour, but more as a relative indication of the potential differences in the processability of the different ores (Fig. 3.9). Lower-grade ores will require more ROM tonnes to produce one tonne of Cu, Pb and Zn concentrate respectively e.g. the AM domain requires 2.5x more ROM tonnes than the QM domain and 3x more ROM tonnes than the PQM domain.

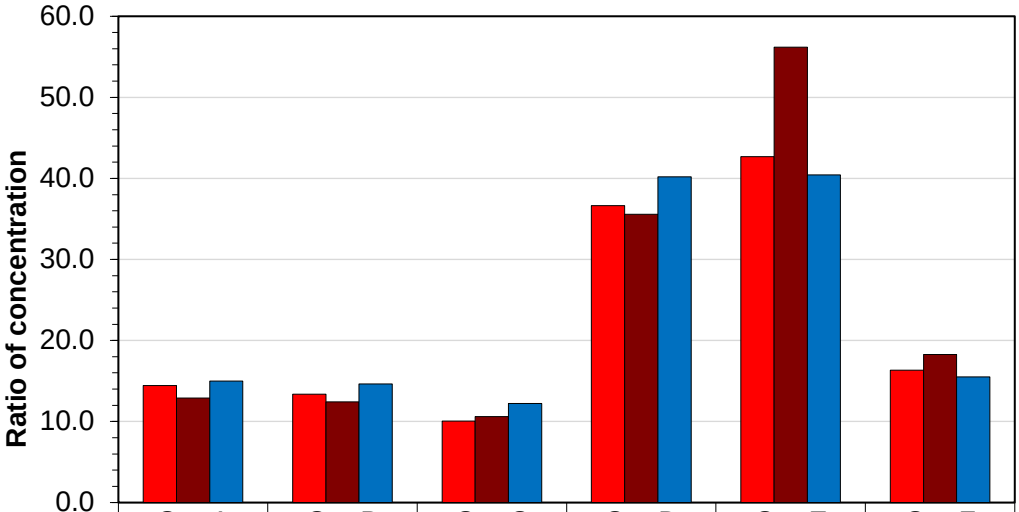

	Ore A	Ore B	Ore C	Ore D	Ore E	Ore F
Cu	14	13	10	37	43	16
Pb	13	12	11	36	56	18
Zn	15	15	12	40	40	16

Figure 3.9: *Concentration ratios for the magnetite dominated ores. The concentration ratio is defined as the weight of the element in the feed (g) relative to the weight of the element in the concentrate (g)*

3.5.3. Predictive elemental proxies in polymetallic sulphide deposits

There is a challenge with integrating the characteristics of the domains back into the geological block model and subsequent grade control practices to be able to predict the characteristics of a feed of ores. To achieve the required predictive capability and selectivity in mining and processing of the domains, fit for purpose ore characterisation data is required on a sample-by-sample basis (Coward et al., 2009; Ehrig, McPhie and Kamenetsky, 2012). Ideally, this data should be readily available, relatively inexpensive and have rapid turnaround times – as is the case for elemental/chemical assay data. Therefore, strong elemental proxies such as the Cu:S ratio derived from routine chemical assay data can potentially substitute for the more costly automated mineralogy datasets. The Cu:S ratio has been used successfully in describing complex copper mineralogies, ROM feeds, copper concentrate grades and smelter throughputs (Dunham and Vann, 2007; Ehrig et al., 2012; Butler et al., 2016, Liebezeit et al., 2016).

Figure 3.10 illustrates the distribution of Cu:S ratios for the three magnetite-dominated domains. Where the Cu: S ratio equals one (Cu = S) ores can be grouped on the premise that mineralisation is predominantly defined by chalcopyrite. Ores that have multiple sulphide minerals, would cluster towards the Cu<S portion of the graph, whereas ores in which other species of copper sulphide are present (in which the amount of Cu in these minerals exceeds the amount of Cu in chalcopyrite), would cluster to the Cu>S portion of the graph. Because of this, ores with similar Cu:S ratios can be considered to behave similarly during minerals processing e.g. ores that plot higher up and closer to the Cu = S line can be inferred as ores that will behave favourably during minerals processing because of its monomineralic ES nature. Ores that plot lower down on the Cu = S line are considered complex and associated with it are

considerations involving liberation and problematic gangue mineral association. Ores that plot towards the S > Cu side can be considered as ores in which there will be competition during flotation (from either ES or SG).

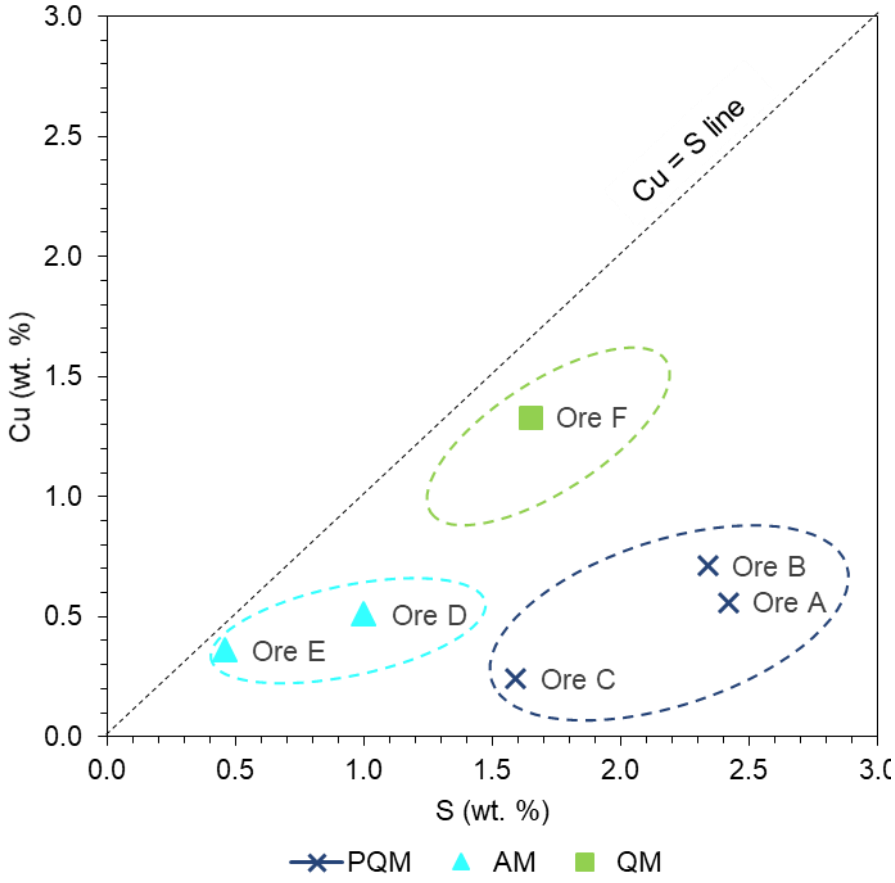

Figure 3.10: *Copper to sulphur ratios of the proposed geometallurgical domains. Ellipses represent the most likely distribution of the ratios.*

The best flotation response for chalcopyrite and galena was obtained from Ore F. Ore F plots the closest to the Cu = S line and hence it is inferred that ores with a similar bulk elemental composition as Ore F will plot in the same vicinity on the Cu:S graph and by extension illustrate the same minerals processing behaviour. The ellipse indicates the most likely distribution of QM type ores. Ore E plots close to the Cu = S line, however the finer-grained and lower grade nature of the AM ores has implications for their processing response. Hence, domains similar to the AM domain can be constrained using a lower grade threshold, possibly between the data points of Ore D and Ore C. The distribution of the PQM domain indicates several processing considerations. The amount of sulphur within the ore greatly exceeds the amount of Cu, hence it can be deduced that the sulphur reports to either galena, sphalerite, pyrrhotite or pyrite, minerals that might be competitive during flotation. The presence of galena and sphalerite can be explored using Pb:S and Zn:S, however, the magnitude of gangue sulphides would prove more difficult to ascertain because of the shared Fe in chalcopyrite and sphalerite as well as other Fe-bearing silicate minerals. By extension, since the

PQM domain is mineralogically complex, the presence of other S-bearing minerals apart from the ES and SG minerals such as barite, bismuthinite, molybdenite, arsenopyrite can be explored using relevant Ba:S, Bi:S, Mo:S and As:S ratios compared to the Cu:S ratio.

3.6. Conclusions

The complex nature of the magnetite-dominated ores of the polymetallic deposit is defined by variable bulk mineralogies, bulk chemistry and textures. This translates to distinct mineral processing responses. Constraining the variability within the magnetite-dominated ores required the use of geometallurgical domains that aim to group ores due to similarities in their physiochemical makeup and their respective flotation behaviours.

The magnetite-dominated ores can be subdivided into three geometallurgical domains: A Cu-Zn-Pb Pyroxmangite-Quartz-Magnetite domain (Ores A, B, C); a Cu-Pb ± Zn Amphibole-Magnetite domain (Ores D, E) and a Cu-Pb ± Zn Quartz Magnetite domain (Ore F). When considering mineralogy, the QM domain is characterised as the most straightforward with the best flotation performance, whereas the PQM is the most variable and the AM has the worst flotation performance. Some key inferences on the processing responses of these ores considered the selectivity (especially when dealing with exsolution textures of chalcopyrite and sphalerite), as well as the undesirable recovery of the penalty element Mn to the concentrate (either through entrainment or recovery of composite ES-Mn mineral middlings).

The Cu: S ratio shows promise for the identification of domains within magnetite-dominated ores in which there are distinct metal zonation patterns that can be used to group ores that will behave the same, prior to minerals processing. A key component of using such an approach is the understanding of the bulk mineralogy, mineral composition and metal zonation. The complexity of such characteristics might require that several such proxies are used concurrently when the mineralogy is variable e.g. Pb:S, Zn:S, Ba:S, Bi:S, As:S etc. However, the limited dataset of the five data points needs validation to truly illustrate the potential heterogeneity of each of the domains when there is variability in head grade.

It is thus suggested that the Cu:S be further explored to constrain the distribution of the domains and boundaries between the domains, such as the lower grade threshold for the AM ores and the distribution of the mineralogically variable PQM ores. Furthermore, it is suggested that the integration of the Cu:S ratio into the Concentrator be based on a reconciliation of head grade data to align variable recoveries with geometallurgical domains, particularly when considering sequential rather than bulk sulfide flotation. Considering that a detailed mineralogical investigation of Ag was beyond the scope of this study, the question as to its response and effect on the geometallurgical domain classification remains unsolved. It is thus suggested that follow up work be conducted on the minerals processing response of Ag from this deposit.

3.7. Acknowledgements

Grateful appreciation is acknowledged to the CMR Process mineralogy and laboratory staff, in particular, Gaynor Yorath, Monde Bekaphi, Lorraine Nkemba and Keshree Pillay for sample preparation, QEMSCAN and QXRD measurements. The authors would also like to acknowledge the efforts of employees at Black Mountain Mining (Pty). Ltd. for providing logistical support during sampling, travelling, site visits and block analysis periods, and the executive management team for providing financial support.

3.8. References

Becker, M, Wightman, E.M and Evans, C.L. (2016). Process Mineralogy. Julius Kruttschnitt Mineral Research Centre, The University of Queensland, Australia. 250-260.

Bojcevski, D., L. Vink, N. W. Johnson, V. Landmark, J. Mackenzie, and M. F. Young. (1998). Metallurgical characterisation of George Fisher ore textures and implications for ore processing. In Proceedings: Mine to Mill Conference, pp. 29-42.

Bradshaw, D.J. (2014). The role of 'process mineralogy' in improving the process performance of complex sulphide ores: In: IMPC 2014, Santiago, Chile.

Bradshaw, D.J., Triffett, B., Latti, D., Wilkie, G. and Adair, B. (2016). Dealing with a problematic ore type at Kennecott Utah Copper Concentrator. (Eds.). Process Mineralogy. Julius Kruttschnitt Mineral Research Centre, The University of Queensland, Australia. 250-260.

Butler, C., Dale, R., Robinson, S. and Turner, A. (2016). Geometallurgy – Bridging the gap between Mine and Mill: A Case Study of the DeGrussa Geometallurgy Program. In: The third AUSIMM International Geometallurgy conference. 77-88. (The Australasian Institute of Mining and Metallurgy: Melbourne).

Cawood, T.R. and Rozendaal, A. (2019). A multistage genetic model for the stratabound Swartberg base metal deposit of the Mesoproterozoic Aggeneys-Gamsberg Ore District, South Africa. Submitted to the journal of Economic Geology.

Cornell, D.H., Thomas, R.J., Moen, H.F.G., Reid, D.L., Moore, J.M. & Gibson, R.L. (2006). The Namaqua-Natal Province. In: Johnson, M.R., Anhaeusser, C.R. & Thomas, R.J. (Eds.) The geology of South Africa. Johannesburg: Geological Society of South Africa & Council for Geoscience. 325-380.

Coward, S., Vann, J., Dunham, S. and Stewart, M. (2009). The primary-response framework for geometallurgical variables. In: Seventh International Mining Geology Conference. 109-113. (The Australasian Institute of Mining and Metallurgy: Melbourne).

Dominy, S.C., O'Connor, L.O. and Xie, Y. (2016). Sampling and Test Work Protocol Development for Geometallurgical Characterisation of a Sheeted Vein Gold Deposit. In: The third AUSIMM International Geometallurgy conference. 97-112. (The Australasian Institute of Mining and Metallurgy: Melbourne).

Dunham, S. and Vann, J. (2007). Geometallurgy, geostatistics and project value—does your block model tell you what you need to know. In Proceedings of the Project Evaluation Conference, Melbourne, Australia (pp. 19-20).

Ehrig, K., McPhie, J. and Kamenetsky, V.S. (2012). Geology and mineralogical zonation of the Olympic Dam iron oxide Cu-U-Au-Ag deposit, South Australia.

Evans, C.L. and Morrison, R.D. (2016). Mineral Liberation, in Becker, M, Wightman, E.M. and Evans, C.L. (Eds.). Process Mineralogy. Julius Kruttschnitt Mineral Research Centre, The University of Queensland, Australia. 219-233.

Fragomeni, D., Boyd, L.J., Charland, A., Kormos, L.J., Lotter, N.O., and Potts, G. (2005). The use of End-Members for Grind-Recovery Modelling, Tonnage Prediction and Flowsheet Development at Raglan, proc. Canadian Mineral Processors, Ottawa, January 2006, Paper 6, pp 75-98.

Gordon, H.J.J, Miller, J.A. and Becker, M. (2018). Using mineralogy for early-stage geometallurgical domain definition: A case study of the Swartberg polymetallic sulphide deposit. In Proceedings: The South African Institute for Mining and Metallurgy (SAIMM), Geometallurgy conference, pp. 121-131. 6-8 August 2018, Cape Town, South Africa.

Gu, Y., Schouwstra, R.P. and Rule, C. (2014). The value of automated mineralogy. Minerals Engineering, 58, pp.100-103.

Hill, H. (2019). Assessing the influence of mineralogy and texture on the ore breakage characteristics of drill core and crushed ore using the JKRBT. On-going Master's Thesis, University of Cape Town.

Johnson, N.W. (2016). Sphalerite and galena liberation levels for the Mt Isa concentrator. In: Becker M, Wightman EM, Evans CL (eds) Process Mineralogy: JKMRC Monograph Series in Mining and Mineral Processing, No 6. Julius Kruttschnitt Mineral Research Centre, Brisbane, Australia, pp 234–249

Johnson, N.W. and Munro, P.D. (2008). Methods for Assigning Domains in the Primary Sulphide Zone of a Sulphide Orebody. In: Ninth International Congress for Applied Mineralogy. 597-603.

Kawatra, S.K. and Eisele, T.C. (2002). Froth Flotation-fundamental principles. Research, Michigan Technical University, pp.1-30.

Kormos, L.J., Oliveira, J., Fragomeni, D., Whiteman, E. and Carrión De la Cruz, J. (2010). Process diagnosis using quantitative mineralogy. In Proceeding of the 42nd Annual Canadian Mineral Processors Conference (pp. 143-162).

Lamberg, P., Rosenkranz, J., Wanhainen, C., Lund, C., Minz, F., Mwanga, A. and Parian, M. (2013). Building a geometallurgical model in iron ores using a mineralogical approach with liberation data. In Proceedings of the Second AusIMM International Geometallurgy Conference, Brisbane, Australia (pp. 317-324).

Lane, D.J., Cook, N.J., Grano, S.R. and Ehrig, K. (2016). Selective leaching of penalty elements from copper concentrates: A review. Minerals Engineering, 98, pp.110-121.

Liebezeit, V., Ehrig, K., Robertson, A., Grant, D., Smith, M. and Bruyn, H. (2016). Embedding geometallurgy into mine planning practices—Practical examples at Olympic Dam. In Proceedings International Geometallurgy Conference; The Australasian Institute of Mining and Metallurgy: Melbourne, Australia (pp. 135-144).

Lotter, N.O. and Fragomeni, D. (2010). High-confidence flotation testing at Xstrata Process Support. Mining, Metallurgy & Exploration, 27(1), pp.47-54

Lotter, N.O., Baum, W., Reeves, S., Arrué, C. and Bradshaw, D.J. (2017). The business value of best practice process mineralogy. Minerals Engineering, 116, pp.226-238.

Lotter, N.O., Kowal, D.L., Tuzun, M.A., Whittaker, P.J. and Kormos, L. (2003). Sampling and flotation testing of Sudbury Basin drill core for process mineralogy modelling. Minerals Engineering, 16(9), pp.857-864.

Lund, C., Lamberg, P. and Lindberg, T. (2013). Practical way to quantify minerals from chemical assays at Malmberget iron ore operations–An important tool for the geometallurgical program. Minerals Engineering, 49, pp.7-16.

McClung, C.R., Gutzmer, J., Beukes, N. Mezger, K., Strauss, H. & Gertloff, E. (2007). Geochemistry of bedded barite of the Mesoproterozoic Aggeneys-Gamsberg Broken Hill-type district, South Africa. Mineralium Deposita, 42: 537-549.

McClung, C.R. and Viljoen, F. (2010). A detailed mineralogical assessment of sphalerites from the Gamsberg zinc deposit, South Africa: The manganese conundrum. Minerals Engineering 24 (2011) pp. 930-938.

McKay, N.A., Vann, J., Ware, W., Morley, C. and Hodkiewicz, P. (2016). Strategic and tactical geometallurgy – a systematic process to add and sustain resource value. In: The Third AusIMM International Geometallurgy Conference. 29-36. (The Australasian Institute of Mining and Metallurgy: Melbourne).

Neufeld, A. (2005). The geology of Black Mountain, Bushmanland Project, Aggeneys, South Africa. Masters dissertation. Southampton: University of Southampton.

Rozendaal, A. (1975). The geology of Gamsberg, Namaqualand, South Africa. Masters dissertation. Stellenbosch: University of Stellenbosch.

Rudnick, T. K. (2016). The Genesis of the Swartberg Base-Metal Sulphide Deposit, South Africa. Unpublished Masters Dissertation. Stellenbosch: University of Stellenbosch.

Ryan, P.J., Lawrence, A.L., Lipson, R.D., Moore, J.M., Paterson, A., Stedman, D.P. & Van Zyl, D. (1986). The Aggeneys base metal sulphide deposits, Namaqualand district. In: Anhausser, C.R. & Maske,

S. (Eds.). Mineral deposits of South Africa. Johannesburg: Geological Society of South Africa. 1447-1473.

Schouwstra, R., De Vaux, D., Hey, P., Malysiak, V., Shackleton, N. and Bramdeo, S. (2010). Understanding Gamsberg–A geometallurgical study of a large stratiform zinc deposit. Minerals Engineering, 23(11-13), pp.960-967.

Stedman, D.P. (1980). The structural geology and metamorphic petrology of Black Mountain, Namaqualand. Masters dissertation. Johannesburg: University of the Witwatersrand.

Strohmayr S.J., Barns K.E., Brindley S.K., and Munro P.D. (1998). Mineralogy Controlling Metallurgy at Ernest Henry Mining., in Proceedings of the Mine to Mill 1998 Conference, Brisbane pp 13-18 (The Australasian Institute of Mining and Metallurgy)

Twidle, T.R. and Engelbrecht, P.C. (1984). Developments in the flotation of copper at Black Mountain. Journal of the Southern African Institute of Mining and Metallurgy, 84(6), pp.164-178.

Williams, S.R. (2013). A historical perspective of the application and success of geometallurgical methodologies. In Proceedings of the International Geometallurgy Conference, Brisbane, Australia (Vol. 30).

CHAPTER 4: Conclusions and recommendations

The following chapter provides an overview of the work completed during the course of this study and presents the way forward using the key learnings from Chapters 2 and 3.

4.1. Key findings of the project

The key findings of Chapter 2 indicated that strong mineral (quartz-dominated vs magnetite dominated) and chalcopyrite grain size differences (very fine, 25 – 350 µm; fine, 25 – 1100 µm and medium, 25 – 2000 µm) seemed to be a natural partition between the three inferred early-stage geometallurgical domains, prior to flotation testing. These were the GQ (quartz-dominated), LOB (quartz-dominated) and UOB (magnetite dominated) domains. The GQ domain was considered to have the most straightforward mineralogy, and even though it is also quartz dominated, it was considered distinct from the LOB domain because it also shared similarities with the UOB. The LOB and UOB domains were considered mineralogically complex. Within the LOB, the mineralogical complexity was expressed as the presence of multiple minerals within a single lithological unit, whereas in the UOB domain mineralogical complexity was expressed as a variety of subordinate lithological units/ secondary lithological units.

The key findings of Chapter 3 indicated that distinct metal zonation and the liberation state of bulk mineralogical configurations proved to be the actual processing partition between the three actual UOB domains, the QM domain, the PQM domain and the AM domain. Ores that are higher grade are better liberated and therefore higher recoveries and mass pulls result. The QM domain is considered the best quality ore, followed by the PQM and AM in order of decreasing quality. Besides the relationship between head grade and recovery, the quality of the ore is also influenced by the potential for processing issues with selectivity (chalcopyrite disease), entrainment (pyroxmangite middlings), flotation rate of dominant metal (sphalerite ores) and the concentration ratio (low-grade ores). As a result of the strong influence of head grade, the Cu:S ratio was presented as a calculable predictive proxy that could illustrate the differences between these geometallurgical domains in both a quantitative 2-D and 3-D spatial context to inform the operational team about the expected variability when a combination of ores are mined.

4.2. Are geometallurgical domains feasible in existing underground operations

The advantages of establishing geometallurgical relationships within a group of ores have been illustrated within this study; however, employing a geometallurgical program in an existing underground mining operation is complicated by several factors.

Firstly, the spatial relationship of ores to one another within a deposit is a crucial factor. Prior to the onset of geometallurgical test work the question should be asked that if the outcomes of the test work indicate that ores should be mined and treated separately, will it be possible to do so. For example, selective mining of sedimentary iron ore deposits or coal deposits that are continuous would be much easier to do than the selective mining of a discontinuous lensoidal Cu-Pb-Zn deposit because the ores within layered deposits are easier to separate. In that sense, employing a geometallurgical program for the selective mining of this deposit would not be feasible unless the mining method is modified to be conducive to selective mining. However, therein also lies a rock engineering and by extension a safety consideration such as the reduced roof stability when a certain volume of ore is mined and a gap is left behind.

Secondly, the feasibility of the geometallurgical program also needs to be explored for the type of mining. The logistics surrounding opencast mining are more favourable for a geometallurgical program than underground mining. In opencast mining operations, a great deal more tonnes are broken and moved compared to underground mines. This means more flexibility for selective loading of ores within opencast mining, whereas in underground mines the logistics surrounding the loading of ores is influenced by the amount of ore that can be hoisted to surface per day. Because of this, there is always pressure on the mining teams to produce and hoist broken tonnes, therefore limited flexibility for selective mining. Considering this factor, the geometallurgical program will only be feasible if a decision is made by the management team to pursue the quality of Cu-Pb-Zn concentrates over the quantity of Cu-Pb-Zn concentrates.

The development of geometallurgical domains within this study has proved that the process mineralogical relationship in ores is best-exploited using quantitative data, and therein lies the final consideration. Quantitative mineralogy data can be produced by a variety of instruments e.g. QEMSCAN, QXRD, MLA, TIMA etc. However, the costing associated with purchasing and maintaining these instruments compared to the financial saving associated with using these instruments on-site at mines is not well known. Therefore, companies are reluctant to invest in such instruments until their value has been proven by R&D initiatives such as this project. This complicates the efficiency of geometallurgical programs that depend on detailed mineralogical data. The aim of a geometallurgical program is to inform the mining and processing of ores in a proactive manner, rather than a reactive manner. Taking this factor into consideration, a proactive geometallurgical program for this deposit will only be efficient if elemental proxies or element to mineral conversion techniques is pursued as an alternative to quantitative mineralogy data. However, therein also lies a limitation. More than just the bulk mineralogy of the ores determined the success of this project. The use of liberation data, mineral association data and image

analysis also contributed greatly to outcomes. Therefore, if companies do decide to invest in a quantitative system, it should be one that adds a spatial context of the minerals to one another.

4.3. Recommendations

It is firstly recommended that a geometallurgical program for this deposit be implemented in increments to assess the value and practicality of the approach to be run as an extension of the current mining operation. In doing this, feed samples should be collected for periods when grade and recovery trends are variable and sent for quantitative size-by-size mineralogical analysis to ascertain the key contributing factors to the reduced recovery and grade of concentrates.

It is secondly recommended an investment be made in a quantitative image analysis instrument such as QEMSCAN, MLA or TESCAN to be able to predict the mineralogical variability of ROM feeds. Considering the operational time required by these instruments it is recommended that the resulting mineralogical data be reconciled with the geological block model to add a spatial context to problematic feeds. This reconciliation process will facilitate the proactive prediction of processing response from a group of ores based on the key process mineralogical variables determined during this study e.g. grade, mineral association and has been identified

Until such time that a quantitative mineralogical instrument is acquired, it is recommended that subsequent testing of the Cu:S elemental proxy be carried out to determine the upper and lower limits of the distribution of geometallurgical domains as indicated in Chapter 3. The addition of other elemental proxies e.g. Pb:S, Zn:S, Ba:S, Bi:S, As:S etc. used in conjunction with the Cu:S ratio should also be used to inform of the potential for competition of ES and SG minerals during flotation and the presence of deleterious elements (Mn, Bi, As, Co, Cd). In addition to this, it is also recommended that a size-by-size mineralogical study be done on the deportment of deleterious elements such as to determine the optimal particle size of ores at which the recovery of deleterious elements, such as Mn, to the concentrates can be minimized or eliminated.

A quantitative mineralogical investigation into the behaviour of Ag as a solid solution element and the behaviour of Ag minerals was beyond the scope of this study; however, it is recommended that a quantitative mineralogical investigation of the Ag be conducted to determine if the behaviour of Ag falls within the same geometallurgical domains as proposed in Chapter 3.

Lastly, since the geological block model informs the grade control approach, it is also important to illustrate the geometallurgical domains in a qualitative way for the use of underground grade control teams. A geometallurgical matrix (Fig. 4.1) of the magnetite-dominated ores was developed to educate the mining team about the process affecting characteristics associated with the geometallurgical domains. It is recommended that the underground grade control geologists make use of this matrix to ensure that the domains are correctly identified and communicated through to the concentrator plant.

Table 4.1: *A geometallurgical matrix that can be used to encourage the identification of minerals to encourage selective mining and processing of the magnetite dominated ores.*

Geometallurgical classification	QM (Ore F) 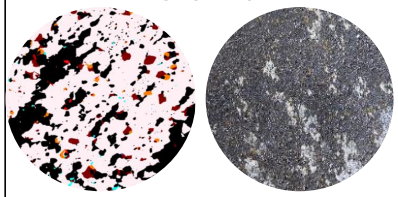	PQM (Ore A, B, C) 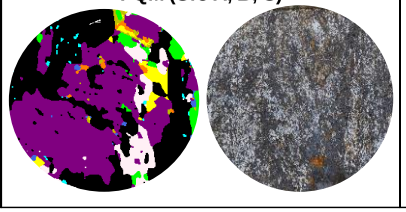	AM (Ore D, E) 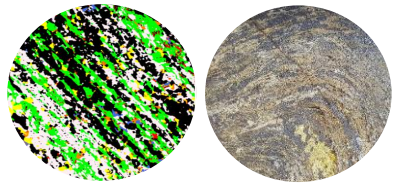
Mineralogy	**Quartz dominated**	**Pyroxmangite dominated**	**Grunerite dominated**
Economic sulphide minerals	*cp>ga*	*sp>cp>ga*	*cp*
Gangue sulphide minerals	*py>po*	*po>py*	*py>po*
Non-Sulphide gangue minerals	*mgt, qtz, ap*	*mgt, pxm, gru, ap, mica*	*mgt, qtz, gru, ap*
Trace minerals			
Mineral association (unliberated)		**Mineral association increases →**	
Chalcopyrite	*mgt>fe- >sp*	*pxm>sp>mgt*	*mgt>pxm>gru>fe-s>oth si*
Galena	*mgt>fe-s>oth>oth di*	*pxm>fe-s>fe-o>oth si*	*gru>fe-s>pxm>oth si>cp>oth*
Sphalerite	*cp>fe-o*	*pxm>cp>fe-o*	*fe-o>cp>gru>fe-s>oth si>oth*
Liberation (> 90 %)		**Liberation decreases →**	
Chalcopyrite (%)	*88*	*63*	*50*
		Liberation decreases →	
Galena	*80*	*51*	*43*
		Liberation decreases →	
Sphalerite	*78*	*65*	*33*
Cu:S (average)	*0.8*	*0.2*	*0.6*
2. Minerals processing			
		Head grade decreases →	
2.1. Head Grade	*High Cu and Pb expected*	*High Cu and Zn. Has potential for high Pb*	*Medium Cu*
2.2. Throughput	*Medium (15 mins)*	*Low(17 mins)*	*High (11 minutes)*
		Liberation decreases →	
2.3. Liberation	*Excellent liberation*	*Chalcopyrite/ Sphalerite and Pyroxmangite middlings. Requires finer grinding*	*Multiple SG and NSG middlings. Requires finer grinding*
		Recovery decreases →	
2.4. Recovery	*High*	*Medium*	*Low*
2.5. Selectivity (Economic sulphides)	*High*	*Medium. Zn to report to Cu conc*	*High*
2.6. Entrainment	*No problem identified*	*Mn from pyroxmangite to conc*	*No problem identified*

REFERENCES

Ayling, B., Rose, P., Petty, S., Zemach, E. and Drakos, P. (2012). QEMSCAN (Quantitative evaluation of minerals by scanning electron microscopy): capability and application to fracture characterization in geothermal systems. In Proc, Thirty-Seventh Workshop on Geotherm Reserv Eng. Stanford, California: Stanford University.

Base Metals Supply and Demand - CME Group. (2019). Available. [Online]. https://www.cmegroup.com/education/courses/introduction-to-base-metals/base-metals-supply-and-demand.html

Baum, W., Lotter, N.O. & Whittaker, P.J. (2004). Process Mineralogy a new generation for ore characterisation and plant optimization. SME Annual Meeting Feb 23-25, Denver, Colorado. Preprint 04-12.

Baumgartner, R., Dusci, M., Gressier, J., Trueman, A., Poos, S., Brittan, M. and Mayta, P. (2011). Building a geometallurgical model for early-stage project development-a case study from the Canahuire epithermal Au-cu-Ag deposit, Southern Peru. In The First AUSIMM International Geometallurgy Conference (pp. 53-60).

Becker, M, Wightman, E.M and Evans, C.L. (2016). Process Mineralogy. Julius Kruttschnitt Mineral Research Centre, The University of Queensland, Australia. 250-260.

Bojcevski, D., L. Vink, N. W. Johnson, V. Landmark, J. Mackenzie, and M. F. Young. (1998). Metallurgical characterisation of George Fisher ore textures and implications for ore processing. In Proceedings: Mine to Mill Conference, pp. 29-42.

Bradshaw, D.J. (2014). The role of 'process mineralogy' in improving the process performance of complex sulphide ores: In: IMPC 2014, Santiago, Chile.

Bradshaw, D.J., Triffett, B., Latti, D., Wilkie, G. and Adair, B. (2016). Dealing with a problematic ore type at Kennecott Utah Copper Concentrator. (Eds.). Process Mineralogy. Julius Kruttschnitt Mineral Research Centre, The University of Queensland, Australia. 250-260.

Butler, C., Dale, R., Robinson, S. and Turner, A. (2016). Geometallurgy – Bridging the gap between Mine and Mill: A Case Study of the DeGrussa Geometallurgy Program. In Proceedings: The third AUSIMM International Geometallurgy conference. 77-88. (The Australasian Institute of Mining and Metallurgy: Melbourne).

Colliston, W.P., Schoch, A.E. and Praekelt, H.E. (2012). Stratigraphy of the Mesoproterozoic Aggeneys Terrane, Western Namaqua Mobile Belt, South Africa. South African Journal of Geology, 115(4), pp.449-464.

Cornell, D.H., Thomas, R.J., Moen, H.F.G., Reid, D.L., Moore, J.M. and Gibson, R.L. (2006). The Namaqua-Natal Province. In: Johnson, M.R., Anhaeusser, C.R. and Thomas, R.J. (Eds.), The Geology of South Africa. Geological Society of South Africa, Johannesburg/ Council for Geoscience, Pretoria, 325-379

Coward, S., Vann, J., Dunham, S. and Stewart, M. (2009). The primary-response framework for geometallurgical variables. In Proceedings: The Seventh International Mining Geology Conference. 109-113. (The Australasian Institute of Mining and Metallurgy: Melbourne).

Cropp, A.F., Goodall, W.R. and Bradshaw, D.J. (2013). The Influence of Textural Variation and Gangue Mineralogy on Recovery of Copper by Flotation from Porphyry Ore – A Review. In Proceedings: The Second AusIMM International Geometallurgy Conference, 279-291, 30 September – 2 October, Brisbane, Queensland, Australia.

Dominy, S.C. and O'Connor, L. (2016). Geometallurgy—Beyond conception. In Proceedings International Geometallurgy Conference; The Australasian Institute of Mining and Metallurgy: Melbourne, Australia (pp. 3-10).

Ehrig, K., McPhie, J. and Kamenetsky, V.S. (2012). Geology and mineralogical zonation of the Olympic Dam iron oxide Cu-U-Au-Ag deposit, South Australia.

Evans, C.L. and Morrison, R.D. (2016). Mineral Liberation, in Becker, M, Wightman, E.M. and Evans, C.L (Eds.). Process Mineralogy. Julius Kruttschnitt Mineral Research Centre, The University of Queensland, Australia. 219-233.

Fragomeni, D., Boyd, L.J., Charland, A., Kormos, L.J., Lotter, N.O., Potts, G. (2005). The use of End-Members for grind-recovery modelling, tonnage prediction and flowsheet development at Raglan. Canadian Mineral Processors, Ottawa, January 2005, Paper No. 6, pp. 75–98.

Gottlieb, P. (2008). The revolutionary impact of automated mineralogy on mining and mineral processing. In The XXIV International Mineral Processing Congress (pp. 165-174).

Hartnady, C.J.H., Joubert, P. and Stowe, C.W. (1985). Proterozoic crustal evolution in south-western Africa. Episodes, 8, 236-244

Howarth, D. F. and Rowlands, J. C. (1987). Quantitative Assessment of Rock Texture and Correlation with Drillability and Strength Properties. Rock Mechanics and Rock Engineering 20: 57-85.

Infomine 5 year Copper prices. (2019, September 30). Available. [Online]. http://www.infomine.com/investment/metal-prices/copper/5-year/

Johnson, N.W. and Munro, P.D. (2008). Methods for assigning domains in the primary sulfide zone of a sulfide orebody. In Proceedings: The Ninth International Congress for Applied Mineralogy, Brisbane, Queensland, 8-10 September. Australasian Institute of Mining and Metallurgy, Melbourne. pp. 597-603.

Johnson, N.W. (2016). Sphalerite and galena liberation levels for the Mt Isa concentrator. In: Becker M, Wightman EM, Evans CL (eds) Process Mineralogy: JKMRC Monograph Series in Mining and Mineral Processing, No 6. Julius Kruttschnitt Mineral Research Centre, Brisbane, Australia, pp 234–249

Kawatra, S.K. and Eisele, T.C. (2002). Froth Flotation-fundamental principles. Research, Michigan Technical University, pp.1-30.

King, G.S. and MacDonald, J.L. (2016). The Business Case for Early-stage Implementation of Geometallurgy – an Example from the Productora Cu-Mo-Au Deposit, Chile. In Proceedings: The third AUSIMM International Geometallurgy conference, 15-16 June 2016, Perth, WA. 125-133. (The Australasian Institute of Mining and Metallurgy: Melbourne).

Klimpel, R. R. (1995). “The Influence of Frother Structure on Industrial Coal Flotation”, High-Efficiency Coal Preparation (Kawatra, ed.), Society for Mining, Metallurgy, and Exploration, Littleton, CO, pp. 141-151International Geometallurgy Conference. 29-36. (The Australasian Institute of Mining and Metallurgy: Melbourne).

Kormos, L.J., Oliveira, J., Fragomeni, D., Whiteman, E. and Carrión De la Cruz, J. (2010). Process diagnosis using quantitative mineralogy. In Proceeding of the 42nd Annual Canadian Mineral Processors Conference (pp. 143-162).

Kuan, S.H. (2009). The effect of solids on gas holdup, bubble size and water overflow rate in flotation (Doctoral dissertation, McGill University).

Lamberg, P., Rosenkranz, J., Wanhainen, C., Lund, C., Minz, F., Mwanga, A. and Parian, M. (2013). Building a geometallurgical model in iron ores using a mineralogical approach with liberation data. In Proceedings of the Second AusIMM International Geometallurgy Conference, Brisbane, Australia (pp. 317-324).

Lane, D.J., Cook, N.J., Grano, S.R. and Ehrig, K. (2016). Selective leaching of penalty elements from copper concentrates: A review. Minerals Engineering, 98, pp.110-121.

Lipson, R.D. (1978). Some aspects of the geology of part of the Aggeneysberge and surrounding gneisses, Namaqualand. Masters dissertation. Johannesburg: University of the Witwatersrand.

Lipson, R.D. (1980). The granitic rocks surrounding the Aggeneysberge-a metamorphosed Rapakivi Suite. South African Journal of Geology, 83(2), pp.179-192.

Lipson, R.D. (1990). Lithogeochemistry and origin of metasediments hosting the Broken Hill deposit, Aggeneys, South Africa, and implications for ore genesis. Doctoral dissertation. Cape Town: University of Cape Town

Lotter, N.O., Kowal, D.L., Tuzun, M.A., Whittaker, P.J., Kormos, L.J. (2003). Sampling and flotation testing of Sudbury Basin drill core for process mineralogy modelling. Miner. Eng. 16, 857–864.

Lotter, N.O. and Fragomeni, D. (2010). High-confidence flotation testing at Xstrata Process Support. Mining, Metallurgy & Exploration, 27(1), pp.47-54

Lotter, N.O., Kormos, L.J., Oliveira, J., Fragomeni, D. and Whiteman, E. (2011). Modern process mineralogy: two case studies. Minerals Engineering, 24(7), pp.638-650.

Lotter, N.O., Baum, W., Reeves, S., Arrué, C. and Bradshaw, D.J. (2017). The business value of best practice process mineralogy. Minerals Engineering, 116, pp.226-238.

Lund, C. (2013). Mineralogical, chemical and textural characterisation of the Malmberget iron ore deposit for a geometallurgical model (Doctoral dissertation, Luleå tekniska universitet).

Lund, C., Lamberg, P. and Lindberg, T. (2013). Practical way to quantify minerals from chemical assays at Malmberget iron ore operations - An important tool for the geometallurgical program. Minerals Engineering, 49, pp.7-16.

Macey, P.H., Minnaar, H., Miller, J.A., Lambert, C.H., Groenewald, C., Diener, J., Le Roux, P. and Frei, D. (2014). The Precambrian geology of the region south of Warmbad from Haib to Velloorsdrif, southern Namibia. Geological Survey of Namibia.

Macey, P.H., Thomas, R.J., Minnaar, H.M., Gresse, P.G., Lambert, C.W., Groenewald, C.A., Miller, J.A., Indongo, J., Angombe, M., Shifotoka, G. and Frei, D. (2017). Origin and evolution of the~ 1.9 Ga Richtersveld Magmatic Arc, SW Africa. Precambrian Research, 292, pp.417-451.

McClung, C.R. (2006). Basin analysis of the Mesoproterozoic Bushmanland Group of the Namaqua Metamorphic Province, South Africa. Doctoral dissertation. Johannesburg: University of Johannesburg.

McKay, N. A., Sztuke, J.C. and Lacouture, B. (2016). Red Dog Zinc concentrator optimization study 2009, in Becker, M, Wightman, E.M. and Evans, C.L (Eds.). Process Mineralogy. Julius Kruttschnitt Mineral Research Centre, The University of Queensland, Australia. 250-260.

Ndlovu, B., Becker, M., Forbes, E., Deglon, D. and Franzidis, J.P. (2011). The influence of phyllosilicate mineralogy on the rheology of mineral slurries. Minerals engineering, 24(12), pp.1314-1322.

Neufeld, A. (2005). The geology of Black Mountain, Bushmanland Project, Aggeneys, South Africa. Masters dissertation. Southampton: University of Southampton.

Petruk, W. and Schnarr, J. R. (1983). The behaviour of minerals during flotation of a base-metal ore from the Brunswick No. 12 Deposit in Canada. Special publication. Geological Society of Southern Africa. 7. (1983). 201-2018.

Petruk, W. (2000). Applied mineralogy in the mining industry. Elsevier.

Rozendaal, A. (1975). The geology of Gamsberg, Namaqualand, South Africa (Doctoral dissertation, Stellenbosch: Stellenbosch University).

Rozendaal, A. (1982). The petrology of the Gamsberg Zinc deposit and the Bushmanland iron formations with special reference to their relationships and genesis. Doctoral dissertation. Stellenbosch: University of Stellenbosch

Rudnick, T. K. (2016). The Genesis of the Swartberg Base-Metal Sulphide Deposit, South Africa. Unpublished Masters dissertation. Stellenbosch: University of Stellenbosch.

Rule, C. and Schouwstra, R.P. (2011). Process mineralogy delivering significant value at Anglo Platinum concentrator operations. In Proceedings of the 10th International Congress for Applied Mineralogy (ICAM) (pp. 613-621). Springer, Berlin, Heidelberg.

Ryan, P.J., Lawrence, A.L., Lipson, R.D., Moore, J.M., Paterson, A., Stedman, D.P. & Van Zyl, D. (1986). The Aggeneys base metal sulphide deposits, Namaqualand district. In: Anhausser, C.R. & Maske, S. (Eds.). Mineral deposits of South Africa. Johannesburg: Geological Society of South Africa. 1447-1473.

Schoch, A.E., Colliston, W.P. & Praekelt, H.E. (1987). The Bushmanland Project Final Report. University of the Free State. 110pp.

Schouwstra, R., De Vaux, D., Muzondo, T. and Prins, C. (2013). A geometallurgical approach at Anglo American Platinum's Mogalakwena operation. In The Second AUSIMM International Geometallurgy Conference/Brisbane, QLD (Vol. 30, pp. 85-92).

Schouwstra, R.P., de Vaux, D.V. and Snyman, Q. (2017). Further development of a chemistry proxy for geometallurgical modelling at the Mogalakwena mine. Journal of the Southern African Institute of Mining and Metallurgy, 117(7), pp.719-726.

South African Commission for Stratigraphy (SACS). (1980). Stratigraphy of South Africa. Part 1 (Comp. L. E. Kent). Lithostratigraphy of the Republic of South Africa, South West Africa/Namibia, and the Republics of Bophuthatswana, Transkei and Venda: Handb. Geol. Surv. S. Afr., 8.

Stedman, D.P. (1980). The structural geology and metamorphic petrology of Black Mountain, Namaqualand. Masters dissertation. Johannesburg: University of the Witwatersrand

Steinmann, P. G. (2016). Grade Control Geologist, Black Mountain Mining. Personal discussion, Aggeneys.

Strohmayr, S. J., Barns, K. E. Brindley, S. K. and Munro, P. D. (1998). Mineralogy controlling metallurgy at Ernst Henry Mining. In Proceedings: Mine to Mill Conference, pp. 13-17. 1998

Strydom, D. (1986). 'n Struktuur-stratigrafiese ondersoek van die gesteentes van Swartberg. The Bushmanland Project Interim Report. University of the Free State. 51pp.

Thomas, R.J., Agenbacht, A.L.D., Cornell, D.H. and Moore, J.M. (1993). The Kibaran of southern Africa: Tectonic evolution and metallogeny. Ore Geology Reviews, 9, 131-160

Thomas, R.J., Cornell, D.H., Moore, J.M. and Jacobs, J. (1994). Crustal evolution of the Namaqua-Natal Metamorphic Province, Southern Africa. South African Journal Geology, 97, 8-14

Twidle, T.R. and Engelbrecht, P.C. (1984). Developments in the flotation of copper at Black Mountain. Journal of the Southern African Institute of Mining and Metallurgy, 84(6), pp.164-178.

Williams, S.R. (2013). A Historical Perspective of the Application and Success of Geometallurgical Methodologies. The Second AusIMM International Geometallurgy Conference. Brisbane, Australia.

APPENDIX A: Location of samples

Sample set A: Drill core samples (The different colours indicate where multiple samples come from the same hole).

Sample	Orebody	Rock type	Description	From (m)	To (m)	Length	Condition
HG-001	UOB	QM	Quartz Magnetite	349.47	349.68	0.21	Half
HG-002	UOB	SQM	Sulphidic Quartz Magnetite	350.27	350.98	0.71	Half
HG-003	UOB	QM	Quartz Magnetite	352.77	353.05	0.28	Half
HG-004	UOB	QM-Cu	Quartz Magnetite Cu-rich	363.59	363.96	0.37	Half
HG-005	MBZ	MB	Magnetite Barite	394.32	394.52	0.20	Half
HG-006	MBZ	MB	Magnetite Barite	395.77	396.02	0.25	Half
HG-007	UOB	QM-Cu	Quartz Magnetite Cu-rich	329.45	329.90	0.45	Half
HG-008	MBZ	MB	Magnetite Barite	412.24	412.37	0.13	Half
HG-009	UOB	QM	Quartz Magnetite	328.35	328.66	0.31	Half
HG-010	MBZ	GAM	Garnet amphibole magnetite	374.14	374.41	0.27	Half
HG-011	LOB	MC	Mineralized schist	351.17	351.34	0.17	Half
HG-012	LOB	MC	Mineralized schist	349.80	350.14	0.34	Half
HG-013	UOB	AM	Amphibole magnetite	322.23	322.50	0.27	Half
HG-014	UOB	QM	Quartz Magnetite	319.69	319.90	0.21	Half
HG-015	UOB	SQM	Sulphidic Quartz Magnetite	327.76	328.13	0.37	Half
HG-016	GQZ	GQ	Garnet Quartzite	306.76	307.16	0.40	Half
HG-017	GQZ	GQ	Garnet Quartzite	313.80	314.39	0.59	Half
HG-018	GQZ	GQ	Garnet Quartzite	324.15	324.34	0.19	Half
HG-019	GQZ	GQ	Garnet Quartzite	328.61	329.02	0.41	Half
HG-020	GQZ	GQ	Garnet Quartzite	336.91	337.18	0.27	Half
HG-021	UOB	AM	Amphibole magnetite	369.35	369.64	0.29	Half
HG-022	GQZ	GQ	Garnet Quartzite	340.77	341.10	0.33	Half
HG-023	UOB	AM	Amphibole magnetite	370.90	371.29	0.39	Half
HG-024	UOB	AM	Amphibole magnetite	364.51	364.78	0.27	Half
HG-025	UOB	AM	Amphibole magnetite	358.53	359.21	0.68	Half
HG-026	P	P	Pegmatite	266.40	266.80	0.40	Half
HG-027	MBZ	MB	Magnetite Barite	754.39	754.70	0.31	Quarter
HG-028	UOB	QM	Quartz Magnetite Cu-rich	726.35	726.97	0.62	Quarter
HG-029	MBZ	MB	Magnetite Barite	755.70	756.07	0.37	Quarter
HG-030	MBZ	MB	Magnetite Barite	758.70	759.11	0.41	Quarter
HG-031	UOB	QM	Quartz Magnetite Cu-rich	739.90	740.18	0.28	Quarter
HG-032	UOB	S-QM	Sulphidic Quartz Magnetite	729.95	730.30	0.35	Quarter
HG-033	LOB	SQ	Sulphidic Quartzite	763.57	763.76	0.19	Quarter
HG-034	MBZ	GM	Garnet Magnetite	761.59	761.89	0.30	Quarter
HG-035	UOB	QM/MM	Quartz Magnetite	716.70	717.06	0.36	Quarter
HG-036	UOB	AM	Amphibole magnetite	727.93	728.31	0.38	Quarter
HG-037	UOB	FQ	Ferruginous Quartzite	747.53	747.99	0.46	Quarter
HG-038	UOB	QM	Quartz Magnetite	741.20	741.50	0.30	Quarter
HG-039	GQZ/UOB	GQ/QM	Garnet Quartzite/ Quartz Magnetite	736.28	736.66	0.38	Quarter
HG-040	LOB	SQ	Sulphidic Quartzite	745.42	745.77	0.35	Quarter
HG-041	LOB	MC	Mineralized schist	764.05	764.70	0.65	Quarter
HG-042	UOB	AM	Amphibole magnetite	302.22	302.55	0.33	Quarter
HG-043	GQZ	GQ	Garnet Quartzite	272.66	272.95	0.29	Quarter

Sample	Orebody	Rock type	Description	From (m)	To (m)	Length	Condition
HG-044	LOB	MC	Mineralized schist (Ferruginous)	229.54	229.97	0.43	Quarter
HG-045	UOB	FQ	Ferruginous Quartzite	293.15	293.30	0.15	Quarter
HG-046	UOB	QM	Quartz Magnetite	296.65	297.02	0.37	Quarter
HG-047	UOB	QM	Quartz Magnetite (Cu)	707.14	707.49	0.35	Quarter
HG-048	UOB	AM	Amphibole Magnetite (Pb)	694.89	695.14	0.25	Quarter
HG-049	UOB	AM	Amphibole Magnetite	702.75	702.98	0.23	Quarter
HG-050	UOB	AM	Amphibole Magnetite	690.50	690.80	0.30	Quarter
HG-051	UOB	AM	Amphibole Magnetite (Pb)	713.08	713.39	0.31	Quarter
HG-052	UOB	AM	Amphibole Magnetite (Pb)	697.08	697.38	0.30	Quarter
HG-053	GQZ	GQ	Garnet Quartzite	726.17	726.68	0.51	Quarter
HG-054	UOB	AM	Amphibole Magnetite	710.52	710.91	0.39	Quarter
HG-055	LOB	SQ	Sulphidic Quartzite	759.37	759.73	0.36	Quarter
HG-056	GQZ	GQ	Garnet Quartzite	688.95	689.13	0.18	Quarter
HG-057	LOB	MC	Mineralized Schist	765.32	765.61	0.29	Quarter
HG-058	GQZ	GQ	Garnet Quartzite	746.02	746.24	0.22	Quarter
HG-059	GQZ	GQ	Garnet Quartzite	746.49	746.69	0.20	Quarter
HG-060	UOB	AM	Amphibole Magnetite	697.49	697.88	0.39	Quarter
HG-061	LOB	SQ	Sulphidic Quartzite	755.65	756.06	0.41	Quarter
HG-062	GQZ	GQ	Garnet Quartzite	688.17	688.45	0.28	Quarter
HG-063	LOB	MC	Mineralized Schist	757.32	757.64	0.32	Quarter
HG-064	GQZ	GQ/SQ	Sulphidic Quartzite	669.08	669.35	0.27	Quarter
HG-065	LOB	MC	Mineralized Schist	753.60	753.99	0.39	Quarter
HG-066	GQZ	MC	Mineralized Schist	639.06	639.35	0.29	Quarter
HG-067	UOB	AM	Amphibole Magnetite	703.12	703.85	0.73	Quarter
HG-068	LOB	MC	Mineralized Schist	756.44	757.00	0.56	Quarter

Sample set B: Bulk underground samples:

Ore bodies	Ore type	Ore	Sampling Location
Upper Ore body	Magnetite quartzite (QM)	A	677 UOB N
		B	677 UOB N
		C	671 UOB N
		F	Drill core*
	Amphibole magnetite quartzite (AM)	D	677 UOB N
		E	671 UOB N

APPENDIX B: Bulk Mineralogy data used in Chapter 2

QM Bulk Mineralogy (wt. %)								
Mineral	HG 002	HG 004	HG 007	HG 009	HG 014	HG 015	HG 031	Ave.
Chalcopyrite	1.6	8.0	17.8	9.5	7.1	10.5	0.5	7.3
Covellite	<0.01	0.0	<0.01	<0.01	<0.01	<0.01	0.4	0.2
Bornite	<0.01	<0.01	<0.01	<0.01	<0.01	<0.01	0.7	0.7
Sphalerite	2.9	0.1	0.0	0.0	0.2	0.8	0.0	0.5
Galena	28.5	0.8	<0.01	0.0	0.0	0.1	0.4	4.6
Pyrrhotite	0.1	0.1	0.1	0.3	0.1	0.2	0.0	0.1
Pyrite	1.1	<0.01	5.4	4.3	1.3	7.1	<0.01	3.6
Arsenopyrite	0.0	0.0	<0.01	<0.01	0.0	<0.01	<0.01	0.0
Magnetite	56.0	48.7	14.4	76.8	59.5	19.7	47.9	43.1
Jacobsite	0.3	0.0	0.2	0.0	0.3	0.1	0.0	0.1
Ilmenite	<0.01	<0.01	0.0	<0.01	<0.01	0.2	0.0	0.1
Quartz	7.3	35.8	51.4	8.1	25.3	34.9	47.7	28.1
Sillimanite	<0.01	0.3	<0.01	<0.01	0.0	0.0	0.2	0.1
Albite	<0.01	0.0	<0.01	<0.01	0.0	<0.01	<0.01	0.0
Grunerite	0.1	0.0	<0.01	<0.01	0.0	0.0	<0.01	0.0
Manganogrunerite	0.7	<0.01	<0.01	<0.01	0.0	<0.01	<0.01	0.3
Pyroxmangite	0.6	0.0	0.0	0.0	1.1	0.5	0.0	0.3
Muscovite	<0.01	0.6	<0.01	<0.01	<0.01	<0.01	0.0	0.3
Annite	<0.01	2.4	7.4	<0.01	<0.01	3.3	0.4	3.1
Chlorite	<0.01	0.3	<0.01	<0.01	<0.01	<0.01	<0.01	0.2
Apatite	0.6	0.3	0.3	0.9	0.1	1.2	<0.01	0.5
Barite	<0.01	0.0	0.0	<0.01	4.9	<0.01	1.1	1.4
Rhodonite	0.2	<0.01	<0.01	<0.01	0.0	0.0	<0.01	0.1
Pyrolusite	0.1	<0.01	<0.01	<0.01	<0.01	<0.01	<0.01	0.0
Spessartine	0.0	0.8	0.0	<0.01	0.0	18.3	0.3	3.0
Almandine	<0.01	1.5	2.5	<0.01	<0.01	2.9	0.3	1.7
Gahnite	<0.01	0.1	<0.01	<0.01	<0.01	0.2	0.1	0.1
Bismuthinite	<0.01	0.0	<0.01	<0.01	<0.01	<0.01	<0.01	0.0
Monazite	0.0	0.0	0.0	<0.01	0.0	0.0	0.0	0.0
Hercynite	<0.01	0.1	0.0	<0.01	<0.01	<0.01	0.1	0.0
Ulvospinel	<0.01	<0.01	0.2	<0.01	<0.01	<0.01	0.1	0.1
Staurolite	<0.01	0.3	0.0	<0.01	<0.01	0.0	0.0	0.1
	100.0	100.0	100.0	100.0	100.0	100.0	100.0	100.0

GQ Bulk Mineralogy (wt. %)					
	HG 017	HG 045	HG 056	HG 062	Ave.
Chalcopyrite	13.0	16.2	8.7	10.2	11.7
Sphalerite	0.1	0.3	0.1	0.1	0.1
Galena	<0.01	<0.01	0.3	0.8	0.5
Pyrrhotite	4.6	3.8	2.0	<0.01	3.4
Pyrite	<0.01	0.0	3.6	0.0	1.2
Magnetite	4.4	21.0	1.6	0.0	6.6
Jacobsite	<0.01	<0.01	0.0	0.0	0.0
Ilmenite	0.1	0.0	0.0	<0.01	0.0
Quartz	61.9	49.2	69.6	72.0	61.4
Sillimanite	3.0	2.5	0.5	<0.01	2.0
Albite	<0.01	<0.01	0.0	<0.01	0.0
Muscovite	<0.01	0.0	0.5	5.3	1.9
Annite	5.9	0.2	3.9	5.5	3.7
Fluorite	<0.01	<0.01	<0.01	0.0	0.0
Apatite	<0.01	1.1	0.2	0.0	0.4
Spessartine	0.0	1.2	5.7	4.5	2.8
Almandine	6.9	4.0	3.6	1.6	3.9
Gahnite	<0.01	0.4	<0.01	<0.01	0.4
Bismuthinite	<0.01	<0.01	<0.01	0.0	0.0
Monazite	0.0	0.1	<0.01	0.0	0.0
Ulvospinel	<0.01	0.0	<0.01	<0.01	0.0
Staurolite	0.0	0.0	0.0	<0.01	0.0
	100.0	100.0	100.0	100.0	100.0

AM Bulk Mineralogy (wt. %)					
Mineral	HG 013	HG 025	HG 048	HG 060	Ave
Chalcopyrite	2.3	1.3	1.3	8.6	2.9
Sphalerite	28.9	1.2	1.4	4.5	7.6
Galena	43.5	4.1	1.3	1.4	10.7
Pyrrhotite	0.0	10.9	13.6	1.6	5.5
Pyrite	1.2	<0.01	0.1	4.1	1.5
Arsenopyrite	<0.01	0.0	<0.01	<0.01	0.0
Magnetite	<0.01	55.3	54.7	62.1	48.7
Jacobsite	<0.01	0.1	0.8	0.4	0.3
Quartz	24.1	12.4	14.3	10.2	13.0
Manganogrunerite	<0.01	12.3	2.6	3.6	5.2
Pyroxmangite	<0.01	2.2	9.0	3.3	4.1
Fluorite	<0.01	<0.01	<0.01	<0.01	0.0
Apatite	<0.01	0.3	0.7	0.4	0.4
Rhodonite	<0.01	0.0	0.2	0.0	0.1
Pyrolusite	<0.01	<0.01	0.0	<0.01	0.0
Spessartine	<0.01	0.0	<0.01	<0.01	0.0
Monazite	<0.01	0.0	0.0	0.0	0.0
	100.0	100.0	100.0	100.0	100.0

Bulk Minerlogy (wt. %)				
	MC			SQ
	HG 041	HG 065	Ave	HG 055
Chalcopyrite	0.6	1.4	1.0	3.6
Sphalerite	0.3	0.1	0.2	0.1
Galena	5.2	28.4	16.1	7.5
Pyrrhotite	7.4	0.1	3.6	0.1
Pyrite	1.0	3.8	2.3	3.3
Arsenopyrite	0.0	0.0	0.0	0.0
Magnetite	0.1	0.8	0.4	3.1
Ilmenite	0.0	0.2	0.1	0.1
Quartz	64.3	30.7	45.4	48.4
Sillimanite	2.4	0.0	1.1	0.2
Albite	0.0	0.0	0.0	<0.01
Pyroxmangite	<0.01	<0.01	0.0	0.0
Muscovite	4.1	0.0	2.0	0.2
Annite	5.8	3.6	4.5	8.9
Chlorite	0.0	<0.01	0.0	0.0
Fluorite	<0.01	0.0	0.0	0.1
Hyalophane	0.3	26.9	13.0	17.1
Apatite	0.1	0.1	0.1	0.1
Barite	<0.01	2.3	2.2	0.4
Spessartine	<0.01	<0.01	0.0	0.9
Almandine	1.3	1.4	1.3	6.0
Andradite	<0.01	0.2	0.2	0.1
Gahnite	6.9	<0.01	6.6	0.0
Monazite	0.0	0.0	0.0	0.0
Ulvospinel	<0.01	0.0	0.0	0.0
Rutile	0.2	0.0	0.1	0.0
Staurolite	0.1	<0.01	0.1	0.0
	100.0	100.0	100.0	100.0

APPENDIX C: Grain size distribution data used in Chapter 2

Chalcopyrite grain size distribution											
Grain size (µm)	QM	AM	GQ	MC	SQ	Grain size (µm)	QM	AM	GQ	MC	SQ
25	0.36	0.07	0.09	0.04	0.02	*1075*	0.00	0.00	0.40	0.00	0.00
50	1.12	1.18	0.21	0.20	0.06	*1100*	0.36	0.62	0.00	0.00	0.00
75	2.72	1.34	0.43	0.36	0.66	*1125*	0.26	0.00	0.00	0.00	0.00
100	3.82	0.76	1.26	0.23	0.48	*1150*	0.00	0.00	0.00	0.00	0.00
125	4.99	0.41	2.32	0.39	0.35	*1175*	0.27	0.00	0.00	0.00	0.00
150	4.56	0.71	3.05	0.20	0.43	*1200*	0.63	0.00	0.00	0.00	0.00
175	3.96	0.81	2.78	0.23	0.39	*1225*	0.00	0.00	0.00	0.00	0.00
275	1.22	0.01	3.13	0.03	0.00	*1250*	0.60	0.00	0.00	0.00	0.00
300	2.83	0.30	2.36	0.03	0.16	*1275*	0.00	0.00	0.00	0.00	0.00
325	2.00	0.85	2.29	0.00	0.09	*1300*	0.00	0.00	0.00	0.00	0.00
350	1.42	0.03	1.98	0.10	0.19	*1325*	0.00	0.00	0.00	0.00	0.00
375	1.14	0.73	1.29	0.05	0.00	*1350*	0.00	0.00	0.00	0.00	0.00
400	0.79	0.01	2.17	0.00	0.00	*1375*	0.00	0.00	0.00	0.00	0.00
425	1.78	0.11	0.50	0.00	0.00	*1400*	0.41	0.00	0.00	0.00	0.00
450	1.18	0.12	1.03	0.00	0.00	*1425*	0.00	0.00	0.00	0.00	0.00
475	0.73	0.24	2.11	0.00	0.00	*1450*	0.00	0.00	0.00	0.00	0.00
500	1.43	0.00	1.66	0.00	0.00	*1475*	0.00	0.00	0.00	0.00	0.00
525	0.63	0.31	0.50	0.00	0.00	*1500*	0.38	0.00	0.00	0.00	0.00
550	0.71	0.00	0.15	0.00	0.00	*1525*	0.43	0.00	0.00	0.00	0.00
575	0.51	0.00	1.31	0.00	0.00	*1550*	0.30	0.00	0.00	0.00	0.00
600	0.14	0.07	0.85	0.00	0.00	*1575*	0.00	0.00	0.00	0.00	0.00
625	0.46	0.61	0.10	0.00	0.00	*1600*	0.00	0.00	0.00	0.00	0.00
650	1.22	0.56	0.45	0.00	0.00	*1625*	0.00	0.00	0.00	0.00	0.00
675	0.37	0.00	0.25	0.00	0.00	*1650*	0.00	0.00	0.00	0.00	0.00
700	0.26	0.61	0.43	0.00	0.00	*1675*	0.00	0.00	0.00	0.00	0.00
725	0.26	0.00	0.58	0.00	0.00	*1700*	0.00	0.00	0.00	0.00	0.00
750	0.78	0.00	2.20	0.00	0.00	*1725*	0.00	0.00	0.00	0.00	0.00
775	0.07	0.00	0.73	0.00	0.00	*1750*	0.00	0.00	0.00	0.00	0.00
800	0.58	0.26	0.00	0.00	0.00	*1775*	0.00	0.00	0.00	0.00	0.00
825	0.60	0.00	0.00	0.00	0.00	*1800*	0.00	0.00	0.00	0.00	0.00
850	0.37	0.59	0.42	0.00	0.00	*1825*	0.00	0.00	0.00	0.00	0.00
875	0.53	0.58	0.25	0.00	0.00	*1850*	0.00	0.00	0.00	0.00	0.00
900	0.62	0.00	0.73	0.00	0.00	*1875*	0.00	0.00	0.00	0.00	0.00
925	0.00	0.00	0.66	0.00	0.00	*1900*	0.19	0.00	0.00	0.00	0.00
950	0.08	0.00	0.00	0.00	0.00	*1925*	0.00	0.00	0.00	0.00	0.00
975	0.51	0.00	0.00	0.00	0.00	*1950*	0.00	0.00	0.00	0.00	0.00
1000	0.56	0.00	0.39	0.00	0.00	*1975*	0.00	0.00	0.00	0.00	0.00
1025	0.06	0.00	0.26	0.00	0.00	*2000*	0.00	0.00	0.00	0.00	0.00
1050	0.00	0.00	0.00	0.00	0.00						

APPENDIX D: Bulk mineralogy data used in Chapter 3

	Bulk Mineralogy (wt. %)				
	Ore A	Ore B	Ore C	Ore D	Ore E
Chalcopyrite	1.6	2.0	0.6	1.4	3.7
Covellite	<0.01	<0.01	<0.01	<0.01	0.0
Sphalerite	3.1	2.6	0.6	0.1	0.4
Galena	0.5	0.5	6.4	0.2	1.7
Pyrrhotite	2.0	2.0	0.8	0.2	0.2
Pyrite	1.1	0.9	1.0	1.2	0.5
Arsenopyrite	0.0	0.1	0.1	0.1	0.0
Magnetite	56.8	53.6	58.3	65.5	73.9
Jacobsite	0.2	0.0	0.3	0.0	0.0
Chromite	0.1	0.1	0.1	0.1	0.1
Quartz	6.8	6.8	2.5	9.2	16.8
Sillimanite	0.0	0.1	0.0	0.0	0.6
Albite	0.0	0.0	0.0	0.0	0.1
Anorthite	0.0	0.0	0.0	0.0	0.0
Grunerite	0.1	0.2	0.1	15.0	0.1
Manganogrunerite	5.4	3.3	0.5	5.3	0.0
Pyroxmangite	21.0	26.2	27.7	0.4	0.1
Muscovite	0.0	0.0	0.0	0.0	0.1
Annite	0.1	0.1	0.1	0.2	0.3
Chlorite	<0.01	<0.01	<0.01	<0.01	0.0
Fluorite	<0.01	0.0	0.0	<0.01	<0.01
Apatite	0.9	0.7	0.5	0.8	0.5
Barite	<0.01	<0.01	<0.01	<0.01	0.2
Rhodonite	0.0	0.0	0.1	<0.01	0.0
Pyrolusite	0.0	0.0	0.2	<0.01	<0.01
Spessartine	0.1	0.6	0.0	0.0	0.2
Almandine	0.0	0.0	0.0	0.1	0.3
Andradite	<0.01	<0.01	0.0	0.0	0.0
Diopside	0.0	0.0	0.0	0.1	0.0
Gahnite	<0.01	0.0	0.0	<0.01	0.0
Bismuthinite	0.0	0.0	<0.01	<0.01	0.0
Monazite	0.0	0.0	0.0	0.1	0.0
Chromohercynite	0.0	0.0	0.0	0.0	0.0
Spinel	<0.01	<0.01	<0.01	<0.01	0.0

APPENDIX E: Flotation data used in Chapter 3

(a). Solids-water recovery

Solids - water recovery data													
Run no.	Reagents	Sample	Time (min)	Mass pull (g)	Water rec (g)	Cum mass (g)	Cum water (g)	Ave cum mass (g)	Std dev cum mass	Std error Cum mass	Ave cum water rec (g)	Std dev Cum water	Std error Cum water
Ore A	SEX (80 g/t)	C1	2	84.4	74.09	84.40	74.09	84.51	0.16	0.09	73.39	0.99	0.57
Float 1	Senkol (6 g/t	C2	6	21.88	59.3	106.28	133.39	104.85	2.02	1.17	133.10	0.41	0.24
	MIBC (25 g/t	C3	12	12.25	101.83	118.53	235.22	117.09	2.04	1.18	235.43	0.29	0.17
		C4	20	11.07	147.27	129.60	382.49	129.50	0.15	0.09	386.21	5.26	3.04
		F		1445.74									
		T		17.63									
		T2		16.97									
		T3		1245.76									
Ore A	SEX (80 g/t)	C1	2	84.62	72.69	84.62	72.69						
Float 2	Senkol (6 g/t	C2	6	18.8	60.12	103.42	132.81						
	MIBC (25 g/t	C3	12	12.23	102.82	115.65	235.63						
		C4	20	13.74	154.3	129.39	389.93						
		F		1462.22									
		T		16.6									
		T2		16.87									
		T3		1264									
Ore B	SEX (80 g/t)	C1	2	80.35	68.27	80.35	68.27	80.49	0.19	0.11	66.74	2.17	1.25
Float 2	Senkol (6 g/t)	C2	6	27.19	51.59	107.54	119.86	107.23	0.45	0.26	118.38	2.09	1.21
	MIBC (25 g/t)	C3	12	15.5	70.71	123.04	190.57	123.39	0.49	0.28	203.56	18.36	10.60
		C4	20	15.14	136.28	138.18	326.85	137.33	1.20	0.69	339.29	17.59	10.15
		F		1430.73									
		T		17.41									
		T2		17.49									
		T3		1223.05									
Ore B	SEX (80 g/t)	C1	2	80.62	65.2	80.62	65.2						
Float 2	Senkol (6 g/t)	C2	6	26.29	51.7	106.91	116.9						
	MIBC (25 g/t)	C3	12	16.82	99.64	123.73	216.54						
		C4	20	12.75	135.18	136.48	351.72						
		F		1418.08									
		T		16.79									
		T2		17.95									
		T3		1216.33									
Ore C	SEX (80 g/t)	C1	2	77.48	57.17	77.48	57.17	#REF!	4.71	2.72	52.36	6.80	3.93
Float 2	Senkol (6 g/t)	C2	6	26.74	77.02	104.22	134.19	#REF!	4.92	2.84	118.41	22.32	12.88
	MIBC (25 g/t)	C3	12	19.91	109.39	124.13	243.58	#REF!	3.35	1.94	225.80	25.15	14.52
		C4	20	13.50	144.84	137.63	388.42	#REF!	0.64	0.37	385.86	3.63	2.09
		F		1238.53									
		T		14.25									
		T2		14.93									
		T3		1042.59									
Ore C	SEX (80 g/t)	C1	2	70.82	47.55	70.82	47.55						
Float 3	Senkol (6 g/t)	C2	6	26.44	55.08	97.26	102.63						
	MIBC (25 g/t)	C3	12	22.13	105.38	119.39	208.01						
		C4	20	17.34	175.28	136.73	383.29						
		F		1228.41									
		T		13.96									
		T2		13.96									
		T3		1057.83									
Ore D	SEX (80 g/t)	C1	2	18.79	18.23	18.79	18.23	21.91	4.41	2.55	24.69	9.13	5.27
Float 1	Senkol (6 g/t)	C2	6	12.04	31.5	30.83	49.73	34.24	4.82	2.78	74.24	34.66	20.01
	MIBC (25 g/t)	C3	12	10.12	71.18	40.95	120.91	43.19	3.17	1.83	155.82	49.36	28.50
		C4	20	7.3	128.88	48.25	249.79	49.67	2.01	1.16	278.06	39.97	23.08
		F		1311.57									
		T		17.51									
		T2		17.77									
		T3		1228.04									
Ore D'	SEX (80 g/t)	C1	2	25.03	31.14	25.03	31.14						
Float 2	Senkol (6 g/t)	C2	6	12.62	67.61	37.65	98.75						
	MIBC (25 g/t)	C3	12	7.78	91.97	45.43	190.72						
		C4	20	5.66	115.6	51.09	306.32						
		F		1233.83									
		T		18.08									
		T2		19.45									
		T3		1145.21									

Ore E	**SEX (80 g/t)**	**C1**	2	25.03	31.14	25.03	31.14	23.27	2.50	1.44	28.01	4.43	2.56
Float 2	**Senkol (6 g/t**	**C2**	6	12.62	67.61	37.65	98.75	35.47	3.09	1.78	79.57	27.13	15.66
	MIBC (25 g/t	**C3**	12	7.78	91.97	45.43	190.72	44.23	1.70	0.98	170.23	28.98	16.73
		C4	20	5.66	115.6	51.09	306.32	50.56	0.76	0.44	289.02	24.47	14.13
		F		1233.83									
		T		18.08									
		T2		19.45									
		T3		1145.21									
Ore E	**SEX (80 g/t)**	**C1**	2	21.5	24.88	21.5	24.88						
Float 3	**Senkol (6 g/t**	**C2**	6	11.78	35.5	33.28	60.38						
	MIBC (25 g/t	**C3**	12	9.75	89.35	43.03	149.73						
		C4	20	6.99	121.98	50.02	271.71						
		F		1322.57									
		T		18.53									
		T2		18.65									
		T3		1235.37									

Ore F	**SEX (80 g/t)**	**C1**	2	61.31	48.56	61.31	48.56	60.95	0.52	0.30	44.88	5.20	3.00
Float 1	**Senkol (6 g/t**	**C2**	6	14.5	70.12	75.81	118.68	76.41	0.84	0.49	122.21	4.99	2.88
	MIBC (25 g/t	**C3**	12	6.43	103.2	82.24	221.88	82.92	0.96	0.56	234.26	17.50	10.10
		C4	20	5.51	154.36	87.75	376.24	88.53	1.10	0.64	393.40	24.26	14.01
		F		1295.01									
		T		15.39									
		T2		16.84									
		T3		1106.54									
Ore F	**SEX (80 g/t)**	**C1**	2	60.58	41.2	60.58	41.2						
Float 2	**Senkol (6 g/t**	**C2**	6	16.42	84.54	77	125.74						
	MIBC (25 g/t	**C3**	12	6.6	120.89	83.6	246.63						
		C4	20	5.71	163.92	89.31	410.55						
		F		1295.01									
		T		6.34									
		T2		15.53									
		T3		1135									

(b). Element mass – water recovery

Cu

Cu grade and recovery																
Run no.	**Reagents**	**Sample**	**Time (min)**	**Cu (%)**	**Cu mass (g)**	**Cum Cu mass (g)**	**Cu grade (%)**	**Cum rec (%)**	**Ave Cu grade (%)**	**Std dev Cu grade**	**Std error Cu grade**	**Ave Cu rec (%)**	**Std dev Cu rec**	**Std error Cu rec**	**Conc ratio**	**Ave Conc ratio**
Ore A	**SEX (80 g/t)**	**C1**	2	0.08	6.65	6.65	7.88	83.93	7.84	0.06	0.04	84.32	0.54	0.38	14.58	14.43
Float 1	**Senkol (6 g/t)**	**C2**	6	0.03	0.72	7.38	6.94	93.03	6.96	0.03	0.02	92.81	0.31	0.22	6.07	6.01
	MIBC (25 g/t)	**C3**	12	0.01	0.10	7.48	6.31	94.31	6.32	0.02	0.02	94.20	0.16	0.11	1.48	1.59
		C4	20	0.01	0.06	7.54	5.82	95.08	5.78	0.06	0.04	95.18	0.14	0.10	0.96	1.07
		F		0.01	8.23		0.57		0.57	0.00	0.00					
		T2		0.00	0.01											
		T3		0.00	0.37											
		Cc+Tt			0.01	7.93										
		Mass Bal				98.81										
Ore A	**SEX (80 g/t)**	**C1**	2	0.08	6.60	6.60	7.80	84.70							14.28	
Float 2	**Senkol (6 g/t)**	**C2**	6	0.03	0.61	7.21	6.98	92.59							5.96	
	MIBC (25 g/t)	**C3**	12	0.01	0.12	7.33	6.34	94.09							1.71	
		C4	20	0.01	0.09	7.42	5.74	95.28							1.18	
		F		0.01	8.37		0.57									
		T2		0.00	0.00											
		T3		0.00	0.36											
		Cc+Tt			0.01	7.79										
		Mass Bal				95.40										

Ore B	**SEX (80 g/t)**	**C1**	2	0.09	7.56	7.56	9.41	81.76	9.34	0.10	0.07	80.95	1.15	0.81	13.97	13.38
Float 2	**Senkol (6 g/t)**	**C2**	6	0.03	0.89	8.45	7.86	91.37	7.89	0.04	0.03	91.05	0.46	0.32	4.81	4.98
	MIBC (25 g/t)	**C3**	12	0.01	0.20	8.65	7.03	93.55	7.03	0.01	0.01	93.31	0.35	0.25	1.88	1.81
		C4	20	0.01	0.10	8.75	6.33	94.63	6.38	0.06	0.05	94.29	0.49	0.35	0.93	0.88
		F		0.01	10.16		0.71		0.72	0.01	0.01					
		T2		0.00	0.01											
		T3		0.00	0.48											
		Cc+Tt			0.01	9.25										
		Mass Bal				93.27										
Ore B	**SEX (80 g/t)**	**C1**	2	0.09	7.48	7.48	9.28	80.13	8.54						12.80	
Float 3	**Senkol (6 g/t)**	**C2**	6	0.04	0.99	8.47	7.92	90.72	7.45						5.15	
	MIBC (25 g/t)	**C3**	12	0.01	0.22	8.69	7.02	93.06	6.68						1.73	
		C4	20	0.01	0.08	8.77	6.42	93.94	6.08						0.83	
		F		0.01	10.23		0.72									
		T2		0.00	0.01											
		T3		0.00	0.55											
		Cc+Tt			0.01	9.33										
		Mass Bal				93.26										

Ore C	**SEX (80 g/t)**	**C1**	2	0.02	1.93	1.93	2.49	69.54	2.47	0.03	0.02	65.95	5.08	3.59	10.97	10.06
Float 2	**Senkol (6 g/t)**	**C2**	6	0.02	0.48	2.41	2.31	86.93	2.33	0.03	0.02	84.60	3.29	2.33	7.93	7.87
	MIBC (25 g/t)	**C3**	12	0.01	0.15	2.56	2.06	92.21	2.08	0.02	0.02	90.99	1.74	1.23	3.20	3.33
		C4	20	0.00	0.06	2.61	1.90	94.30	1.89	0.01	0.01	93.46	1.20	0.85	1.84	1.75
		F		0.00	2.98		0.24		0.26	0.03	0.02					
		T2		0.00	0.00											
		T3		0.00	0.15											
		Cc+Tt			0.00	2.77										
		Mass Bal				95.42										
Ore C	**SEX (80 g/t)**	**C1**	2	0.02	1.74	1.74	2.45	62.36	5.93						9.14	
Float 3	**Senkol (6 g/t)**	**C2**	6	0.02	0.55	2.29	2.36	82.28	5.11						7.81	
	MIBC (25 g/t)	**C3**	12	0.01	0.21	2.50	2.09	89.76	4.56						3.46	
		C4	20	0.00	0.08	2.58	1.89	92.61	4.11						1.65	
		F		0.00	3.50		0.29									
		T2		0.00	0.00											
		T3		0.00	0.20											
		Cc+Tt			0.00	2.78										
		Mass Bal				79.89										

Ore D	**SEX (80 g/t)**	**C1**	2	0.17	3.15	3.15	16.79	67.77	17.05	0.37	0.26	67.69	0.11	0.08	35.36	36.64
Float 1	**Senkol (6 g/t)**	**C2**	6	0.07	0.86	4.02	13.03	86.31	13.91	1.24	0.88	86.61	0.43	0.30	15.07	18.25
	MIBC (25 g/t)	**C3**	12	0.02	0.22	4.24	10.35	91.02	11.58	1.74	1.23	90.92	0.14	0.10	4.52	5.74
		C4	20	0.01	0.09	4.33	8.98	93.04	10.26	1.82	1.29	92.59	0.62	0.44	2.66	2.95
		F		0.00	6.55		0.50		0.50	0.00	0.00					
		T2		0.00	0.00											
		T3		0.00	0.32											
		Cc+Tt			0.00	4.65										
		Mass Bal				71.02										
Ore D	**SEX (80 g/t)**	**C1**	2	0.17	4.33	4.33	17.30	67.61	15.74						37.93	
Float 2	**Senkol (6 g/t)**	**C2**	6	0.10	1.24	5.57	14.79	86.92	13.77						21.44	
	MIBC (25 g/t)	**C3**	12	0.03	0.25	5.82	12.80	90.82	11.95						6.96	
		C4	20	0.02	0.09	5.90	11.55	92.15	10.77						3.23	
		F		0.00	6.14		0.50									
		T2		0.00	0.01											
		T3		0.00	0.49											
		Cc+Tt			0.01	6.41										
		Mass Bal				104.34										

Ore E	**SEX (80 g/t)**	**C1**	2	0.14	3.55	3.55	14.17	65.54	14.22	0.07	0.05	67.44	2.68	1.89	40.04	42.67
Float 2	**Senkol (6 g/t)**	**C2**	6	0.10	1.25	4.80	12.75	88.71	12.21	0.77	0.54	88.21	0.72	0.51	28.05	24.96
	MIBC (25 g/t)	**C3**	12	0.03	0.24	5.04	11.10	93.22	10.31	1.12	0.79	92.88	0.47	0.33	8.80	7.86
		C4	20	0.01	0.06	5.11	10.00	94.39	9.15	1.20	0.85	94.12	0.38	0.27	3.10	2.82
		F		0.00	4.67		0.38		0.36	0.03	0.02					
		T2		0.00	0.00											
		T3		0.00	0.29											
		Cc+Tt			0.00	5.41										
		Mass Bal				115.74										
Ore E	**SEX (80 g/t)**	**C1**	2	0.14	3.07	3.07	14.27	69.33	12.57						45.30	
Float 3	**Senkol (6 g/t)**	**C2**	6	0.07	0.81	3.88	11.66	87.70	10.86						21.87	
	MIBC (25 g/t)	**C3**	12	0.02	0.21	4.10	9.52	92.55	9.47						6.93	
		C4	20	0.01	0.06	4.15	8.30	93.85	8.71						2.54	
		F		0.00	4.44		0.34									
		T2		0.00	0.00											
		T3		0.00	0.26											
		Cc+Tt			0.00	4.43										
		Mass Bal				99.60										

Ore F	**SEX (80 g/t)**	**C1**	2	0.22	13.76	13.76	22.44	83.74	21.91	0.75	0.53	82.57	1.65	1.17	17.00	16.35
Float 1	**Senkol (6 g/t)**	**C2**	6	0.14	1.97	15.73	20.75	95.74	20.41	0.48	0.34	96.44	0.99	0.70	10.29	10.74
	MIBC (25 g/t)	**C3**	12	0.03	0.18	15.91	19.34	96.84	19.05	0.41	0.29	97.70	1.22	0.86	2.10	2.31
		C4	20	0.01	0.06	15.97	18.20	97.23	17.92	0.40	0.28	98.13	1.28	0.90	0.85	0.90
		F		0.01	17.58		1.36		1.37	0.01	0.01					
		T2		0.00	0.01											
		T3		0.00	0.44											
		Cc+Tt			0.01	16.43										
		Mass Bal				92.90										
Ore F	**SEX (80 g/t)**	**C1**	2	0.21	12.95	12.95	21.38	81.40							15.70	
Float 2	**Senkol (6 g/t)**	**C2**	6	0.15	2.50	15.45	20.07	97.14							11.20	
	MIBC (25 g/t)	**C3**	12	0.03	0.23	15.68	18.76	98.57							2.52	
		C4	20	0.01	0.07	15.75	17.64	99.03							0.94	
		F		0.01	17.79		1.37									
		T2		0.00	0.00											
		T3		0.00	0.15											
		Cc+Tt			0.01	15.91										
		Mass Bal				89.69										

Pb

Pb grade and recovery															
Run no.	Reagents	Sample	Pb (%)	Pb mass (g)	Cum Pb mass (g)	Pb grade (%)	Pb rec (%)	Ave Pb grade (%)	Std dev Pb grade	Std error Pb grade	Ave Pb rec (%)	Std dev Pb rec	Std error Pb rec	Conc ratio	Ave Conc ratio
Ore A	**SEX (80 g/t)**	**C1**	0.06	4.79	4.79	5.68	67.66	5.60	0.11	0.08	68.14	0.68	0.48	12.81	12.89
Float 1	**Senkol (6 g/t)**	**C2**	0.03	0.56	5.36	5.04	75.60	5.01	0.04	0.03	75.61	0.02	0.01	5.66	5.74
	MIBC (25 g/t)	**C3**	0.01	0.14	5.50	4.64	77.59	4.61	0.03	0.02	77.73	0.20	0.14	2.38	2.57
		C4	0.01	0.11	5.60	4.32	79.08	4.28	0.07	0.05	79.67	0.83	0.59	1.94	2.26
		F	0.01	7.95		0.55		0.54	0.02	0.01					
		T1	0.00	0.02											
		T2	0.00	1.42											
		Cc+Tt		0.00	7.08										
		Mass Bal			91.37										
Ore A	**SEX (80 g/t)**	**C1**	0.06	4.68	4.68	5.53	68.62	6.27						12.97	
Float 2	**Senkol (6 g/t)**	**C2**	0.03	0.48	5.16	4.98	75.63	5.48						5.83	
	MIBC (25 g/t)	**C3**	0.01	0.15	5.31	4.59	77.88	4.78						2.75	
		C4	0.01	0.16	5.47	4.23	80.25	4.37						2.57	
		F	0.01	7.63		0.52									
		T1	0.00	0.02											
		T2	0.00	1.31											
		Cc+Tt		0.00	6.82										
		Mass Bal			91.52										
Ore B	**SEX (80 g/t)**	**C1**	0.07	5.36	5.36	6.67	68.51	6.63	0.06	0.04	67.49	1.45	1.02	12.31	12.42
Float 2	**Senkol (6 g/t)**	**C2**	0.02	0.66	6.02	5.60	77.00	5.60	0.00	0.00	76.31	0.97	0.69	4.38	4.76
	MIBC (25 g/t)	**C3**	0.01	0.22	6.24	5.08	79.88	5.08	0.01	0.00	79.24	0.90	0.64	2.51	2.50
		C4	0.01	0.16	6.41	4.64	81.98	4.63	0.01	0.01	81.07	1.29	0.91	1.83	1.74
		F	0.01	9.22		0.64		0.64	0.01	0.00					
		T1	0.00	0.02											
		T2	0.00	1.37											
		Cc+Tt		0.01	7.82										
		Mass Bal			86.91										
Ore B	**SEX (80 g/t)**	**C1**	0.07	5.29	5.29	6.58	66.46	6.06						12.52	
Float 3	**Senkol (6 g/t)**	**C2**	0.03	0.73	6.02	5.60	75.63	5.29						5.15	
	MIBC (25 g/t)	**C3**	0.01	0.24	6.26	5.09	78.60	4.84						2.49	
		C4	0.01	0.12	6.38	4.62	80.16	4.42						1.65	
		F	0.01	9.08		0.63									
		T1	0.00	0.02											
		T2	0.00	1.54											
		Cc+Tt		0.01	7.96										
		Mass Bal			89.61										
Ore C	**SEX (80 g/t)**	**C1**	0.59	44.72	44.72	57.72	74.77	55.48	3.16	2.23	72.03	3.88	2.74	11.63	10.62
Float 2	**Senkol (6 g/t)**	**C2**	0.32	8.60	53.32	51.16	89.16	49.88	1.82	1.28	87.10	2.90	2.05	6.30	6.06
	MIBC (25 g/t)	**C3**	0.07	1.45	54.77	44.13	91.58	43.48	0.91	0.64	90.44	1.61	1.14	1.27	1.55
		C4	0.04	0.58	55.36	40.22	92.56	39.73	0.69	0.49	91.62	1.32	0.93	0.72	0.71
		F	0.05	65.22		5.27		5.86	0.85	0.60					
		T1	0.00	0.06											
		T2	0.00	4.33											
		Cc+Tt		59.81	59.81										
		Mass Bal		0.92	91.38										
Ore C	**SEX (80 g/t)**	**C1**	0.58	41.26	41.26	53.25	69.29	29.96						9.62	
Float 3	**Senkol (6 g/t)**	**C2**	0.36	9.39	50.65	48.59	85.05	27.10						5.83	
	MIBC (25 g/t)	**C3**	0.11	2.53	53.18	42.84	89.31	23.96						1.82	
		C4	0.05	0.82	54.00	39.24	90.69	21.94						0.71	
		F	0.07	80.03		6.46									
		T1	0.01	0.07											
		T2	0.01	5.40											
		Cc+Tt		59.55	59.55										
		Mass Bal			74.77										
Ore D	**SEX (80 g/t)**	**C1**	0.07	1.29	1.29	6.87	55.93	6.94	0.10	0.07	58.98	4.32	3.06	34.10	35.57
Float 1	**Senkol (6 g/t)**	**C2**	0.03	0.35	1.64	5.32	71.12	5.65	0.46	0.33	75.35	5.99	4.23	14.34	17.52
	MIBC (25 g/t)	**C3**	0.01	0.10	1.74	4.25	75.47	4.61	0.51	0.36	77.70	3.16	2.23	4.75	2.60
		C4	0.01	0.05	1.79	3.72	77.78	4.11	0.56	0.39	79.61	2.59	1.83	3.45	3.62
		F	0.00	3.16		0.24		0.24	0.01	0.01					
		T1	0.00	0.01											
		T2	0.00	0.50											
Ore D	**SEX (80 g/t)**	**C1**	0.07	1.75	1.75	7.01	62.04	21.07						37.05	
Float 2	**Senkol (6 g/t)**	**C2**	0.04	0.50	2.25	5.98	79.59	17.41						20.69	
	MIBC (25 g/t)	**C3**	0.00	0.01	2.26	4.97	79.93	14.80						0.45	
		C4	0.01	0.04	2.30	4.51	81.44	13.31						3.79	
		F	0.00	2.83		0.23									
		T1	0.00	0.01											
		T2	0.00	0.47											
		Cc+Tt		0.00	2.83										
		Mass Bal			99.96										

Ore E	**SEX (80 g/t)**	**C1**	0.35	8.80	8.80	35.14	71.09	33.01	3.01	2.13	72.64	2.19	1.55	53.38	56.18
Float 2	**Senkol (6 g/t)**	**C2**	0.16	2.07	10.86	28.85	87.79	26.35	3.53	2.50	87.00	1.12	0.79	24.80	21.07
	MIBC (25 g/t)	**C3**	0.04	0.32	11.19	24.62	90.41	22.54	2.94	2.08	89.83	0.83	0.59	6.21	5.71
		C4	0.02	0.11	11.29	22.11	91.29	20.26	2.61	1.84	90.81	0.67	0.48	2.78	2.67
		F	0.01	9.22		0.75		0.72	0.04	0.03					
		T1	0.00	0.02											
		T2	0.00	1.04											
		Cc+Tt		0.01	12.37										
		Mass Bal			134.12										
Ore E	**SEX (80 g/t)**	**C1**	0.36	7.73	7.73	30.88	74.19	16.91						58.97	
Float 3	**Senkol (6 g/t)**	**C2**	0.11	1.25	8.98	23.85	86.20	13.38						17.34	
	MIBC (25 g/t)	**C3**	0.03	0.32	9.30	20.46	89.24	11.63						5.21	
		C4	0.02	0.11	9.41	18.42	90.34	10.57						2.56	
		F	0.01	9.09		0.69									
		T1	0.00	0.01											
		T2	0.00	0.98											
		Cc+Tt		0.01	10.42										
		Mass Bal			114.61										

Ore F	**SEX (80 g/t)**	**C1**	0.23	14.40	14.40	23.48	83.37	23.25	0.33	0.23	82.61	1.08	0.76	18.43	18.26
Float 1	**Senkol (6 g/t)**	**C2**	0.12	1.76	16.16	21.31	93.58	21.26	0.08	0.05	94.73	1.62	1.15	9.51	10.47
	MIBC (25 g/t)	**C3**	0.02	0.13	16.29	19.81	94.33	19.77	0.05	0.04	95.58	1.77	1.25	1.52	1.72
		C4	0.01	0.07	16.36	18.64	94.72	18.60	0.06	0.04	96.00	1.81	1.28	0.91	0.96
		F	0.01	17.48		1.35		1.33	0.03	0.02					
		T1	0.00	0.01											
		T2	0.00	0.89											
		Cc+Tt		0.01	17.27										
		Mass Bal			98.21										
Ore F	**SEX (80 g/t)**	**C1**	0.23	13.94	13.94	23.01	81.84							18.09	
Float 2	**Senkol (6 g/t)**	**C2**	0.15	2.39	16.33	21.21	95.87							11.43	
	MIBC (25 g/t)	**C3**	0.02	0.16	16.49	19.73	96.84							1.93	
		C4	0.01	0.08	16.57	18.55	97.28							1.02	
		F	0.01	16.96		1.31									
		T1	0.00	0.01											
		T2	0.00	0.45											
		Cc+Tt		0.01	17.03										
		Mass Bal			100.69										

Zn

Zn grade and recovery															
Run no.	**Reagents**	**Sample**	**Zn (%)**	**Zn mass (g)**	**Cum Zn mass (g)**	**Zn grade (%)**	**Zn rec (%)**	**Ave Zn grade (%)**	**Std dev Zn grade**	**Std error Zn grade**	**Ave Zn rec (%)**	**Std dev Zn rec**	**Std error Zn rec**	**Conc ratio**	**Ave Conc ratio**
Ore A	**SEX (80 g/t)**	**C1**	0.25	21.04	21.04	24.93	81.35	25.02	0.13	0.09	81.63	0.40	0.28	14.62	15.00
Float 1	**Senkol (6 g/t)**	**C2**	0.11	2.45	23.48	22.10	90.80	22.39	0.41	0.29	90.60	0.29	0.21	6.50	6.80
	MIBC (25 g/t)	**C3**	0.02	0.24	23.72	20.01	91.72	20.27	0.37	0.26	91.62	0.14	0.10	1.05	1.22
		C4	0.01	0.07	23.79	18.36	91.99	18.39	0.05	0.04	91.96	0.05	0.04	0.28	0.32
		F	0.02	26.83		1.86		1.82	0.05	0.04					
		T1	0.00	0.03											
		T2	0.00	2.01											
		Cc+Tt		0.02	25.86										
		Mass Bal			98.83										
Ore A	**SEX (80 g/t)**	**C1**	0.25	21.25	21.25	25.12	81.91							15.38	
Float 2	**Senkol (6 g/t)**	**C2**	0.12	2.20	23.45	22.68	90.39							7.11	
	MIBC (25 g/t)	**C3**	0.02	0.29	23.74	20.53	91.52							1.38	
		C4	0.01	0.10	23.85	18.43	91.92							0.36	
		F	0.02	26.09		1.78									
		T1	0.00	0.03											
		T2	0.00	2.04											
		Cc+Tt		0.02	25.94										
		Mass Bal			101.90										

Ore B	**SEX (80 g/t)**	**C1**	0.22	17.39	17.39	21.64	78.30	21.24	0.57	0.40	77.28	1.45	1.02	14.88	14.63
Float 2	**Senkol (6 g/t)**	**C2**	0.08	2.20	19.58	18.21	88.19	18.10	0.16	0.11	87.72	0.66	0.47	5.48	5.89
	MIBC (25 g/t)	**C3**	0.02	0.38	19.97	16.23	89.92	16.08	0.22	0.15	89.67	0.36	0.26	1.60	1.72
		C4	0.01	0.11	20.08	14.53	90.41	14.51	0.02	0.02	90.10	0.44	0.31	0.37	0.35
		F	0.02	23.07		1.89		1.75	0.19	0.14					
		T1	0.00	0.03											
		T2	0.00	2.07											
		Cc+Tt		0.02	22.21										
		Mass Bal			98.63										
Ore B	**SEX (80 g/t)**	**C1**	0.21	16.80	16.80	20.84	76.26							14.39	
Float 3	**Senkol (6 g/t)**	**C2**	0.09	2.42	19.23	17.98	87.26							6.30	
	MIBC (25 g/t)	**C3**	0.03	0.47	19.70	15.92	89.41							1.84	
		C4	0.01	0.08	19.78	14.50	89.79							0.33	
		F	0.02	22.91		1.62									
		T1	0.00	0.03											
		T2	0.00	2.19											
		Cc+Tt		0.02	22.03										
		Mass Bal			98.28										

Ore C	**SEX (80 g/t)**	**C1**	0.04	3.47	3.47	4.48	58.66	4.45	0.05	0.04	56.24	3.42	2.42	13.31	12.23
Float 2	**Senkol (6 g/t)**	**C2**	0.02	0.59	4.06	3.90	68.62	3.93	0.04	0.03	67.49	1.60	1.13	6.30	6.56
	MIBC (25 g/t)	**C3**	0.01	0.13	4.19	3.38	70.79	3.39	0.02	0.01	70.36	0.61	0.43	1.50	1.78
		C4	0.00	0.05	4.25	3.09	71.68	3.06	0.04	0.03	71.47	0.29	0.21	0.72	0.74
		F	0.00	5.97		0.57		0.55	0.03	0.02					
		T1	0.00	0.02											
		T2	0.00	1.63											
		Cc+Tt		5.92	5.92										
		Mass Bal		0.99	101.67										
Ore C	**SEX (80 g/t)**	**C1**	0.04	3.12	3.12	4.41	53.83							11.16	
Float 3	**Senkol (6 g/t)**	**C2**	0.03	0.73	3.85	3.96	66.36							6.81	
	MIBC (25 g/t)	**C3**	0.01	0.21	4.06	3.40	69.93							2.05	
		C4	0.00	0.08	4.14	3.03	71.27							0.77	
		F	0.01	6.58		0.54									
		T1	0.00	0.02											
		T2	0.00	1.62											
		Cc+Tt		0.00	5.80										
		Mass Bal			88.70										

Ore D	**SEX (80 g/t)**	**C1**	0.02	0.36	0.36	1.94	34.19	1.96	0.02	0.02	37.63	4.86	3.44	35.86	40.20
Float 1	**Senkol (6 g/t)**	**C2**	0.01	0.11	0.48	1.54	44.57	1.62	0.11	0.08	48.90	6.11	4.32	16.56	21.13
	MIBC (25 g/t)	**C3**	0.00	0.03	0.51	1.24	47.45	1.35	0.17	0.12	51.56	5.81	4.11	4.90	6.31
		C4	0.00	0.01	0.52	1.08	48.82	1.21	0.18	0.13	52.73	5.53	3.91	2.98	3.36
		F	0.00	1.26		0.10		0.09	0.01	0.00					
		T1	0.00	0.01											
		T2	0.00	0.53											
Ore D	**SEX (80 g/t)**	**C1**	0.02	0.49	0.49	1.97	41.07							44.53	
Float 2	**Senkol (6 g/t)**	**C2**	0.01	0.15	0.64	1.70	53.22							25.70	
	MIBC (25 g/t)	**C3**	0.00	0.03	0.67	1.47	55.67							7.72	
		C4	0.00	0.01	0.68	1.33	56.64							3.73	
		F	0.00	1.08		0.09									
		T1	0.00	0.01											
		T2	0.00	0.51											
		Cc+Tt		0.00	1.20										
		Mass Bal			111.50										

Ore E	**SEX (80 g/t)**	**C1**	0.01	0.19	0.19	0.75	26.88	0.76	0.01	0.01	26.20	0.95	0.67	43.02	40.44
Float 2	**Senkol (6 g/t)**	**C2**	0.01	0.08	0.27	0.72	38.48	0.69	0.04	0.03	36.22	3.19	2.25	36.54	29.37
	MIBC (25 g/t)	**C3**	0.00	0.02	0.29	0.64	41.71	0.60	0.06	0.04	39.56	3.05	2.15	15.41	12.76
		C4	0.00	0.01	0.30	0.59	42.95	0.54	0.06	0.04	40.89	2.91	2.06	7.18	6.21
		F	0.00	0.62		0.05		0.05	0.00	0.00					
		T1	0.00	0.01											
		T2	0.00	0.39											
		Cc+Tt		0.00	0.70										
		Mass Bal			112.45										
Ore E	**SEX (80 g/t)**	**C1**	0.01	0.16	0.16	0.76	25.53							37.86	
Float 3	**Senkol (6 g/t)**	**C2**	0.00	0.05	0.22	0.66	33.97							22.21	
	MIBC (25 g/t)	**C3**	0.00	0.02	0.24	0.56	37.40							10.10	
		C4	0.00	0.01	0.25	0.50	38.84							5.24	
		F	0.00	0.67		0.05									
		T1	0.00	0.01											
		T2	0.00	0.38											
		Cc+Tt		0.00	0.64										
		Mass Bal			96.74										

Ore F	**SEX (80 g/t)**	**C1**	0.03	2.03	2.03	3.30	64.46	3.45	0.21	0.15	67.08	3.72	2.63	14.77	15.52
Float 1	**Senkol (6 g/t)**	**C2**	0.05	0.73	2.76	3.64	87.68	3.62	0.01	0.01	88.32	0.91	0.64	22.57	19.57
	MIBC (25 g/t)	**C3**	0.01	0.04	2.79	3.40	88.89	3.39	0.01	0.01	89.56	0.95	0.67	2.54	2.58
		C4	0.00	0.01	2.80	3.20	89.24	3.19	0.02	0.01	89.92	0.97	0.68	0.76	0.80
		F	0.00	3.26		0.25		0.25	0.00	0.00					
		T1	0.00	0.01											
		T2	0.00	0.33											
		Cc+Tt		0.00	3.14										
		Mass Bal			95.99										
Ore F	**SEX (80 g/t)**	**C1**	0.04	2.18	2.18	3.60	69.71							16.27	
Float 2	**Senkol (6 g/t)**	**C2**	0.04	0.60	2.78	3.61	88.96							16.58	
	MIBC (25 g/t)	**C3**	0.01	0.04	2.82	3.38	90.23							2.61	
		C4	0.00	0.01	2.83	3.17	90.61							0.83	
		F	0.00	3.17		0.25									
		T1	0.00	0.00											
		T2	0.00	0.29											
		Cc+Tt		0.00	3.13										
		Mass Bal			98.84										

Fe

Fe grade and recovery													
Run no.	**Reagents**	**Sample**	**Fe (%)**	**Fe mass (g)**	**Cum Fe mass (g)**	**Fe grade (%)**	**Fe rec (%)**	**Ave Fe grade (%)**	**Std dev Fe grade**	**Std error Fe grade**	**Ave Fe rec (%)**	**Std dev Fe rec**	**Std error Fe rec**
Ore A	**SEX (80 g/t)**	**C1**	0.29	24.31	24.31	28.81	3.07	28.90	0.13	0.10	3.03	0.05	0.04
Float 1	**Senkol (6 g/t)**	**C2**	0.43	9.39	33.70	31.71	4.25	31.61	0.14	0.10	4.11	0.20	0.14
	MIBC (25 g/t)	**C3**	0.51	6.22	39.92	33.68	5.04	33.55	0.18	0.13	4.87	0.23	0.16
		C4	0.48	5.36	45.28	34.94	5.71	34.90	0.06	0.04	5.60	0.15	0.11
		F	0.56	810.19		56.04		56.59	0.78	0.55			
		T1	0.58	9.91									
		T2	0.58	727.17									
		Cc+Tt		0.55	792.65								
		Mass Bal			100.32								
Ore A	**SEX (80 g/t)**	**C1**	0.29	24.54	24.54	29.00	2.99	29.32					
Float 2	**Senkol (6 g/t)**	**C2**	0.43	8.06	32.59	31.52	3.97	31.39					
	MIBC (25 g/t)	**C3**	0.50	6.06	38.65	33.42	4.71	32.79					
		C4	0.47	6.44	45.10	34.85	5.50	33.81					
		F	0.57	835.51		57.14							
		T1	0.60	10.08									
		T2	0.60	755.48									
		Cc+Tt		0.56	820.58								
		Mass Bal			100.65								
Ore B	**SEX (80 g/t)**	**C1**	0.29	23.29	23.29	28.99	2.93	29.63	0.91	0.64	3.03	0.14	0.10
Float 2	**Senkol (6 g/t)**	**C2**	0.45	12.21	35.51	33.02	4.47	33.35	0.48	0.34	4.55	0.11	0.08
	MIBC (25 g/t)	**C3**	0.47	7.23	42.74	34.73	5.38	35.19	0.64	0.45	5.52	0.20	0.14
		C4	0.47	7.18	49.92	36.13	6.28	36.43	0.42	0.30	6.36	0.11	0.08
		F	0.58	830.12		58.02		58.15	0.19	0.13			
		T1	0.59	10.35									
		T2	0.59	724.01									
		Cc+Tt		0.56	794.59								
		Mass Bal			98.09								
Ore B	**SEX (80 g/t)**	**C1**	0.30	24.41	24.41	30.27	3.13	29.64					
Float 3	**Senkol (6 g/t)**	**C2**	0.44	11.61	36.02	33.69	4.62	32.60					
	MIBC (25 g/t)	**C3**	0.48	8.08	44.10	35.64	5.66	34.53					
		C4	0.47	6.03	50.12	36.73	6.43	35.79					
		F	0.58	826.54		58.29							
		T1	0.61	11.04									
		T2	0.55	669.80									
		Cc+Tt		0.55	779.17								
		Mass Bal			96.34								
Ore C	**SEX (80 g/t)**	**C1**	0.09	7.21	7.21	9.30	1.04	9.21	0.14	0.10	0.98	0.09	0.06
Float 2	**Senkol (6 g/t)**	**C2**	0.29	7.78	14.99	14.39	2.16	13.78	0.86	0.61	1.99	0.25	0.17
	MIBC (25 g/t)	**C3**	0.43	8.59	23.58	18.99	3.40	18.60	0.56	0.40	3.24	0.23	0.16
		C4	0.45	6.04	29.62	21.52	4.28	21.48	0.05	0.04	4.22	0.08	0.06
		F	0.59	735.00		59.34		59.72	0.54	0.38			
		T1	0.62										
		T2	0.62	645.04									
		Cc+Tt		0.56	692.71								
		Mass Bal			96.52								
Ore C	**SEX (80 g/t)**	**C1**	0.09	6.45	6.45	9.11	0.91	19.05					
Float 3	**Senkol (6 g/t)**	**C2**	0.24	6.36	12.81	13.17	1.82	23.09					
	MIBC (25 g/t)	**C3**	0.40	8.92	21.73	18.20	3.08	26.47					
		C4	0.44	7.59	29.32	21.44	4.16	28.79					
		F	0.60	738.33		60.10							
		T1	0.62	8.69									
		T2	0.62	658.57									
		Cc+Tt		0.57	705.27								
		Mass Bal			95.99								

Ore D	**SEX (80 g/t)**	**C1**	0.29	5.51	5.51	29.32	0.77	29.48	0.23	0.16	0.94	0.24	0.17
Float 1	**Senkol (6 g/t)**	**C2**	0.37	4.46	9.97	32.35	1.39	31.81	0.77	0.54	1.57	0.27	0.19
	MIBC (25 g/t)	**C3**	0.35	3.57	13.54	33.06	1.88	32.61	0.64	0.45	2.04	0.22	0.15
		C4	0.40	2.91	16.45	34.10	2.29	33.44	0.94	0.66	2.40	0.16	0.11
		F	0.54	714.40		54.47		54.94	0.66	0.47			
		T1	0.56	9.89									
		T2	0.56	683.66									
Ore D	**SEX (80 g/t)**	**C1**	0.30	7.42	7.42	29.64	1.11	22.07					
Float 2	**Senkol (6 g/t)**	**C2**	0.34	4.35	11.77	31.27	1.76	24.34					
	MIBC (25 g/t)	**C3**	0.36	2.84	14.61	32.16	2.19	26.01					
		C4	0.38	2.14	16.75	32.78	2.51	27.10					
		F	0.55	683.64		55.41							
		T1	0.55	0.00									
		T2	0.55	629.97									
		Cc+Tt		0.54	667.36								
		Mass Bal			97.62								

Ore E	**SEX (80 g/t)**	**C1**	0.14	3.63	3.63	14.49	0.53	15.48	1.39	0.99	0.52	0.03	0.02
Float 2	**Senkol (6 g/t)**	**C2**	0.23	2.93	6.56	17.42	0.97	18.48	1.50	1.06	0.94	0.04	0.03
	MIBC (25 g/t)	**C3**	0.32	2.47	9.02	19.86	1.33	21.09	1.74	1.23	1.34	0.01	0.01
		C4	0.34	1.92	10.95	21.42	1.61	22.89	2.07	1.46	1.66	0.07	0.05
		F	0.54	669.66		54.27		54.08	0.27	0.19			
		T1	0.56	10.03									
		T2	0.56	646.32									
		Cc+Tt		0.55	678.44								
		Mass Bal			101.31								
Ore E	**SEX (80 g/t)**	**C1**	0.16	3.54	3.54	16.47	0.50	31.90					
Float 3	**Senkol (6 g/t)**	**C2**	0.25	2.96	6.50	19.54	0.91	33.09					
	MIBC (25 g/t)	**C3**	0.32	3.10	9.61	22.32	1.35	34.24					
		C4	0.37	2.57	12.18	24.35	1.71	34.97					
		F	0.54	712.76		53.89							
		T1	0.55	0.00									
		T2	0.55	680.29									
		Cc+Tt		0.54	712.94								
		Mass Bal			100.03								

Ore F	**SEX (80 g/t)**	**C1**	0.22	13.24	13.24	21.59	1.99	22.19	0.84	0.60	2.01	0.02	0.02
Float 1	**Senkol (6 g/t)**	**C2**	0.28	4.12	17.35	22.89	2.61	23.29	0.57	0.40	2.65	0.05	0.03
	MIBC (25 g/t)	**C3**	0.37	2.37	19.72	23.98	2.97	24.36	0.54	0.38	3.00	0.05	0.03
		C4	0.37	2.06	21.79	24.83	3.28	25.19	0.51	0.36	3.32	0.05	0.03
		F	0.53	691.02		53.36		52.88	0.69	0.48			
		T1	0.56	9.49									
		T2	0.56	0.25									
		Cc+Tt		0.51	663.82								
		Mass Bal			95.52								
Ore F	**SEX (80 g/t)**	**C1**	0.23	13.80	13.80	22.78	2.03						
Float 2	**Senkol (6 g/t)**	**C2**	0.27	4.44	18.24	23.69	2.68						
	MIBC (25 g/t)	**C3**	0.37	2.44	20.68	24.74	3.04						
		C4	0.37	2.14	22.82	25.55	3.35						
		F	0.52	678.46		52.39							
		T1	0.57	8.84									
		T2	0.57	0.09									
		Cc+Tt		0.53	680.97								
		Mass Bal			100.67								

Mn

Mn grade and recovery													
Run no.	**Reagents**	**Sample**	**Mn (%)**	**Mn mass (g)**	**Cum Mn mass (g)**	**Mn grade (%)**	**Mn rec (%)**	**Ave Mn grade (%)**	**Std dev Mn grade**	**Std error Mn grade**	**Ave Mn rec (%)**	**Std dev Mn rec**	**Std error Mn rec**
Ore A	**SEX (80 g/t)**	**C1**	0.02	1.88	1.88	2.23	2.42	2.41	0.26	0.18	2.62	0.28	0.20
Float 1	**Senkol (6 g/t)**	**C2**	0.04	0.89	2.77	2.61	3.57	2.75	0.20	0.14	3.70	0.19	0.13
	MIBC (25 g/t)	**C3**	0.06	0.72	3.49	2.95	4.49	3.08	0.19	0.13	4.63	0.19	0.14
		C4	0.07	0.79	4.28	3.31	5.51	3.48	0.25	0.18	5.79	0.40	0.28
		F	0.06	81.05		5.61		5.56	0.07	0.05			
		T1	0.06	0.97									
		T2	0.06	71.44									
		Cc+Tt		0.05	77.71								
		Mass Bal			98.31								
Ore A	**SEX (80 g/t)**	**C1**	0.03	2.20	2.20	2.59	2.81	1.57					
Float 2	**Senkol (6 g/t)**	**C2**	0.04	0.79	2.99	2.89	3.83	1.77					
	MIBC (25 g/t)	**C3**	0.06	0.73	3.72	3.21	4.76	1.97					
		C4	0.07	1.02	4.74	3.66	6.08	2.24					
		F	0.06	80.51		5.51							
		T1	0.06	0.95									
		T2	0.06	71.35									
		Cc+Tt		0.05	77.98								
		Mass Bal			99.26								
Ore B	**SEX (80 g/t)**	**C1**	0.02	1.63	1.63	2.02	2.11	2.10	0.11	0.08	2.20	0.12	0.08
Float 2	**Senkol (6 g/t)**	**C2**	0.05	1.38	3.01	2.80	3.91	2.72	0.11	0.08	3.78	0.17	0.12
	MIBC (25 g/t)	**C3**	0.06	0.95	3.96	3.22	5.15	3.17	0.07	0.05	5.08	0.10	0.07
		C4	0.08	1.16	5.12	3.70	6.65	3.61	0.14	0.10	6.43	0.31	0.22
		F	0.06	82.85		5.79		5.76	0.05	0.03			
		T1	0.06	1.00									
		T2	0.06	69.88									
		Cc+Tt		0.05	76.99								
		Mass Bal			95.23								
Ore B	**SEX (80 g/t)**	**C1**	0.02	1.76	1.76	2.18	2.28	2.39					
Float 3	**Senkol (6 g/t)**	**C2**	0.04	1.07	2.82	2.64	3.66	2.77					
	MIBC (25 g/t)	**C3**	0.06	1.04	3.86	3.12	5.01	3.17					
		C4	0.07	0.93	4.79	3.51	6.21	3.59					
		F	0.06	81.20		5.73							
		T1	0.06	1.01									
		T2	0.06	70.32									
		Cc+Tt		0.05	77.12								
		Mass Bal			97.07								
Ore C	**SEX (80 g/t)**	**C1**	0.02	1.20	1.20	1.56	1.47	1.53	0.04	0.03	1.37	0.14	0.10
Float 2	**Senkol (6 g/t)**	**C2**	0.06	1.71	2.92	2.80	3.55	2.65	0.21	0.15	3.23	0.46	0.32
	MIBC (25 g/t)	**C3**	0.11	2.09	5.01	4.04	6.11	3.96	0.10	0.07	5.82	0.40	0.29
		C4	0.11	1.42	6.43	4.67	7.84	4.71	0.05	0.04	7.79	0.08	0.05
		F	0.07	86.98		7.02		6.97	0.07	0.05			
		T1	0.07	1.05									
		T2	0.07	73.55									
		Cc+Tt		0.07	82.04								
		Mass Bal			96.59								
Ore C	**SEX (80 g/t)**	**C1**	0.01	1.06	1.06	1.50	1.26	1.76					
Float 3	**Senkol (6 g/t)**	**C2**	0.05	1.38	2.44	2.51	2.90	2.65					
	MIBC (25 g/t)	**C3**	0.10	2.21	4.64	3.89	5.53	3.55					
		C4	0.11	1.85	6.49	4.75	7.73	4.23					
		F	0.07	85.08		6.93							
		T1	0.07	1.00									
		T2	0.07	75.43									
		Cc+Tt		0.07	83.91								
		Mass Bal			99.10								

Ore D	**SEX (80 g/t)**	**C1**	0.01	0.11	0.11	0.58	0.86	0.57	0.01	0.01	1.02	0.23	0.17
Float 1	**Senkol (6 g/t)**	**C2**	0.01	0.12	0.22	0.73	1.78	0.69	0.06	0.04	1.93	0.21	0.15
	MIBC (25 g/t)	**C3**	0.01	0.13	0.35	0.86	2.79	0.80	0.09	0.06	2.83	0.05	0.04
		C4	0.02	0.11	0.46	0.96	3.69	0.89	0.10	0.07	3.63	0.08	0.06
		F	0.01	13.04		0.99		0.98	0.02	0.01			
		T1	0.01	0.17									
		T2	0.01	11.79									
Ore D	**SEX (80 g/t)**	**C1**	0.01	0.14	0.14	0.56	1.19	0.44					
Float 2	**Senkol (6 g/t)**	**C2**	0.01	0.10	0.24	0.65	2.08	0.58					
	MIBC (25 g/t)	**C3**	0.01	0.09	0.33	0.74	2.86	0.70					
		C4	0.01	0.08	0.42	0.82	3.57	0.79					
		F	0.01	12.00		0.97							
		T1	0.01	0.19									
		T2	0.01	10.91									
		Cc+Tt		0.01	11.69								
		Mass Bal			97.35								

Ore E	**SEX (80 g/t)**	**C1**	0.00	0.08	0.08	0.32	0.69	0.38	0.09	0.06	0.74	0.06	0.05
Float 2	**Senkol (6 g/t)**	**C2**	0.01	0.12	0.20	0.52	1.69	0.61	0.12	0.08	1.78	0.12	0.09
	MIBC (25 g/t)	**C3**	0.01	0.11	0.31	0.67	2.64	0.77	0.14	0.10	2.84	0.28	0.20
		C4	0.01	0.08	0.39	0.76	3.35	0.87	0.15	0.11	3.66	0.43	0.31
		F	0.01	11.66		0.94		0.94	0.01	0.01			
		T1	0.01	0.17									
		T2	0.01	0.17									
		Cc+Tt		0.01	11.58								
		Mass Bal			99.31								
Ore E	**SEX (80 g/t)**	**C1**	0.00	0.10	0.10	0.45	0.78	0.25					
Float 3	**Senkol (6 g/t)**	**C2**	0.01	0.13	0.23	0.69	1.87	0.39					
	MIBC (25 g/t)	**C3**	0.01	0.14	0.37	0.87	3.04	0.49					
		C4	0.02	0.11	0.49	0.97	3.96	0.55					
		F	0.01	12.26		0.93							
		T1	0.01	0.18									
		T2	0.01	11.45									
		Cc+Tt		0.01	12.28								
		Mass Bal			100.13								

Ore F	**SEX (80 g/t)**	**C1**	0.00	0.07	0.07	0.11	2.11	0.11	0.00	0.00	2.11	0.00	0.00
Float 1	**Senkol (6 g/t)**	**C2**	0.00	0.04	0.11	0.14	3.50	0.14	0.01	0.00	3.47	0.04	0.03
	MIBC (25 g/t)	**C3**	0.01	0.03	0.14	0.17	4.59	0.17	0.01	0.00	4.56	0.04	0.03
		C4	0.00	0.03	0.17	0.19	5.41	0.19	0.00	0.00	5.41	0.00	0.00
		F	0.00	3.24		0.25		0.25	0.01	0.00			
		T1	0.00	0.04									
		T2	0.00	0.00									
		Cc+Tt		0.00	3.09								
		Mass Bal			94.80								
Ore F	**SEX (80 g/t)**	**C1**	0.00	0.06	0.06	0.11	2.10	0.05					
Float 2	**Senkol (6 g/t)**	**C2**	0.00	0.04	0.10	0.14	3.44	0.07					
	MIBC (25 g/t)	**C3**	0.00	0.03	0.14	0.16	4.53	0.08					
		C4	0.00	0.03	0.16	0.18	5.41	0.09					
		F	0.00	3.12		0.24							
		T1	0.00	0.04									
		T2	0.00	0.00									
		Cc+Tt		0.00	3.03								
		Mass Bal			97.43								

APPENDIX F: Liberation data used in Chapter 3

Note: -10/0 particle size fraction liberation data assumed to be the same as the -38/10 particle size fraction.

(a). Chalcopyrite

Chalcopyrite liberation													
Ore	Size	0.0	<= 10%	<= 20%	<= 30%	<= 40%	<= 50%	<= 60%	<= 70%	<= 80%	<= 90%	< 100%	100.0	Weight
Ore A	-300/75	0.0	19.2	11.2	4.7	4.3	2.4	5.4	1.2	1.6	5.7	26.7	17.5	37.4
	-75/38	0.0	8.3	6.1	2.5	3.5	2.3	3.1	2.9	2.4	4.8	19.1	45.1	30.2
	-38/10	0.0	3.5	2.1	1.4	1.3	0.9	1.2	1.2	2.0	2.0	13.7	70.8	20.7
	-10/0	0.0	3.1	4.0	2.7	2.7	3.1	2.2	3.3	5.1	7.6	10.8	55.4	11.7
	Comb	0.0	8.1	5.6	2.7	2.9	2.1	2.9	2.1	2.8	4.9	17.3	48.8	100.0
Ore B	-300/75	0.0	25.2	9.0	3.7	3.5	4.5	2.0	1.4	3.3	5.3	15.9	26.3	41.1
	-75/38	0.0	8.6	4.6	2.8	2.6	2.7	2.5	2.4	2.9	4.9	21.5	44.7	24.6
	-38/10	0.0	3.9	2.7	1.9	1.6	1.7	1.2	2.0	2.1	3.4	15.8	63.9	28.5
	-10/0	0.0	3.7	3.5	2.5	2.4	2.8	1.7	2.6	4.1	7.4	11.2	58.2	5.8
	Comb	0.0	10.1	4.7	2.6	2.3	2.7	1.7	2.0	2.8	4.6	16.5	50.0	100.0
Ore C	-300/75	0.0	29.4	13.4	4.3	7.1	0.7	0.4	1.4	1.6	1.5	14.8	25.4	33.8
	-75/38	0.0	10.0	4.8	4.1	3.5	1.3	2.5	2.7	1.9	3.8	19.2	46.3	32.4
	-38/10	0.0	3.1	2.5	1.5	1.2	0.6	0.8	0.8	1.2	1.9	13.1	73.3	17.4
	-10/0	0.0	3.6	3.5	2.5	1.8	2.4	1.5	2.6	3.6	6.7	9.3	62.4	16.5
	Comb	0.0	9.1	5.1	2.9	2.9	1.3	1.4	1.9	2.2	3.7	13.7	56.0	100.0
Ore D	-300/75	0.0	16.6	10.4	7.3	7.0	9.9	5.8	8.8	8.1	2.4	14.8	8.9	36.4
	-75/38	0.0	6.4	4.6	4.8	5.1	3.6	5.1	4.4	5.2	6.4	22.2	32.3	34.6
	-38/10	0.0	2.5	2.3	2.2	2.2	1.9	2.2	2.4	2.6	4.5	14.9	62.3	17.9
	-10/0	0.0	2.1	2.3	1.7	1.7	2.2	1.1	2.2	2.9	4.4	9.5	69.9	11.2
	Comb	0.0	6.3	4.5	3.9	3.9	4.0	3.5	4.2	4.5	4.7	16.0	44.5	100.0
Ore F	-300/75	0.0	3.9	2.1	0.9	1.3	0.7	1.5	3.2	2.2	2.6	31.4	50.1	26.2
	-75/38	0.0	1.3	0.6	0.6	1.0	0.5	1.2	1.3	1.5	3.8	24.2	64.1	37.5
	-38/10	0.0	0.8	0.7	0.5	0.6	0.6	0.6	0.7	0.8	1.6	14.4	78.8	28.9
	-10/0	0.0	3.1	3.4	2.4	2.2	2.6	1.9	2.7	3.7	6.4	8.9	62.7	7.5
	Comb	0.0	1.8	1.2	0.8	1.0	0.8	1.1	1.6	1.7	3.2	19.8	67.0	100.0

(b). Galena

Galena liberation													
Ore	Size	0.0	<= 10%	<= 20%	<= 30%	<= 40%	<= 50%	<= 60%	<= 70%	<= 80%	<= 90%	< 100%	100.0	Weight
Ore A	-300/75	0.0	54.8	12.2	7.4	6.5	2.2	2.5	0.0	0.0	0.0	13.5	1.0	37.4
	-75/38	0.0	24.0	6.3	2.3	6.9	0.1	0.0	0.6	5.2	6.5	43.4	4.9	30.2
	-38/10	0.0	5.3	2.7	1.7	1.0	1.0	1.3	0.7	1.4	2.8	51.9	30.3	20.7
	-10/0	0.0	2.4	3.3	2.4	3.1	5.0	3.8	6.3	11.8	15.6	18.8	27.6	11.7
	Comb	0.0	19.4	5.7	3.2	4.1	2.0	1.9	2.0	4.6	6.4	33.3	17.6	100.0
Ore B	-300/75	0.0	61.7	12.6	7.5	2.9	3.6	0.0	0.0	0.0	1.0	7.1	3.7	41.1
	-75/38	0.0	26.0	8.8	5.7	6.5	1.4	1.5	0.1	0.0	2.1	40.0	8.0	24.6
	-38/10	0.0	5.8	3.1	1.9	1.3	1.2	1.1	1.7	2.8	6.5	42.4	32.2	28.5
	-10/0	0.0	3.0	3.1	2.0	1.8	3.7	3.2	5.2	9.9	20.1	21.8	26.2	5.8
	Comb	0.0	22.2	6.3	3.9	2.6	2.0	1.1	1.3	2.3	5.6	31.9	20.8	100.0
Ore C	-300/75	0.0	40.7	19.0	8.9	2.9	2.8	0.6	0.9	1.4	0.4	18.6	3.9	33.8
	-75/38	0.0	7.7	3.9	2.1	1.8	1.1	0.9	0.6	1.2	1.4	52.1	27.1	32.4
	-38/10	0.0	2.0	1.4	0.9	0.7	0.7	0.5	0.7	1.1	2.1	46.8	43.3	17.4
	-10/0	0.0	1.9	2.0	1.5	1.6	2.2	1.6	2.6	4.8	9.9	18.6	53.4	16.5
	Comb	0.0	6.5	3.7	2.1	1.5	1.6	1.1	1.4	2.7	5.0	33.9	40.6	100.0
Ore D	-300/75	0.0	51.5	10.9	0.0	11.9	0.0	0.0	5.6	2.8	0.0	17.4	0.0	36.4
	-75/38	0.0	15.7	6.5	5.0	5.7	2.4	4.0	5.2	4.5	9.3	34.7	7.2	34.6
	-38/10	0.0	3.5	2.4	2.0	1.3	2.4	1.9	1.4	2.2	5.6	42.8	34.5	17.9
	-10/0	0.0	1.7	1.5	1.4	1.3	2.1	1.6	2.0	5.1	11.9	23.7	47.9	11.2
	Comb	0.0	14.0	4.7	2.5	4.2	1.9	2.1	3.3	3.7	7.5	31.5	24.6	100.0
Ore F	-300/75	0.0	22.5	10.6	1.8	2.4	0.0	0.0	0.0	9.4	2.0	44.8	6.6	26.2
	-75/38	0.0	2.6	1.8	0.1	1.3	1.3	0.7	1.3	1.6	0.6	80.6	8.1	37.5
	-38/10	0.0	0.9	0.6	0.4	0.4	0.6	0.4	0.8	1.1	3.2	49.2	42.4	28.9
	-10/0	0.0	2.9	3.5	3.0	3.2	4.7	3.8	5.8	9.8	16.0	19.8	27.5	7.5
	Comb	0.0	2.5	1.8	0.9	1.3	1.6	1.2	1.9	3.3	5.0	51.9	28.7	100.0

(c). Sphalerite

Sphalerite liberation													
Ore	Size	0.0	<= 10%	<= 20%	<= 30%	<= 40%	<= 50%	<= 60%	<= 70%	<= 80%	<= 90%	< 100%	100.0	Weight
Ore A	-300/75	0.0	12.8	4.9	3.6	5.0	3.7	2.4	2.4	2.1	5.2	44.7	13.3	37.4
	-75/38	0.0	2.7	1.3	1.1	0.8	0.8	0.9	0.8	2.1	3.7	56.4	29.4	30.2
	-38/10	0.0	1.4	0.7	0.4	0.4	0.5	0.6	0.8	1.4	3.2	32.2	58.5	20.7
	-10/0	0.0	2.8	3.4	2.2	2.2	2.6	2.1	2.9	5.1	7.7	11.9	57.2	11.7
	Comb	0.0	3.9	2.2	1.5	1.7	1.6	1.3	1.5	2.5	4.7	36.4	42.7	100.0
Ore B	-300/75	0.0	16.0	8.7	3.2	3.7	1.9	0.7	1.6	0.9	4.5	45.3	13.5	41.1
	-75/38	0.0	4.1	2.0	1.8	1.5	1.0	1.5	1.4	1.7	4.6	57.4	22.9	24.6
	-38/10	0.0	2.3	1.3	0.9	1.0	0.9	0.9	1.1	1.6	5.1	32.3	52.6	28.5
	-10/0	0.0	2.9	3.1	2.2	2.0	2.3	1.5	2.6	4.1	7.4	13.2	58.7	5.8
	Comb	0.0	5.6	3.2	1.7	1.8	1.3	1.1	1.4	1.8	5.1	38.0	39.1	100.0
Ore C	-300/75	0.0	41.3	11.1	5.3	3.0	3.9	1.0	6.7	0.3	5.0	22.1	0.3	33.8
	-75/38	0.0	15.2	5.2	3.9	2.1	2.2	1.1	4.2	3.3	15.8	39.4	7.6	32.4
	-38/10	0.0	4.5	2.4	1.6	1.1	1.3	1.1	2.3	5.4	14.3	42.2	23.9	17.4
	-10/0	0.0	3.9	3.3	2.2	2.1	1.9	1.8	2.8	6.2	9.9	16.0	50.0	16.5
	Comb	0.0	13.7	5.0	3.0	2.0	2.2	1.3	3.7	4.2	11.6	29.5	23.7	100.0
Ore D	-300/75	0.0	62.4	6.7	16.3	2.0	1.2	4.4	1.8	0.0	0.0	5.2	0.0	36.4
	-75/38	0.0	27.7	9.4	6.0	3.3	2.9	4.9	5.4	1.0	3.9	32.4	3.2	34.6
	-38/10	0.0	7.2	4.1	3.7	1.9	2.1	2.9	5.1	3.6	7.4	29.1	33.0	17.9
	-10/0	0.0	3.4	3.6	1.6	2.3	1.9	2.8	2.3	3.0	7.3	14.0	57.8	11.2
	Comb	0.0	20.6	5.8	5.8	2.4	2.1	3.6	3.9	2.2	5.2	21.9	26.6	100.0
Ore F	-300/75	0.0	6.4	1.0	0.0	4.4	0.0	1.0	1.3	7.3	9.9	66.3	2.3	26.2
	-75/38	0.0	3.7	1.2	0.7	1.5	0.6	1.6	3.8	1.2	8.1	53.4	24.3	37.5
	-38/10	0.0	1.7	0.7	0.5	0.9	0.7	0.6	1.4	3.8	6.0	38.5	45.3	28.9
	-10/0	0.0	5.0	3.9	2.5	2.4	2.4	1.7	3.2	5.1	7.8	13.9	52.0	7.5
	Comb	0.0	3.4	1.3	0.8	1.8	0.8	1.1	2.4	3.6	7.5	43.9	33.4	100.0

APPENDIX G: Mineral association data used in Chapter 3

Chalcopyrite, galena and sphalerite mineral association											
		Background	Ccp	Ga	Sp	Fe sul	Fe ox	Gru	Pxm	Oth Mn Si	Oth Si	Oth
Ore A	Background	0.0	72.1	52.9	83.6	67.7	93.0	42.5	52.9	28.1	61.2	53.3
	Ccp	3.40	0.00	0.90	5.40	1.60	0.20	0.40	2.70	0.90	1.10	1.20
	Ga	0.80	0.30	0.00	0.20	1.10	0.10	0.30	2.20	0.50	1.30	1.60
	Sp	6.90	9.40	1.00	0.00	1.50	0.50	0.80	1.70	0.50	1.00	1.70
	Fe sul	5.20	2.50	6.20	1.30	0.00	1.80	0.50	2.00	0.70	1.60	11.90
	Fe ox	67.30	3.10	3.30	4.10	17.40	0.00	3.90	11.10	5.20	7.10	20.60
	Gru	2.90	0.60	1.30	0.60	0.40	0.40	0.00	18.40	5.90	1.40	1.40
	Pxm	9.50	10.20	27.50	3.70	4.80	2.80	49.10	0.00	50.20	21.40	3.90
	Oth Mn Si	0.40	0.30	0.60	0.10	0.10	0.10	1.40	4.30	0.00	1.90	1.90
	Oth Si	2.10	0.80	3.10	0.40	0.70	0.30	0.70	4.10	4.30	0.00	2.50
	Oth	1.60	0.80	3.40	0.60	4.70	0.90	0.60	0.70	3.80	2.20	0.00
Ore B	Background	0.0	73.3	51.0	82.3	65.4	93.2	30.8	50.0	52.5	61.3	49.9
	Ccp	4.4	0.0	1.0	4.3	2.2	0.3	0.7	3.7	1.3	1.5	1.4
	Ga	0.7	0.2	0.0	0.2	1.1	0.1	0.3	2.2	0.4	1.3	1.3
	Sp	6.1	5.3	0.9	0.0	1.2	0.5	0.8	1.9	0.5	1.3	2.3
	Fe sul	5.3	3.0	6.2	1.3	0.0	1.9	0.5	2.7	0.7	1.4	15.2
	Fe ox	67.5	3.4	2.8	4.5	17.3	0.0	3.6	9.4	8.0	7.1	21.3
	Gru	2.5	1.0	1.4	0.9	0.5	0.4	0.0	25.4	3.4	2.0	1.2
	Pxm	10.0	12.3	31.2	5.1	6.8	2.6	62.0	0.0	23.4	22.2	3.5
	Oth Mn Si	0.2	0.1	0.1	0.0	0.0	0.1	0.2	0.5	0.0	0.1	1.5
	Oth Si	2.1	0.9	3.0	0.6	0.6	0.3	0.8	3.8	0.8	0.0	2.4
	Oth	1.3	0.6	2.4	0.8	4.9	0.8	0.4	0.5	9.2	1.8	0.0
Ore C	Background	0.0	69.2	72.6	62.5	56.1	91.1	39.6	65.8	22.5	47.9	46.7
	Ccp	1.3	0.0	0.2	9.8	1.0	0.1	0.1	0.9	0.2	0.3	0.5
	Ga	7.7	1.0	0.0	1.9	10.1	0.6	0.9	7.0	0.9	3.3	6.1
	Sp	1.2	10.1	0.3	0.0	0.8	0.3	0.2	0.8	0.3	0.5	1.0
	Fe sul	3.1	3.0	5.4	2.5	0.0	1.8	0.3	1.3	0.4	1.0	3.2
	Fe ox	67.9	4.1	4.0	10.9	24.4	0.0	2.9	11.9	20.5	25.0	25.5
	Gru	1.1	0.2	0.2	0.3	0.1	0.1	0.0	6.9	0.6	0.2	0.8
	Pxm	14.3	11.0	14.3	9.1	5.1	3.5	54.8	0.0	29.9	18.2	5.0
	Oth Mn Si	0.2	0.1	0.1	0.1	0.1	0.2	0.2	1.2	0.0	0.9	6.7
	Oth Si	2.0	0.6	1.3	1.2	0.7	1.4	0.3	3.6	4.3	0.0	4.4
	Oth	1.3	0.7	1.6	1.5	1.5	0.9	0.8	0.6	20.7	2.8	0.0
Ore D	Background	0.0	72.0	62.0	60.9	72.0	95.2	73.4	22.2	21.1	64.7	51.0
	Ccp	2.9	0.0	2.9	9.6	5.3	0.4	1.8	13.8	4.2	2.4	1.1
	Ga	0.3	0.3	0.0	0.7	1.3	0.0	0.3	1.3	1.1	0.4	0.5
	Sp	0.2	0.9	0.7	0.0	0.5	0.1	0.3	0.6	0.6	0.3	0.4
	Fe sul	2.1	3.9	8.9	3.7	0.0	0.5	0.4	1.8	0.7	0.6	2.9
	Fe ox	84.9	9.9	6.8	10.8	15.3	0.0	14.2	40.9	9.2	21.1	28.9
	Gru	5.0	3.2	5.3	5.6	1.0	1.1	0.0	13.3	6.8	3.5	9.2
	Pxm	0.4	6.2	5.4	2.6	1.1	0.8	3.5	0.0	15.3	1.6	0.3
	Oth Mn Si	0.1	0.2	0.6	0.4	0.1	0.0	0.2	1.9	0.0	2.0	0.1
	Oth Si	2.9	2.6	4.6	3.1	0.9	1.0	2.2	3.8	39.8	0.0	5.7
	Oth	1.4	0.7	2.9	2.7	2.6	0.9	3.6	0.5	1.3	3.4	0.0
Ore F	Background	0.0	86.4	78.5	74.4	54.3	95.4	38.2	28.7	35.6	71.8	48.1
	Ccp	6.2	0.0	2.0	12.5	5.8	0.4	0.8	5.3	3.5	2.2	2.6
	Ga	1.9	0.7	0.0	1.1	5.3	0.1	0.3	4.3	1.8	0.9	3.8
	Sp	0.7	1.6	0.4	0.0	0.4	0.1	0.1	1.0	0.6	0.2	0.6
	Fe sul	1.6	2.4	6.3	1.3	0.0	1.0	0.6	1.3	0.7	0.9	2.0
	Fe ox	82.9	5.1	3.8	6.1	29.4	0.0	43.1	36.5	12.4	16.1	32.7
	Gru	0.2	0.1	0.1	0.1	0.1	0.3	0.0	7.0	2.0	0.4	1.0
	Pxm	0.1	0.2	0.5	0.3	0.1	0.1	3.6	0.0	3.9	0.4	0.2
	Oth Mn Si	0.2	0.2	0.3	0.3	0.1	0.1	1.6	6.2	0.0	2.3	1.0
	Oth Si	4.5	2.0	2.3	1.6	2.0	1.2	4.8	7.9	31.7	0.0	8.2
	Oth	1.8	1.3	5.7	2.3	2.5	1.4	6.9	2.0	7.9	4.8	0.0

APPENDIX H: Theoretical grade-recovery data used in Chapter 3

Theoretical grade-recovery of chalcopyrite, galena and sphalerite										
Mineral	Ore A		Ore B		Ore C		Ore D		Ore F	
	Rec	Gr	Rec	Gr	Rec	Gr	Rec	Gr	Rec	Gr
Chalcopyrite	100.0	2.0	100.0	2.5	100.0	0.7	100.0	1.8	100.0	4.5
	89.7	82.1	89.9	83.1	90.4	84.3	91.9	75.3	97.8	92.5
	84.6	92.0	85.5	91.9	85.8	94.1	84.9	87.1	96.0	96.4
	80.2	96.3	81.1	96.5	82.8	97.4	77.5	93.8	94.4	98.0
	75.7	98.5	76.7	98.6	79.4	99.0	68.4	98.3	91.4	99.2
	61.0	100.0	62.0	100.0	69.8	100.0	53.5	100.0	79.2	100.0
Galena	100.0	0.7	100.0	0.6	100.0	7.5	100.0	0.3	100.0	2.0
	86.9	79.3	85.9	79.3	95.0	88.7	88.7	79.5	97.8	91.5
	81.2	90.5	79.3	92.4	91.9	95.6	84.0	89.1	95.9	95.9
	76.4	95.9	75.0	97.4	89.7	97.9	77.4	95.4	93.9	97.7
	72.0	98.1	72.3	98.8	87.1	99.0	71.4	98.1	91.1	98.9
	52.9	100.0	53.9	100.0	73.4	100.0	51.2	100.0	73.8	100.0
Sphalerite	100.0	4.1	100.0	3.4	100.0	0.7	100.0	0.5	100.0	0.1
	95.3	88.4	93.5	87.3	86.6	81.4	96.6	90.9	79.3	73.9
	92.3	95.0	90.3	94.8	81.6	91.8	94.5	95.4	71.3	88.3
	89.8	97.4	87.8	97.5	78.0	95.3	92.7	97.3	65.1	95.1
	86.6	98.8	85.1	98.8	72.8	97.7	89.4	98.7	60.0	98.3
	64.5	100.0	60.6	100.0	44.7	100.0	55.5	100.0	46.5	100.0

APPENDIX I: Published manuscript of Chapter 3

Using mineralogy for early stage Geometallurgical domain definition: a case study of the Swartberg polymetallic sulphide deposit

H.J.J. Gordon[1,2], J. A. Miller[1], and M. Becker[3]

[1]University of Stellenbosch, South Africa
[2]Black Mountain Complex (Pty) Ltd, a subsidiary of Vedanta Resources Plc, South Africa
[3]University of Cape Town, South Africa

The Swartberg deposit, Northern Cape Province, South Africa, is a low-grade, polymetallic base metal sulphide deposit. Reworking during the Namaquan Orogeny generated complex mineralogical and textural variability in the deposit. This variability is expressed through several different geological ore 'types' defined on texture and mineralogy. However, it is not clear how this petrographic definition of ore 'type' relates to the processing response of each ore type. In order to clarify the linkages between ore type defined geologically and ore type defined metallurgically, this study re-evaluates the geologically defined ore types by reviewing the silicate, oxide, and sulphide mineralogy, grain size, and mineral associations for each. Ore textures manifest as intricate intergrowths of sulphide, silicate, and oxide minerals, and are problematic for metallurgical processing, resulting in poor copper recovery. The geological ore types are then reclassified as distinct early-stage geometallurgical ore types on the basis of gangue mineralogy, copper mineral grain size distribution, and gangue mineral associations. The results have important implications for establishing controls on ore variability regarding mineral processing performance, and which mineralogical parameters ideally need to be incorporated when building a geometallurgical block model for the deposit.

Keywords: Polymetallic, block model, mineralogy.

INTRODUCTION

The growth in demand for copper, lead, zinc, and silver, coupled with high base metal prices, is driving the need for more efficient extraction of larger metal tonnages (Bradshaw, 2014; Rosenkranz and Lamberg, 2014). At the same time, known high-grade, large-tonnage deposits are being depleted, causing mining companies to invest in the development of complex, lower-grade deposits. Ore variability in these types of deposits presents one of the most significant processing challenges (Lotter *et al*., 2017). Variability in mineralogy, mineralization style, grade, grain size, alteration, gangue mineral association, and the spatial arrangement of these characteristics within ores presents a limitation to metallurgical extraction, and hampers the development of these deposits (Lotter *et al*., 2011, 2017; Bradshaw, 2014; McKay *et al*., 2016a). The Pb-Zn ores of the Mount Isa deposit, Australia (Johnson, 2016) and the Zn-Pb-Ag-Ba ores of the Red Dog deposit, Alaska (McKay, Sztuke, and Lacouture, 2016b) are world-class examples illustrating the extent of such challenges. The block modelling of geometallurgical response variables, along with qualitative resource information, provides a new direction for proactive decision-making. This is especially so in an economic climate where financial sustainability of mining operations requires mitigation of mineralogical and metallurgical uncertainty (Coward *et al*., 2009; Lamberg, 2011, Sepulveda *et al*., 2015)

The Aggeneys-Gamsberg ore district (A-GOD) in South Africa's Northern Cape Province is a 10 × 30 km area known to host four polymetallic, sedimentary-exhalative and Broken Hill-type deposits in mid-Proterozoic metasediments (Bailie, Armstrong, and Reid, 2007; Rudnick, 2016). The westernmost portion of the A-GOD, the Swartberg deposit, forms the focus of this study. The metal distribution within the Swartberg deposit follows the decreasing order of lead>zinc>copper>silver as disseminated, stratiform and recrystallized lead (galena), zinc (sphalerite), and copper sulphides (chalcopyrite and bornite) contained within an enclosing isoclinal fold nappe (Stedman, 1980). Two distinct stacked orebodies, the Upper (UOB) and Lower (LOB) orebody define the centre of the fold nappe, with an alteration halo, the garnet quartzite zone (GQ), defining a third orebody, encompassing the UOB and LOB (Ryan *et al.*, 1986; Rudnick, 2016). Ore textures manifest as intricate intergrowths of sulphide, oxide, and silicate minerals, resulting in poor copper recovery during metallurgical processing. This has led to the recognition that established mineralogical end-member characteristics for the Swartberg deposit as applied to processing have not yet been quantified on a geometallurgical end-member level.

This paper examines the current lithological domains as distinct early-stage geometallurgical ore types based on gangue mineralogy, copper mineral grain size distribution, and gangue mineral associations found within the main and down-plunge resource. A review of the mineralogical variability will have implications for constraining fixed boundaries between geological ore types, establish controls on ore variability regarding flotation performance, and identify which mineralogical parameters need to be incorporated when building a geometallurgical block model for the deposit. This paper focuses on attributes relevant to the copper flotation circuit. Characteristics relevant to the lead and zinc circuits will be addressed in a subsequent paper.

GEOMETALLURGICAL BLOCK MODELLING

Model Input

A geometallurgical block model is a multivariate extension of a conventional 3D geological block model based on both geological and metallurgical data (Lotter *et al.*, 2017). This model utilizes a combination of subordinate models, of which, focus is placed on developing mineralogical and metallurgical trends that are consolidated to display geometallurgical domains in a block-by-block, 3D spatial context (Coward *et al.*, 2009; Lamberg, 2011; McKay *et al.*, 2016a). Viewing orebodies by means of such domains defines the metallurgical variability and contributes toward the development of more robust mining and processing approaches (*e.g.*, Butler *et al.*, 2016; King and McDonald, 2016; Liebezeit *et al.*, 2016). The geometallurgical programme as defined by Lamberg (2011) is based on joint input from three subordinate models that link geology and metallurgy through the consideration of minerals and particles: the geological model, particle breakage model, and the process model. The geological model provides quantitative mineralogical and textural information per ore block. The particle breakage model forecasts the resultant particle properties from the breakdown of different ore blocks, and the unit process model forecasts how particles will respond in a unit process. The combination of these three models feeds quantitative data into the geometallurgical model.

Model Considerations

This synergy between mineralogy and mineral processing starts with representative sample material regarding the type, size, and quantity of minerals (Lotter *et al.*, 2017). A successful geometallurgical programme requires that the sampling strategy for the major domains within a deposit on which testing is conducted should be designed in accordance with the mineralization type (Coward *et al.*, 2009). This ensures statistically sound chemical, mineralogical, and metallurgical data (Lotter *et al.*, 2017). Representativity across samples requires that sample locations be spatially distributed throughout the deposit, or that the spatial location of drill-holes be optimized to allow for adequate coverage of the deposit as more drilling is done (McKay *et al.*, 2016a, 2016b). The multivariate nature of geometallurgical domains can be missed when samples from different metallurgical units are blended and treated as one sample (Lotter *et al.*, 2017). This is commonly considered the weak point of a geometallurgical programme as assumptions regarding the representativity of variability within the orebody are made at this stage (Lamberg, 2011).

Due care should be taken not to collect metallurgical samples based only on geological information, as the representativity and full variability within the deposit will be known only once metallurgical analysis has been completed (Lamberg, 2011). This makes for the case that using resource drill core in conjunction with bulk samples from underground workings and reject pulps from chemical assay analyses is beneficial towards establishing representativity and considering variability (McKay *et al*., 2016a, 2016b; Dominy, O'Connor, and Xie, 2016). From the work of Coward *et al*. (2009) there are three important considerations associated with variability: (1) rock variables are classified as 'primary' in light of their characteristics, or 'response' in light of their response processes; (2) variables are often commodity, deposit-type, or mining/processing specific; and (3) the distinction between variables is not always apparent, but has important implications for their modelling capability, and defines the manner in which modelling is carried out. Directly measurable characteristics such as mineral grade, metal grade, mass, rock density, colour, grain size, and alteration are considered primary. Response variables describe the ore's reaction to processing and are often multivariate. Throughput, recovery, grindability, size distribution, particle density, and distribution are examples of response variables (Coward *et al*., 2009).

The revision of model inputs is beneficial towards the planning of a geometallurgical block model. As illustrated by Lotter *et al*. (2017), the foundation for a geometallurgical block model is existing data and prior knowledge. Within the scope of this paper, attention will be focused on the variability in bulk mineralogy, grain size distribution, and gangue mineral association, *i.e.* the primary variables, to gain an understanding of the variability within early-stage geometallurgical domains.

MATERIALS AND METHODS

Thirty-five drill core samples were selected from the five main geological ore types of the Swartberg deposit, from which 30 mm samples were cut, impregnated in resin, polished, and carbon coated in a Quorum Q150T E coater for QEMSCAN analysis at the University of Cape Town. Polished blocks were run on a QEMSCAN 650F with two Bruker XFlash 6130 detectors operating at 25 kV, 10 nA using the field image analysis routine at a 1500 µm field size and a 15 µm pixel size. The Species Identification Protocol (SIP) was utilized to create a secondary Swartberg mineral list from the primary list by using the iExplorer software offline. In the process of establishing and refining the mineral classifications, reference was made to previous works on the orebody (*e.g*. Rudnick, 2016).

RESULTS

The main economic, geological end-members examined in this study are the magnetite quartzite (QM), amphibole magnetite quartzite (AM), garnet quartzite (GQ), mineralized quartz schist (MC), and sulphidic quartzite (SQ). The QM and AM, along with barite magnetite quartzite (MB) and garnet magnetite quartzite (GM), define the Upper Orebody, whereas the MC and SQ define the Lower Orebody. For the purpose of this paper, the MB and GM are disregarded due to their relatively low copper sulphide content in the down-plunge extent of the deposit. The following sections summarize the bulk mineralogy (Table I), grain size distribution of copper minerals (Figure 2), and main gangue mineral associations of each of the copper minerals for the geological end-members listed above. Mineral percentages here are reported as mineral mass per cent, with 'trace' amounts indicating less than 1%.

Mineral and textural characterization of preliminary end-members

Garnet Quartzite (GQ)

The GQ (Figure 1a) end-member is composed of quartz (approx. 59%), magnetite (approx. 11), almandine garnet (approx. 6%), muscovite-chlorite mica (approx. 4%), as well as sillimanite (approx. 2.5%), with trace amounts of feldspars, apatite, and ilmenite, and contains around 17% sulphide minerals. The three dominant sulphides are chalcopyrite (approx. 13%), pyrrhotite (approx. 3%), and pyrite (approx. 1%), although minor amounts of bornite, galena, and sphalerite are present. The ratio of

chalcopyrite to total sulphides is 2.5:1, and the ratio of chalcopyrite to other economic sulphides (galena and sphalerite) is 16:1. Chalcopyrite occurs as coarse and massive grains overprinting the fabric and is primarily associated with quartz, magnetite, sphalerite, sillimanite, and pyrrhotite. Bornite, galena, and sphalerite proportions are too low to establish statistical associations but these minerals appear to be associated with quartz and chalcopyrite. Of the main sulphide gangue minerals, pyrrhotite dominates pyrite in a 3:1 ratio. Pyrrhotite and pyrite, along with mica, occur as rims on chalcopyrite, or as pyrite-pyrrhotite-quartz inclusions within chalcopyrite.

Magnetite Quartzite (QM)

Magnetite (53%) and quartz (27%) together account for the bulk of the mineralogy in the QM unit. The remainder consists of chalcopyrite (7%), galena (4.5%), pyrite (approx. 2%), chlorite-muscovite mica (approx. 1.5%), barite (approx. 1%), amphiboles (approx. 1%), and trace amounts of garnet, sphalerite, apatite, pyrrhotite, and bornite. Chalcopyrite dominates galena in a 1.8:1 ratio, and the ratio of chalcopyrite to total sulphides is approximately 1:1. Chalcopyrite is commonly associated with magnetite, quartz, and pyrrhotite. Bornite is present in trace concentrations but may locally exceed 1.5%. Where present it is associated with chalcopyrite, quartz, garnet, and magnetite. Sphalerite does not exceed 2%. Pyrite is the dominant gangue sulphide mineral, with lesser sphalerite in an 8:1 ratio and pyrrhotite in a 6:1 ratio. A combination of coarse, euhedral and subhedral chalcopyrite and galena overprints an association of finely banded quartz, magnetite, pyrite, and pyrrhotite grains. The overall texture displays a combination of massive and well-defined compositional layering (Figure 1b). Quartz-magnetite-chalcopyrite-galena interfaces are often arranged in triple junctions with distinct grain boundaries.

Amphibole Magnetite Quartzite (AM)

The AM unit is dominated by magnetite (approx. 56%), with lesser amounts of manganogrunerite-actinolite-amphibole (approx. 12%), quartz (approx. 10%), and manganese minerals (approx. 3%) with trace amounts of apatite. Galena (approx. 5%), sphalerite (approx. 4%), and chalcopyrite (approx. 3%) comprise the economic sulphides, whereas pyrrhotite (approx. 6%) and pyrite (approx. 1%) comprise the gangue sulphides. Chalcopyrite is primarily associated with manganogrunerite amphibole, magnetite, sphalerite, pyrrhotite, and pyroxmangite. The association of coarse-grained, massive galena-chalcopyrite-sphalerite-pyrrhotite-pyrite is common. Pyrite occurs as inclusions within pyrrhotite, chalcopyrite, and sphalerite, and is rarely found outside this arrangement. The presence of pyroxmangite with rhodonite is widespread, and associated with manganogrunerite along the grain boundaries and as inclusions in quartz veins and magnetite grains. The AM texture is characterized by the presence of coarse-grained, centimetre-scale chalcopyrite, galena, and pyrrhotite overprinting a wavy compositional fabric defined by magnetite, elongated amphibole, and quartz with manganogrunerite and magnetite (Figure 1c).

Mineralized Quartzitic Schist (MC)

The MC consists of quartz (approx. 45%), hyalophane (barium feldspar) (approx. 13%), biotite-muscovite (approx. 6%), gahnite (approx. 3.5 %), with lesser amounts of garnet (approx. 1%), sillimanite (approx. 1%), ilmenite (approx. 1%), magnetite (approx. 1.5%), and barite (approx. 1.5%). The sulphide population is dominated by galena (approx. 17%), with lesser amounts of pyrrhotite (approx. 4.5%), pyrite (approx. 2%), chalcopyrite (approx. 1%), and trace amounts of sphalerite and bornite. Chalcopyrite is randomly associated with the sulphide gangue minerals, most commonly as chalcopyrite-pyrrhotite-biotite and chalcopyrite-pyrrhotite-pyrite associations. Trace amounts of bornite are seen closely associated with chalcopyrite, Ba-feldspar, and quartz. Variability in the economic sulphides is common, where locally chalcopyrite dominates galena (62:1), and sphalerite concentrations exceed 5%. Pyrrhotite and pyrite are the main sulphide gangue minerals and although pyrrhotite is generally dominant, locally pyrite can dominate pyrrhotite in a ratio up to 5:1. Certain varieties of mineralized schist have hyalophane dominant over quartz in a 2:1 ratio. In the MC, compositional banding defined by gahnite-quartz-pyrrhotite with finer grained biotite-pyrrhotite-chalcopyrite-quartz alternates with the main fabric defined by muscovite-biotite-sillimanite and coarse-grained galena-gahnite-quartz (Figure 1d).

Sulphidic Quartzite (SQ)

The SQ end-member is dominated by quartz (approx. 45%) and hyalophane (19%), with lesser amounts of magnetite (approx. 9%), biotite-muscovite mica (5%), garnet (2%), ilmenite (approx. 1.5%), sillimanite (approx. 1%), barite (approx. 1%) and alkali feldspar (1%). The sulphide population consists of galena (approx. 8%), chalcopyrite (approx. 4%), and pyrite (approx. 3%) with generally trace amounts of pyrrhotite, bornite, and sphalerite, although sphalerite can locally be up to approximately 5%. Chalcopyrite and galena are closely associated, with galena appearing on the rims of chalcopyrite grains. Chalcopyrite similarly displays occasional inclusions of pyrite and pyrrhotite. Bornite is associated with quartz and chalcopyrite. Quartz, Ba-feldspar, and mica comprise the matrix of the SQ unit, while quartz-galena-pyrite, mica-Ba-feldspar-magnetite, and quartz-chalcopyrite-galena-garnet associations define a compositional fabric (Figure 1e). Disseminated chalcopyrite, pyrite, pyrrhotite, and galena also locally overprint the fabric.

Grain Size Distribution of Copper Minerals

The grain size distribution of the copper minerals for the different rock types is illustrated in Figure 2. The grain size distributions show a clustering into two groups, a finer grained mineralization for the MC and SQ with a *d*50 of approximately 150 µm, and a coarser grained mineralization for the GQ, QM and AM with a *d*50 of approximately 250 µm. Given the dominance of chalcopyrite in the ore relative to bornite, the grain size distributions largely reflect those of chalcopyrite. In general, bornite is relatively fine-grained (< 50 µm) other than in the QM, where bornite grains can be as large as 150 µm.

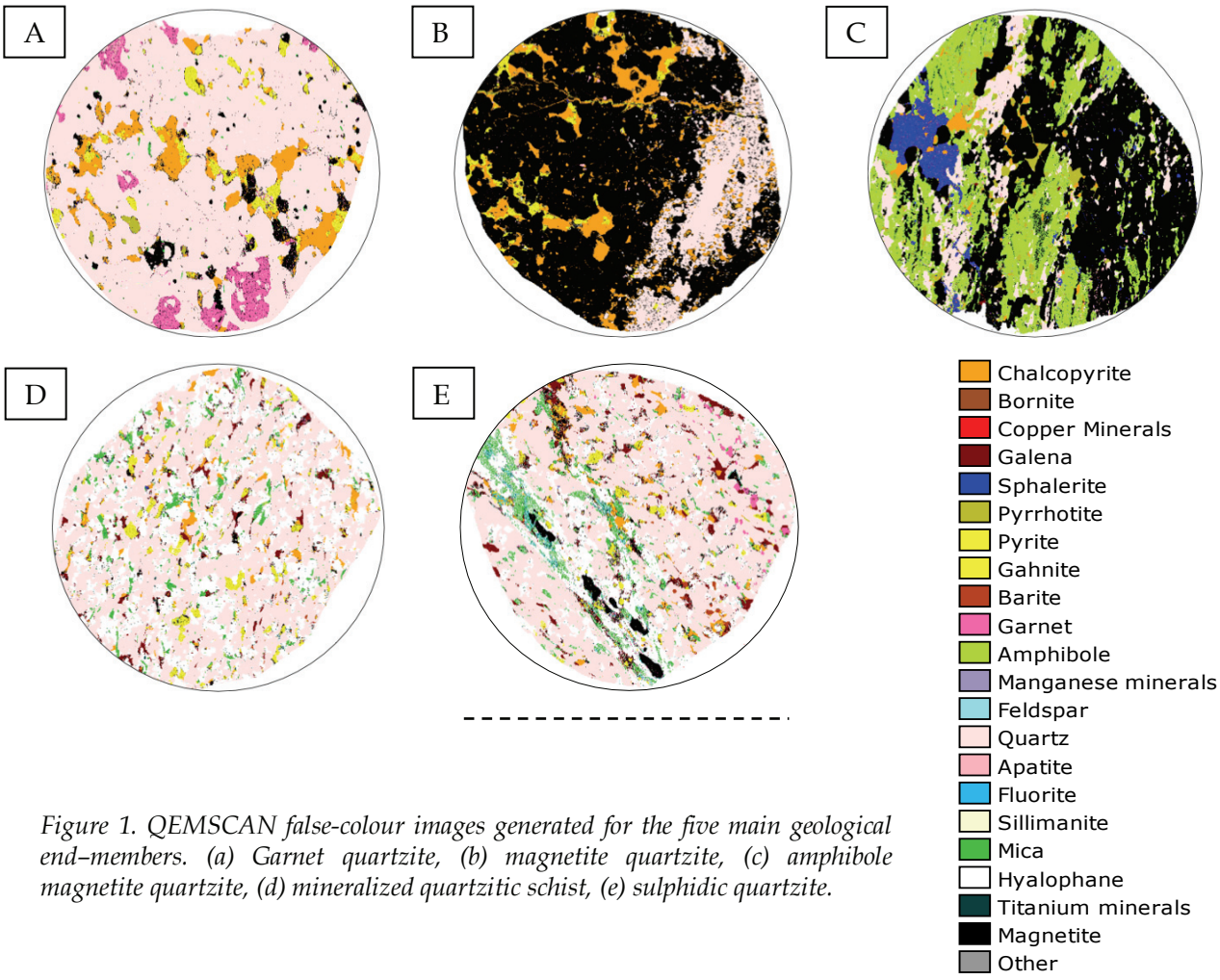

Figure 1. QEMSCAN false-colour images generated for the five main geological end–members. (a) Garnet quartzite, (b) magnetite quartzite, (c) amphibole magnetite quartzite, (d) mineralized quartzitic schist, (e) sulphidic quartzite.

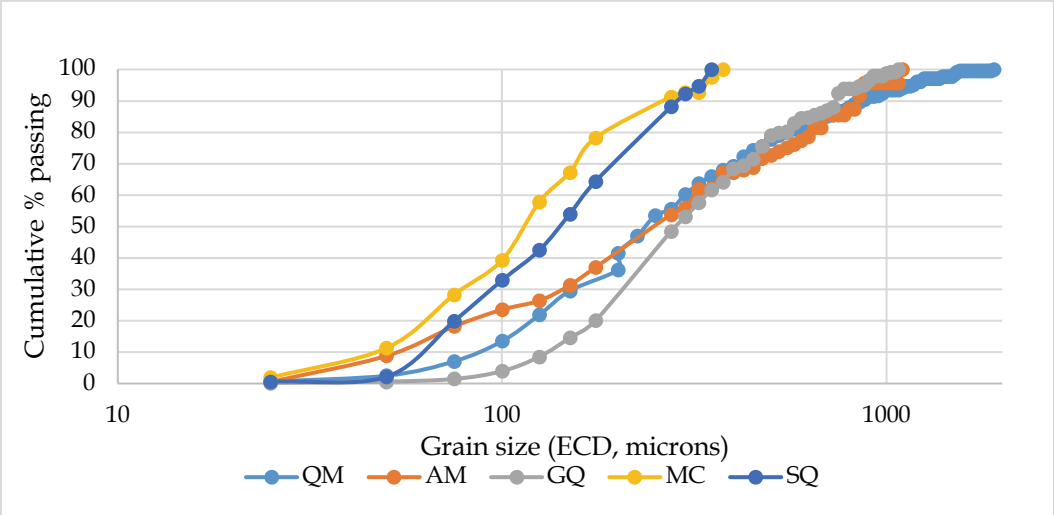

Figure 2. Grain size distribution patterns of copper minerals within the GQ, QM, AM, MC, and SQ early-stage mineralogical ore types.

DISCUSSION

Understanding the Mineralogical Characteristics for Geological Subdivisions of Ore Types

Five potential ore types were investigated in an attempt to establish the foundation for early-stage geometallurgical domaining by verifying that these five geological end-members are distinct. Ore types were compared based on mineralogy (Tables I and II) and textural characteristics (fabric and grain size) (Table III). The UOB ore types (QM and AM) share similarities in their bulk mineralogy and are differentiated on the amounts of quartz and amphibole present. The QM displays the greatest textural variability. This is illustrated as a combination of fabrics and grain sizes ranging from micrometre-scale up to centimetre-scale. This characteristic feature of the QM ore, along with its mineralogical variability, has led to the establishment of subordinate ore types for improved underground grade control targeting. Three further variants of the QM ore type are identified: S-QM, QM Cu, and QM Zn (Steinmann, 2016, personal communication). The main characteristic feature of the S-QM is the dominance of centimetre-scale euhedral-massive galena and chalcopyrite over all other sulphides. In comparison, the QM Cu ore is characterized by the absence of coarse galena and sphalerite, and the presence of coarse pyrrhotite and pyrite along with very coarse (centimetre-scale) chalcopyrite. The QM Zn is defined by centimetre-scale recrystallized, anomalous and lensoid massive sphalerite with subordinate galena and minor chalcopyrite.

The AM ore type displays both the greatest elemental and mineralogical variability, defined by a combination of amphibole, pyroxenoid, and manganese minerals. Mn-absent amphiboles such as grunerite and actinolite, and similarly amphibole- and pyroxenoid-poor varieties are also considered characteristic of the AM ore. The mobility of manganese within the AM complicates the classification of amphiboles, pyroxenoids, and other manganese minerals. Manganese, iron, magnesium, and calcium can substitute for one another in these minerals, creating the possibility for a wide range of silicate and manganese minerals. Subordinate ore types might be required to constrain the variable nature of the abovementioned minerals into distinct classes, *e.g.* manganese-rich, manganese-poor, foliated, and non-foliated varieties, which might behave differently during metallurgical, processing based on the study by Schouwstra *et al.* (2010) on the neighbouring Gamsberg orebody. A close association of pyroxmangite and manganogrunerite is most prevalent in the AM ore. However, this association is also encountered in the QM ore where subordinate amounts of sphalerite are present. The manganese minerals might not necessarily be associated with only the AM ore type, but with sphalerite in general. The AM ore type is the only UOB ore type where sphalerite is widespread in high mineral grades, and this might explain why manganese minerals are concentrated here.

The variable amount of quartz in each of the UOB end-members is also problematic. Besides the QM and AM ore types described above, the GM and MB ores are also quartz-bearing. After discounting dominant magnetite, these ores are usually labelled according to the dominant silicate present. An important question is that where there is abundant quartz in these ore types, can the metallurgical responses of the QM, AM, MB, and GM ore types be distinguished from each other? The hardness of quartz overshadows that of the major silicate gangue minerals (amphibole and barite) with the exception of garnet. This raises a concern as to the metallurgical influence of garnet, amphibole, and barite relative to the amount of quartz, and how this can be better mitigated, *i.e.* forecasting the metallurgical performance based on the ratio of quartz to the dominant silicate gangue mineral (garnet, amphibole, or barite).

The establishment of the LOB end-members, MC and SQ, is based on the presence of hyalophane, quartz, mica, sillimanite, and muscovite, generally without magnetite. The MC and SQ ore types also have distinctly finer-grained foliated and non-foliated economic chalcopyrite and galena (Table III). The GQ is much closer in bulk mineralogy, grain size distribution, and mineral association to the LOB ore types.

The definitions of these early-stage ore types are still immature and will evolve depending on whether mineralogical or metallurgical variables have greater impacts on processing, *e.g*. the presence of pyrite and pyrrhotite *vs*. quartz, amphibole, and hyalophane (barium feldspar). Distinct mineral associations are present within each of the GQ, UOB, and LOB end–members. With the understanding of the elemental distribution within such geological ore types, the forecasting of mineral assemblages through element-to-mineral conversion (*e.g*. Nthlabane *et al*., 2018) as an alternative to QEMSCAN and XRD data allows for further refining of 'early-stage mineralogical domains'.

Development of Early Stage Metallurgical Domains

The definition of geometallurgical domains is ultimately based on the response of the different ore types to mineral processing, as determined by experimental test work (Johnson and Munro, 2008). The effects of mineralogy on processing have been extensively described in the literature, specifically for polymetallic sulphide ores (*e.g*. Johnson, 2016; McKay *et al*. 2016a, 2016b; Bojcevski *et al*. 1998). This allows us to make some general inferences in terms of key characteristics affecting processing performance that can be used to explore possible early-stage metallurgical domains.

The first of these is the relationship between grain size distribution and liberation – the coarser the grain size distribution of the valuable minerals, the better the liberation. The copper minerals in the GQ-QM-AM ores have a considerably coarser grain size distribution than in MC-SQ ores. This could present a natural subdivision into two different geometallurgical domains. Furthermore, valuable minerals cannot be recovered unless they are adequately liberated – the better the liberation, the better the flotation recovery. This presents a natural subdivision into the same two geometallurgical domains. It also highlights the potential need for finer grinding of the MC-SQ ores to liberate the copper minerals.

The second inference is the relationship between texture, rock strength, and mill throughput – the stronger the ore, the lower the throughput for a given set of milling conditions. Rock strength is a function of both the hardness of the individual minerals present and the texture, including both grain size distribution and grain orientation (Howarth and Rowland, 1987). Considering the hardness of the major gangue minerals using Moh's scale, this suggests that quartz- (hardness 7) dominant rock types are likely to show a lower mill throughput than the amphibole- (hardness 5-6) and magnetite- (hardness 6) dominant rock types in the UOB. This is similar for the LOB ores, where there will be a difference in mill throughput for ores that are richer in quartz in comparison to hyalophane and micas. This presents a similar subdivision to that outlined above for liberation, except that the GQ ores are more similar to MC-SQ than to QM-AM.

The third of these inferences is the effect of mineral association on the nature of composite particles and the possible effects on flotation concentrate grade. Because of the finer grain size distribution of the MC-SQ ores the mineral association becomes more relevant. Both these ore types show notable associations with economic (galena, sphalerite) and gangue sulphide minerals (pyrite, pyrrhotite). Both

these ore types also have significant galena (> 10 wt.%) and as such are likely to exhibit similar problems relating to selectivity between the different sulphide concentrates (*i.e.* whether composite chalcopyrite-galena particles report to the Cu or the Pb concentrate). This affirms the logic in considering a single geometallurgical domain for the MC-SQ ores.

An additional factor to be considered is the role of the feed grade, which follows a general trend in that the higher the feed grade of the economic metals, the better the performance of the ore in processing (Bojcevski *et al*. 1998). In this case the GQ-QM ores would be expected to display the best copper grade and recovery during flotation (> 7% chalcopyrite in the feed), whereas the SQ-MC ores would be expected to display the best lead grade and recovery (> 8% galena in the feed). The reverse of this is, however, also possible, in that ores with the highest content of iron sulphide gangue minerals (pyrite, pyrrhotite) are likely to be the most problematic in achieving selectivity during sequential flotation, *i.e.* the AM and MC ores.

From the above discussion considering the five geological ore types, taking into account predicted response variables, three possible geometallurgical domains have been identified: (1) garnet quartzite, (2) magnetite quartzite and amphibole magnetite quartzite (both from the upper orebody), and (3) the mineralized quartz schist and sulphidic quartzite (both from the lower orebody). Further experimental work is needed to verify these divisions, and also to investigate whether the ore variability within each of these 'early-stage metallurgical domains' would warrant additional subdivisions (*e.g.* presence of S-QM and QM-Cu both within the QM ore type). Similarly, a more detailed investigation is needed to fully explore the variability within the Pb and Zn mineralization for this polymetallic sulphide orebody.

Table I. Bulk mineralogical comparison of Swartberg geological end-members (wt.%).

Geological ore types					
Minerals	**GQ**	**QM**	**AM**	**SQ**	**MC**
Chalcopyrite (cp)	12.6	7.2	2.9	3.7	1.1
Bornite (bor)	<0.1	0.2	<0.1	<0.1	<0.1
Galena (ga)	0.6	4.6	4.8	8.1	17.3
Sphalerite (sph)	0.3	0.6	4.0	0.1	0.2
Pyrrhotite (po)	2.9	0.3	5.9	0.7	4.4
Pyrite (py)	0.8	1.9	0.9	2.9	2.0
Gahnite (gah)	0.1	<0.1	<0.1	<0.1	3.5
Barite (ba)	<0.1	1.0	<0.1	0.8	1.4
Garnet (gt)	5.5	0.6	<0.1	2.0	1.2
Amphibole (amph)	<0.1	0.7	12.1	0.1	0.1
Manganese minerals (mn)	<0.1	0.4	2.7	<0.1	<0.1
Feldspar (fsp)	0.2	0.1	<0.1	1.0	0.6
Quartz (qtz)	59.1	27.0	9.7	44.9	44.6
Apatite (ap)	0.3	0.3	0.5	0.1	0.1
Fluorite (fl)	<0.1	<0.1	<0.1	0.1	<0.1
Sillimanite (sill)	2.3	0.2	<0.1	1.0	1.2
Mica	4.5	1.5	<0.1	5.0	6.3
Hyalophane (hyal)	<0.1	<0.1	<0.1	19.0	13.4
Ti-minerals (ilm)	0.2	0.1	<0.1	1.4	1.0
Magnetite (mgt)	10.6	53.3	56.3	9.2	1.5
Other (oth)	0.1	0.1	<0.1	0.1	0.2
Minerals	100	100	100	100	100

Table II. A summary of sulphide, oxide, silicate, and trace minerals present within the Swartberg geological end-members. Refer to Table I for mineral abbreviations.

Ore type	Sulphides		Oxides	Silicates	Trace
	Economic	Gangue			
GQ	cp	po, py	mgt	qtz, gt, mic, sill	
QM	cp, ga, sph, bor	py , po	mgt	qtz, ba, mica, amph, mn	amph, pyrox, ap
AM	ga, sph, cp	po	mgt	amph, qtz, pyrox	ap, bor, py, gt, gah, fsp, fl, ilm
MC	ga, cp, sph	po, py	mgt, ilm	qtz, hyal, mica, gah	gt, fsp, sill, ap
SQ	ga, cp	py	mgt, ilm	qtz, hyal, mica, gt	bor, sph, po, ba, ep, amph, ap, fl, sill

Table III. Grain size, mineral association, and textural arrangements as summarized from the Swartberg geological end-members. Refer to Table I for mineral abbreviations.

Ore body	Ore type	Grain size (μm)			Mineral association (%) **	Textural arrangement of chalcopyrite***	
		Copper minerals			Copper minerals	Grain shape	Fabric
		Min.	Max.	Med.		Euh/sub/anh	Fol/band/brec
GQ	**GQ**	<25	<1075	225-275	qtz, mgt, sph, sill, po	anh (massive)	mass/ non-fol
UOB	**QM**	<25	<2000	100-150	mgt, qtz, po	euh/ anh	mass/ fol/ non-fol
	AM	<25	<1100	50-100	amph, mgt, sph, po, pyrox	anh (stretched)	fol
LOB	**MC**	<25	<375	100-150	po, py, mica	sub	fol
	SQ	<25	<350	50-100	ga, py, po	anh (massive)	mass/ fol

** See Table I for mineral abbreviations
*** Grain shapes as euhedral (euh), subhedral (sub), anhedral (anh), and fabric as massive (mass), foliated (fol), and non-foliated (non-fol)

CONCLUSIONS

The Swartberg deposit is a complex polymetallic sulphide orebody, for which there is motivation to initiate the development of a geometallurgical block model. Mineralogical variability within the Swartberg ore manifests as an intricate association of sulphide, oxide, and silicate minerals across different lithological domains. A quantitative mineralogical study of the five geological ore types was essential to understand the disposition of these ores, specifically with a focus on copper mineralization. The resultant early-stage mineralogical domains, as based on the association of copper mineralization with silicate gangue minerals, is immature, and will evolve.

Mineralogical attributes such as chalcopyrite head grade, grain size distribution, mineral grades of economic sulphide, gangue sulphide, and other major gangue minerals, were most critical during the review of mineral processing responses. Characteristics of this nature should henceforth be primary variable inputs into the geometallurgical block model, and will prove useful towards the rationalization and interpretation of mineral relationships. Consideration of the potential mineral processing response of the five mineralogical ore types on the basis of liberation, mill throughput, and flotation grade, recovery, and selectivity revealed three 'early-stage geometallurgical domains'. Defining subordinate geometallurgical domains within these early-stage geometallurgical domains might have further implications for mitigating elemental variability during mineral processing, and developing element-to-mineral conversion parameters for the generation of quantitative mineralogy from chemical assays.

It is recommended that subordinate ore types be pursued by expanding the focus of the geometallurgical block model to incorporate lead-zinc-dominated ores.

ACKNOWLEDGEMENTS

The authors would like to acknowledge the efforts of employees at Black Mountain Mining (Pty) Ltd. in providing logistical support during sampling, travelling, site visits, and block analysis, and the executive management team for financial support. This work is based on research supported in part by the National Research Foundation of South Africa (grant numbers 86054, 99005). The authors would also like to acknowledge Gaynor Yorath and the QEMSCAN team for assistance with the QEMSCAN analysis.

REFERENCES

Bailie, R., Armstrong, R., and Reid. D. (2007). Composition and single zircon U-Pb emplacement and metamorphic ages of the Aggeneys Granite Suite, Bushmanland, South Africa. *South African Journal of Geology*, 110: 87-110.

Bojcevski, D., Vink, L., Johnson, N.W., Landmark, V., Mackenzie, J., and Young, M.F. (1998). Metallurgical characterization of George Fisher ore textures and implications for ore processing. *Proceedings of the AusIMM Mine to Mill Conference*, Brisbane, Australia, 11-14 October. Australasian Institute of Mining and Metallurgy, Melbourne. pp. 29-41.

Bradshaw, D.J. (2014). The role of 'process mineralogy' in improving the process performance of complex sulphide ores. *Proceedings of IMPC 2014*, Santiago, Chile. Gecamin, Santiago. pp. 1-23.

Butler, C., Dale, R., Robinson, S., and Turner, A. (2016). Geometallurgy – Bridging the gap between mine and mill: A case study of the DeGrussa geometallurgy program. *Proceedings of the Third AUSIMM International Geometallurgy Conference,* Perth, WA, 15-16 June 2016. Australasian Institute of Mining and Metallurgy, Melbourne. pp. 77-88.

Coward, S., Vann, J., Dunham, S., and Stewart, M. (2009). The primary-response framework for geometallurgical variables. *Proceedings of the Seventh International Mining Geology Conference.* Australasian Institute of Mining and Metallurgy, Melbourne. pp. 109-113.

Dominy, S.C., O'Connor, L.O., and Xie, Y. (2016). Sampling and test work protocol development for geometallurgical characterisation of a sheeted vein gold deposit. *Proceedings of the Third AUSIMM International Geometallurgy Conference,* Perth, WA, 15-16 June 2016. Australasian Institute of Mining and Metallurgy, Melbourne. pp. 97-112.

Howarth, D.F. and Rowlands, J.C. (1987). Quantitative assessment of rock texture and correlation with drillability and strength properties. *Rock Mechanics and Rock Engineering*, 20, 57-85.

Johnson, N.W. (2016). Sphalerite and galena liberation levels for the Mount Isa concentrator. *Process Mineralogy*. Becker, M, Wightman, E.M., and Evans, C.L. (eds). Julius Kruttschnitt Mineral Research Centre, University of Queensland, Australia. pp. 234-249.

Johnson, N.W. and Munro, P.D. (2008). Methods for assigning domains in the primary sulfide zone of a sulfide orebody. *Proceedings of the Ninth International Congress for Applied Mineralogy*, Brisbane, Queensland, 8-10 September. Australasian Institute of Mining and Metallurgy, Melbourne. pp. 597-603.

King, G.S. and MacDonald, J.L. (2016). The business case for early-stage implementation of geometallurgy – an example from the Productora Cu-Mo-Au deposit, Chile. *Proceedings of the Third AUSIMM International Geometallurgy Conference*, Perth, WA, 15-16 June 2016. Australasian Institute of Mining and Metallurgy, Melbourne. pp. 125-133.

Lamberg, P. (2011). Particles – the bridge between geology and metallurgy. https://www.researchgate.net/publication/267386265

Liebezeit, V., Ehrig, K., Robertson, A., Grant, D., Smith, M., and Bruyn, H. (2016). Embedding geometallurgy into mine planning practices – Practical examples at Olympic Dam. *Proceedings of the Third AUSIMM International Geometallurgy Conference*, Perth, WA, 15-16 June 2016. Australasian Institute of Mining and Metallurgy, Melbourne. pp. 135-143.

Lotter, N.O., Kormos, L.J., Oliveira, J., Fragomeni, D., and Whiteman, E. (2011). Modern process mineralogy: Two case studies. *Minerals Engineering*, 24, 638–650.

Lotter, N.O., Baum, W., Reeves, S., Arrué, C., and Bradshaw, D.J. (2017). The business value of best practice process mineralogy. *Minerals Engineering*, http://dx.doi.org/10.1016/j.mineng.2017.05.008

McKay, N.A., Vann, J., Ware, W., Morley, C., and Hodkiewicz, P. (2016a). Strategic and tactical geometallurgy – a systematic process to add and sustain resource value. *Proceedings of the Third AUSIMM International Geometallurgy Conference*, Perth, WA, 15-16 June 2016. Australasian Institute of Mining and Metallurgy, Melbourne. pp. 29-36.

McKay, N. A., Sztuke, J.C. and Lacouture, B. (2016b). Red Dog Zinc concentrator optimization study 2009. *Process Mineralogy.* Becker, M., Wightman, E.M., and Evans, C.L. (eds). Julius Kruttschnitt Mineral Research Centre, University of Queensland, Australia. pp. 250-260.

Nthlabane, S., Becker, M., Charikinya, E., Voight, M., Schouwstra, R., and Bradshaw, D. (2018). Towards the development of an integrated modelling framework underpinned by mineralogy. *Minerals Engineering*, 116, 123-131.

Rosenkranz, J. and Lamberg, P. (2014). Sustainable processing of mineral resources. *International Journal of the Society of Materials Engineering for Resources*, 20 (1), 17-22.

Rudnick, T.K. (2016). The genesis of the Swartberg base-metal sulphide deposit, South Africa. Master's dissertation, University of Stellenbosch.

Ryan, P.J., Lawrence, A.L., Lipson, R.D., Moore, J.M., Paterson, A., Stedman, D.P., and van Zyl, D. (1986). The Aggeneys base metal sulphide deposits, Namaqualand district. *Mineral Deposits of South Africa.* Anhaeusser, C.R. and Maske, S. (eds). Geological Society of South Africa, Johannesburg. pp. 1447-1473.

Schouwstra, R., de Vaux, D., Hey, P., Malysiak, V., Shackleton, N., and Bramdeo, S. (2010). Understanding Gamsberg – A geometallurgical study of a large stratiform zinc deposit. *Minerals Engineering,* 23 (11-13), 960-967.

Sepulveda, E., Dowd, P., and Xu, C. (2015). Modelling geometallurgical response variables using Projection Pursuit regression. *Proceedings of the 11th International Mineral Processing Conference.* Gecamin, Santiago.

Stedman, D.P. (1980). The structural geology and metamorphic petrology of Black Mountain, Namaqualand. Master's dissertation. University of the Witwatersrand, Johannesburg.

Steinmann, P.G. (2016). Grade Control Geologist, Black Mountain Mining, Aggeneys. Personal communication.

Henry Justinian Jnr Gordon

Exploration Geologist
Black Mountain Mining (Pty). Ltd.

As of 2015, Henry Gordon has been employed by Black Mountain Mining, Aggeneys. Henry has experience in grade control, resource development and mineral resource management pertaining to copper, lead and zinc base metals. As of 2017, he has been part of the Vedanta Zinc International minerals development team in the capacity of Exploration Geologist. He is responsible for resource drill planning - and management of on-mine base metal projects, formulating - and interpretation of geological models, and database - and QA/QC management. Henry aspires to manage brownfields project geometallurgy as part of the resource development team. Henry holds a BSc Hons degree in Applied Geology from Stellenbosch University, and as of 2017, is an MSc Geology candidate (Stellenbosch University) focussing on the geometallurgical delineation of complex, polymetallic, sedimentary exhalative base metal deposits.